

Ph.D. THESIS DISSERTATION:

Novel non-linear approaches to understanding the dynamic brain: knowledge from
rsfMRI and EEG studies.

Ph.D. candidate: Lucía Penalba

Supervisor: Dr. Ignacio Cifre León (Universitat Ramon Llull)

Research group: Comunicació i Salut (COMSAL)

Cosupervisors: Dr. Patricia Oliveira-Silva (Universidade Catolica Portuguesa), Dr. Alexander Sumich
(Nottingham Trent University)

Research groups: Human Neurobehavioral Laboratory (HNL) in the Research Center for Human
Development (CEDH), Affect,

Personality and the Embodied Brain (APE) in the Centre for Public and Psychosocial Health

Program: Ph.D. program in Applied Psychology, Adaptation and Change in Contemporary Societies

December 2022



UNIVERSIDADE
CATOLICA
PORTUGUESA

NOTTINGHAM
TRENT UNIVERSITY

Acknowledgments

I would like to express my deepest gratitude to Ignacio, Patrícia and Alex, the best supervisory team I could ever have. Each of them provided me with invaluable and complementary insights for this thesis and for my career. I could not have undertaken this journey without Ignacio, who offered me his great knowledge, technical support, patience, and guidance. Words cannot express my gratitude to Patrícia who encouraged me to savour every moment of my Ph.D. journey and inspired me with her words, actions and by offering countless opportunities to step outside my comfort zone, grow personally and professionally and connect with different researchers. I am extremely grateful to Alex, who taught me to think big, out of the box, creatively and critically and offered to share and discuss my research in several international meetings.

Special thanks to Mark for his tremendous generosity, for sharing his collected EEG data with me and helping me with the EEG preprocessing steps. Many thanks to Gabriel and Pedro for guiding me through the EEG analysis and for sharing a novel and promising machine learning technique with me.

Heartfelt thanks also go to my colleagues at UCP, especially to Rosario and Elisa for the countless coffees, walks, talks and “pomodoros” we did together. So much needed to make it through this “cognitive marathon”. Many thanks to Ana, Sofía and Inés for their great professional and personal support.

Lastly, I would like to extend my sincere thanks to Adrian for his continuous encouragement and for believing in me since the beginning of this adventure. Also, to my caring family and friends who offered me their unconditional love and support.

Content

Abstract

1. Introduction	
1.1. Neuroimaging techniques to study the brain spatio-temporal dynamics: rsfMRI and rsEEG	12
1.2. Linear and non-linear rsfMRI methods.....	12
1.3. Presentation of the rsfMRI studies and characterization of the samples	14
1.4. Challenges of dynamic rsfMRI.....	16
1.5. A novel non-linear rsEEG machine learning method (ML) to classify aging and sleep quality.....	18
1.6. Contribution of authors and co-authors of the studies	21
2. Study 1. Revisiting Nonlinear Functional Brain Co-activations: Directed, Dynamic, and Delayed.....	27
3. Study 2. Increased Functional connectivity patterns in mild Alzheimer’s Disease: A rsfMRI study.....	43
4. Study 3. The distance-dependent brain functional connectivity is normal in ipsilateral but disturbed between homologous-contralateral regions in Alzheimer disease.....	75
5. Study 4. Classification of sleep quality and aging as a function of brain complexity: A multiband non-linear EEG analysis.....	90
6. General discussion.....	129

Abstract

Advances in neuroimaging techniques have been critical to identifying new biomarkers for brain diseases. Resting State Functional Magnetic Resonance Imaging (rsfMRI) non-invasively quantifies the Blood Oxygen Level Dependent (BOLD) signal across brain regions with high spatial resolution; whilst temporal resolution of Electroencephalography (EEG) in measuring the brain's electrical response is unsurpassed. Most of the statistical and machine learning methods used to analyze rsfMRI and EEG data, are static and linear, fail to capture the dynamics and complexity of the brain, and are prone to residual noise. The general goals of this thesis dissertation are i) to provide methodological insight by proposing a statistical method namely point process analysis (PPA) and a machine learning (ML) multiband non-linear EEG method. These methods are especially useful to investigate the brain configuration of older participants and individuals with neurodegenerative diseases, and to predict age and sleep quality; and ii) to share biological insights about synchronization between brain regions (i.e., functional connectivity and dynamic functional connectivity) in different stages of mild cognitive impairment and in Alzheimer's disease. The findings, reported and discussed in this thesis, open a path for new research ideas such as applying PPA to EEG data, adjusting the non-linear ML algorithm to apply it to rsfMRI and use these methods to better understand other neurological diseases.

Resumen

Los avances en las técnicas de neuroimagen han sido fundamentales para identificar nuevos biomarcadores de enfermedades cerebrales. La resonancia magnética funcional en estado de reposo (rsfMRI) cuantifica de forma no invasiva la señal dependiente del nivel de oxígeno en sangre (BOLD) en todas las regiones del cerebro con una alta resolución espacial, mientras que la resolución temporal de la electroencefalografía (EEG) para medir la respuesta eléctrica del cerebro es insuperable. La mayoría de los métodos estadísticos y de aprendizaje automático utilizados para analizar datos de rsfMRI y EEG son estáticos y lineales, no captan el dinamismo y la complejidad del cerebro y son propensos al ruido residual. Los objetivos generales de esta tesis doctoral son i) proporcionar una visión metodológica proponiendo un método estadístico, llamado análisis por proceso de puntos (PPA), y un método de aprendizaje automático (ML) multibanda no lineal de EEG. Estos métodos son especialmente útiles para investigar la configuración cerebral de participantes de edad avanzada y de individuos con enfermedades neurodegenerativas, y para predecir la edad y la calidad del sueño; y ii) compartir conocimientos biológicos sobre la sincronización entre regiones cerebrales (es decir, la conectividad funcional y la conectividad funcional dinámica) en diferentes etapas del deterioro cognitivo leve y en la enfermedad de Alzheimer. Los hallazgos, comunicados y discutidos en esta tesis, abren un camino para nuevas ideas de investigación, como la aplicación de PPA a datos de EEG, el ajuste del algoritmo ML no lineal para aplicarlo a rsfMRI y el uso de estos métodos para comprender mejor otras enfermedades neurológicas.

Resum

Els avenços en les tècniques de neuroimatge han estat fonamentals per identificar nous biomarcadors de malalties cerebrals. La ressonància magnètica funcional en estat de repòs (rsfMRI) quantifica de manera no invasiva el senyal dependent del nivell d'oxigen a la sang (BOLD) a totes les regions del cervell amb una alta resolució espacial, mentre que la resolució temporal de l'electroencefalografia (EEG) per mesurar la resposta elèctrica del cervell és insuperable. La majoria dels mètodes estadístics i d'aprenentatge automàtic utilitzats per analitzar dades de rsfMRI i EEG són estàtics i lineals, no capten el dinamisme i la complexitat del cervell i són propensos al soroll residual. Els objectius generals d'aquesta tesi doctoral són i) proporcionar una visió metodològica proposant un mètode estadístic, anomenat anàlisi per procés de punts (PPA), i un mètode d'aprenentatge automàtic (ML) multibanda no lineal d'EEG. Aquests mètodes són especialment útils per investigar la configuració cerebral de participants d'edat avançada i d'individus amb malalties neurodegeneratives, i per predir l'edat i la qualitat del son; i ii) compartir coneixements biològics sobre la sincronització entre regions cerebrals (és a dir, la connectivitat funcional i la connectivitat funcional dinàmica) en diferents etapes del deteriorament cognitiu lleu i en la malaltia d'Alzheimer. Les troballes, comunicades i discutides en aquesta tesi, obren un camí per a noves idees de recerca, com l'aplicació de PPA a dades d'EEG, l'ajust de l'algorisme ML no lineal per aplicar-lo a rsfMRI i l'ús d'aquests mètodes per comprendre'n millor d'altres malalties neurològiques.

1. Introduction

1.1. Neuroimaging techniques to study the brain spatio-temporal dynamics: rsfMRI and rsEEG

Rapid advances in statistics, technology and neuroscience are enabling the identification of biomarkers to predict and diagnose brain diseases. The present thesis applies innovative statistical and machine learning (ML) methods to resting-state functional magnetic resonance imaging (rsfMRI) and electroencephalography (rsEEG) data, in order to better understand mechanisms of healthy and pathological ageing.

rsfMRI and rsEEG are commonly used to measure intrinsic spatial-temporal brain dynamics¹, and each offer advantages to understanding brain function (Bandettini, 2009). rs-fMRI measures spontaneous brain activity, indirectly by quantifying the changes in blood oxygenation, the Blood Oxygen Level Dependent (BOLD) response. This non-invasive technique provides excellent spatial resolution (i.e., 1-2 mm), although temporal resolution has a time scale in seconds. On the other hand, EEG measures the electrical signals produced by the brain via electrodes attached to the scalp, and thus provides a high temporal resolution (sample rates between 250 and 2000 Hz), but poorer spatial resolution. EEG is also typically more easily accessible, portable, and has lower cost. The passive assessments involved in resting-state methods are also advantageous for participants who might find completion of experimental tasks challenging (e.g., those with neurodegenerative diseases or psychiatric illnesses).

Subsequent sections in this introduction will provide i) a brief explanation of the linear and non-linear rsfMRI methods used in the present thesis studies to study synchronicity between brain regions, i.e., functional connectivity (FC); ii) a synthetic description of the studies and the main characteristics of the samples, i.e., aging and Alzheimer's disease (AD); iii) an explanation of the challenges of using rs-fMRI data; iiiii) an introduction to a novel non-linear rsEEG machine learning method (ML) to classify aging, with particular reference to interactions with sleep quality².

1.2. Linear and non-linear rsfMRI methods

¹ Understanding the healthy brain and the brain with pathology requires of techniques that capture the brain changes in activity and connectivity of specific regions over time, i.e., spatial and temporal dynamic data. rsfMRI and EEG are tools that provide this type of information.

² It is worth noting that 3 out of the 4 studies in the present thesis dissertation are rsfMRI studies, for this reason much of the space dedicated in this introduction is related to this specific neuroimaging technique.

Functional connectivity (FC) is a popular neuroscience method for determining the temporal correlation or synchronization between activity from spatially distant brain regions. FC can be obtained by means of the rsfMRI BOLD response, which is sensitive to capturing the spontaneous and intrinsic neural activity (Biswal et al., 1995; Fingelkurts et al., 2005; Chen et al., 2016). Traditional rs-fMRI methods to explore FC, have applied single or windowed frame analysis. The outcome when conducting this type of analysis, is a single value of statistical dependence, i.e., the Pearson's Correlation Coefficient (PCC) between pairs of regions when using the whole time series, or as many values as windows when segmenting the timeseries. In this latter approach, namely sliding windows analysis (SWA) the variability in FC over the scan, i.e., dynamic FC (dFC), can be captured. Nevertheless, the fact that in both approaches the mean of the segment/s' BOLD signal is computed, i.e., in the classic FC the average of each entire timeseries and in SWA the average of each segment of each time series the relevant transient changes over the scan are hindered, as these are cancelled out when averaging the signals.

Whilst from a classic FC point of view, the linear PCC of two whole timeseries has been considered robust as all the volumes or time points are included in the analysis, alternative approaches that captures neural avalanches of information might reduce noise and provide us with insight that reflects more accurately the biological nature of the brain (Keilholz et al., 2017). In this sense, transient changes detected in the BOLD signal, might be of great relevance when considering the FC from a neurophysiological perspective. Neurons do not function in isolation; they organize throughout the cortex in large groups, forming transient assemblies. In contrast to single neurons, these assemblies are strong, i.e., damage of single neurons do not influence the way the information is presented. Additionally, these assemblies represent avalanches of intrinsic neuronal information that produce a hemodynamic response, similar to the response that occurs when participants respond to a stimulus or task. Considering the characteristics of neuronal assemblies, non-linear methods that capture uniquely those spontaneous events, might yield more accurate information of the brain spatio-temporal dynamics, while at the same time reduce computational demands (D'Atri et al., 2021). Most of the nonlinear approach focuses on the amplitude of the signal, and assumes that time points or volumes with a higher activation, are caused by the avalanche of intrinsic neuronal information (Tagliazucchi et al., 2012, 2016).

Identifying relevant events or points in the signal seems to be especially relevant when comparing healthy cohorts with groups with psychiatric or neurological diseases (Keilholz et al., 2017); for instance, in post-traumatic stress disorder (Li et al., 2014), attention-deficit hyperactivity disorder (Ou et al., 2014), schizophrenia (Miller et al., 2016; Yu et al., 2015), major depression (Demirtas et al., 2016), autism spectrum (de Lacy et al., 2017; Falahpour et al., 2016) and mild

cognitive impairment³ (MCI) (Chen et al., 2016). It is worth noting that another study detected differences between patients with schizophrenia and patients with bipolar disorder, and that these two groups are difficult to be differentiated with classic FC methods (Rashid et al., 2016). In conclusion, the PPA capability to detect non-linearity and time varying changes in FC is a promising method to differentiate stages of neurological diseases, such as Alzheimer's disease (AD).

1.3. Presentation of the rsfMRI studies and characterization of the samples

The present thesis is composed of a compendium of four articles. In the first three, rsfMRI data was used while in the last one rsEEG data was used. In this present section (i.e., 2.2), only the rsfMRI studies (i.e., studies 1-3) will be introduced.

Study 1 presents a in depth description of a novel method based on the detection of relevant events of the signal, i.e., amplitude-based events in the BOLD signals. This approach allows the extraction of FC, as well as additional measures, such as the delay and directionality, i.e., causal or directed FC, also introduced in this paper. Additionally, the performance of the method was applied in two samples, one composed by healthy participants and another one by individuals with autism from the Autism Brain Imaging Data Exchange (ABIDE) database (Craddock et al., 2013), to explore non-linear FC. For comparison purposes the classic whole time-series correlation FC analysis was also applied.

While in study 1 the most relevant goal was to thoroughly describe the method and show its performance with a couple of examples. The second and third studies focused on providing biological insights and less on contributing with methodological novelty. More specifically, study 2 aimed to explore differences in FC between healthy participants, participants with MCI and patients with AD using the classic FC, SWA and the novel PPA, an approach derived from the method based on events introduced in the first study (in this second study directionality is not explored, only FC).

Study 3 aimed to investigate whether the functional connectivity (FC) between pairs of brain regions decays as a function of their mutual distance in Alzheimer's disease. Additionally, it explored whether age, atrophy, lower scores in executive functioning and global cognition are correlated with an FC deficit between contralateral distant homologous regions (Meguro et al., 2003; Oosterman et al., 2012). Data taken from the Alzheimer's Disease Neuroimaging Initiative (ADNI) was used for studies 2 and 3, <https://adni.loni.usc.edu/>

³ Mild Cognitive Impairment (MCI) is often considered a prodromal stage of AD. However, some patients develop other types of neurodegenerative disease, others do not develop any and others recover their cognition completely.

The motivation to apply novel linear and non-linear rsfMRI methods on MCI and AD data and extract neurological insight from it was two-fold. First, AD is the most common neurodegenerative disorder associated with age that conveys a significant economic and societal impact (Scarapicchia et al., 2018). By 2050 it is projected that 115 million people worldwide will have Alzheimer's disease (Rice, L and Bisdas, S, 2017). For this reason, the World Health Organization set as a priority in the health agenda around the globe to increase awareness, diagnose the disease at an early stage and offer better support to families, caregivers, and patients with AD (Cassani et al., 2018). Hence, advances in AD research are essential to find ways that reduce the negative impact of the disease. Second, considering these facts, it is crucial to find efficient techniques to diagnose AD at a very incipient phase and differentiate the stages of the disease. Research studies are key to finding biomarkers that guide the development of individualized interventions to reduce the burden of the disease. Until now, AD remains a clinical diagnosis, i.e., it can be detected when cognitive symptoms are clear and measurable by means of cognitive tests⁴ and supported by structural MRI to detect atrophy. These tools are time consuming and need well-prepared clinicians for an appropriate application and interpretation. Moreover, several studies revealed that changes in the brain, such as aberrant functional connectivity, appear 10 to 20 years before the onset of structural atrophy and cognitive symptoms (Dubois et al., 2016). rsfMRI might enable the detection of these early changes in AD. Although several studies have explored FC in patients with MCI and AD, until now results are inconsistent, especially in MCI (Badhwar et al., 2017). For this reason, a good cognitive and biological characterization of the samples, appropriate rsfMRI preprocessing methods and novel analysis that captures relevant neural intrinsic events might be the path to find accurate AD prognostic biomarkers.

MCI is usually a symptomatic prodromal stage of AD. Patients who suffer from it score lower than their normative age group in neuropsychological tests but still preserve their autonomy and their daily life activities are not affected (Csukly et al., 2016). The pathological changes detected in patients with MCI are neuritic plaques, neurofibrillary tangles, and loss of basal forebrain cholinergic neurons (Braak and Braak in Yamasaki 2012). The conversion rate from MCI to dementia (including AD) is of 10-15% every year. MCI is classified into amnesic MCI (aMCI) and non-amnesic MCI (naMCI). While aMCI is associated with a loss of episodic memory and usually evolves towards AD, naMCI affects other cognitive functions and evolves towards another type of dementia, such as diffuse Body Lewis or frontotemporal dementia (Csukly et al., 2016).

⁴ The mini mental state examination (MMSE), the Montreal cognitive assessment (MOCA) and the Alzheimer's Disease Assessment Scale-Cognitive (ADASCog) are the cognitive tests more widely used in the clinical practice for screening and assessment of the level of cognitive impairment.

Several studies in the context of AD have included group samples of participants with MCI without characterizing the type. This could explain the contradictory findings in the literature, e.g., some studies reported an increased FC between several brain regions in MCI in contrast to healthy participants, while others reported the opposite (Badhwar et al., 2017). In light of this, to better characterize the MCI sample in study 2⁵, only patients with aMCI were included. Additionally, the groups were divided into two aMCI groups, depending on the results of the Wechsler Memory Scale Logical Memory II (WMS-R), as suggested by the ADNI. The cutoff scores for EMCI out of 25 were 9-11 for a minimum of 16 years of education and a score of 5-9 for 8-15 years of education. For LMCI a score of 8 or below for 16 years of education or more and a maximum score of 4 for those who had 8 to 15 years of education (see the following ADNI link for further information on inclusion and exclusion criteria of this group and the AD group see)⁶:

<https://adni.loni.usc.edu/wp-content/uploads/2008/07/adni2-procedures-manual.pdf>

1.4. Challenges of dynamic rsfMRI

Despite the potential benefits that BOLD rsfMRI analysis yield to understanding neurological diseases, several challenges in the data processing should be considered to avoid spurious results. This section provides an explanation of the most relevant issues in rsfMRI analysis that are yet to be resolved in the field of neuroscience.

1. One of the primary sources of signal noise in rsfMRI is head movement during the scan, which poses a significant challenge in signal processing. In the currently reported studies, DPARSF pipelines were applied to correct head motion artefacts (Chao-Gan et al., 2010). DPARSF, is a user-friendly software that calls the functions in Statistic Parametric Mapping (SPM), a Matlab-based package for signal processing. DPARSF ensures that all brain volumes are aligned and generates a report with details on the realignment parameters estimated. As suggested by the DPARSF developers, participants with a head movement of rotation or translation over 2 mm needed to be excluded (Chao-Gan et al., 2010). Although these procedures based on realignment and regression cannot completely remove the noise caused of the signals by head motion, they are able to reduce it considerably and are the best choice available until the moment (Keilholz et al., 2017).

⁵ MCI participants were only included in study 2.

⁶ Further characterization of the MCI and AD samples can be found in the ADNI website or in the method section of studies 2 and 3 of the present dissertation.

2. Another issue in neuroscience, yet unresolved, that deserves special attention is how to parcellate the brain so that results are valid and that comparison across studies is possible. Until now, there is no consensus regarding the best way to segment the brain for rsfMRI analysis. However, the most common approaches to map the brain can be divided into two groups: the data-driven and the atlas-based (i.e., using a template) parcellations. Data-driven parcellations do not consider anatomy or function. Conversely, the parcellation depends on certain parameters that the researcher sets, such as that the size between nodes does not differ, that nodes do not occupy space in the two hemispheres or that the parcellation contains a specific number of nodes (Alexander-Bloch et al., 2012). The main disadvantage of this type of parcellation is that it is sensitive to the clustering parameters used. Additionally, interpreting and comparing results with other studies is difficult using a data-driven approach (Shen et al., 2013). On the other hand, although using an atlas or a template is limited due to variability in neuroanatomy across brains, in general, it enables a good delineation of the structures of the brain. There are several parcellation atlases available for the analysis of structural and functional networks, e.g., the Harvard-Oxford, the Talarach Daemon and the LONI probabilistic brain atlas (LPBA40) to mention a few (Yao et al., 2015). Nevertheless, the most popular one is the automated anatomical labelling (AAL) atlas (Tzourio-Mazoyer et al., 2002) which segments the brain into 90 or 116 regions⁷, a manageable number for whole-brain analysis. The AAL yields an excellent delineation of cortical areas, which is essential for network analysis (Arslan et al., 2018). Additionally, its popularity makes it a good option of choice for interpretation and comparison purposes. For these reasons, the AAL atlas was used in studies 1-3 of this dissertation.
3. As mentioned, the SWA is a commonly used dFC, based on the linear correlation between signals. Applying this method, the variability of brain region synchronicity across time is captured. This method is considered a dynamic FC approach, in contrast to the classic FC method, based on the correlation of average across the entire time series. The degree of time-varying changes in FC captured by the SWA depends on the window size. Smaller windows are more sensitive in detecting changes over time but present a reduced signal to noise ratio (SNR). On the other hand, wider windows, average the windows over longer segments approaching the classic FC method, and consequently losing dynamic information (Keilholz et al., 2017). The perfect size to preserve stability and dynamicity would probably be the one that captures a whole brain configuration, i.e., a state of the brain in time and space, however the amount of time the brain takes to change from one state to another is unknown. Some researchers, however, have discussed other ways to

⁷ The AAL 116 includes the cerebellum, the AAL 90 excludes it.

choose an optimal window size. According to several investigators, an appropriate size should be selected by considering the lowest frequency. If the lowest frequency is not present in the first window, usually windows of 50 to 100 sec, then spurious fluctuations might be present (Leonardi and Van De Ville, 2015). Considering these findings, to ensure a good trade-off between sensitivity and robustness, in study 2, where a SWA was conducted and the frequency of the BOLD signal ranged between 0.1 and 0.001 Hz, time series were split into windows of 90 seconds (i.e., 30 timepoints or volumes in our case). In addition to the suggestions found in the literature, an analysis to optimize the window size was conducted and can be found in study 2.

These aforementioned challenges are relevant as they have an impact in the results and explain heterogeneity across findings.

1.5. A novel non-linear rsEEG machine learning method (ML) to classify aging and sleep quality

Apart from the use of statistical methods, based on correlations, the amplitude of the signal and null hypothesis testing by finding P values (methods used in studies 1, 2 and 3), another way to study biological systems is by using machine learning (ML). The selection of which method to use should typically be based on the purpose of the study⁸. The use of traditional statistics is suitable to obtain mechanistic insight, as it allows exploration and inference, whilst ML is appropriate when the aim is to classify and predict groups or variables, i.e., a class label can be guessed for a given input data with more or less accuracy depending on the algorithms used and the optimization parameters (Bzdok & Ioannidis, 2019).

When dealing with big data, e.g., a large number of characteristics or features from the brain, algorithms that predict patterns are an optimal alternative to traditional statistics. It is relevant to underline that when using ML to predict and classify, the primary goal has traditionally been to achieve the highest performance possible, rather than gain insight into the biological significance of the results, e.g., the directionality of the results and their interpretation (Bzdok & Ioannidis, 2019). For instance, in traditional statistics, one could infer that a decrease of activity in the default mode network (DMN) in resting state in patients with Alzheimer's disease in contrast to healthy participants might be associated with the accumulation of pathologic protein in this region. Conversely, in ML one could predict whether it is possible to distinguish between healthy

⁸ I highly believe that researchers, especially in the field of neuroscience, should work in collaboration, as different disciplines and skills are required for the study of the brain. Instead of using the same methods because of one's expertise, one should think about the appropriate method for each research question. As a psychologist, when choosing the novel ML method of this dissertation, assistance from engineers was needed and highly appreciated.

participants versus individuals with MCI as a function of brain configuration; or whether an intervention works for participants as a function of a combination of brain patterns. Usually, these patterns are non-linear, difficult to identify by the researchers and can be processed only with specific ML algorithms.

In contrast to the aims in studies 1-3, that were exploratory and inferential, the aim of study 4 was to classify older and younger adults with good and bad sleep quality as a function of awake electroencephalography (EEG) brain complexity. Conducting this study and including it as part of this present dissertation was motivated by different reasons. First, the relevance of good sleep in healthy aging and its relationship with brain configuration⁹. Second, the presentation of another neuroimaging technique (i.e., EEG), that yields an excellent temporal resolution to study the brain and, third, the presentation of a novel non-linear ML method (i.e., note that in the first three studies, linear and non-linear methods using traditional statistics were presented while in this last one a non-linear ML method was used).

Sleep is essential to maintain one's mental and physical health. Although demographics show that poor sleep is more prevalent in older adults, evidence indicates that age *per se* cannot explain this tendency (Dregan & Armstrong, 2009; Sculin et al., 2017). Conversely, brain complexity, understood as the ability of the neuronal circuits to interact at different spatial and temporal scales enabling the individual to adapt flexibly to the environment, is a measure that might enable one to better understand and classify individuals. Determining whether brain complexity can be used to differentiate young and older adults with good and bad sleep quality is a first step to develop age and lifestyle interventions.

Several studies have used single non-linear features of complexity from wake EEG signals and demonstrated their usefulness to classify participants as a function of sleep quality and / or aging. Some of these are the correlation dimension (D_2), a measure of the connectedness of the system (Jeong et al., 2001); the Hurst Exponent (H), a measure of statistical self-dependence of the brain activity over multiple scales of time and space, e.g., the self-similarity of the time series (Colombo et al., 2016); and, the entropy, a measure of complexity that indicates the level of disorder in a dynamic system (Faust and Bairy, 2012)¹⁰. Proceeding from these results that suggest the appropriateness of these features to classify aging and sleep quality, here we propose an algorithm, already used in a recent study to classify Alzheimer's disease, developed by coauthors of study 4 of the present dissertation (Silva et al., 2022). The novelty of this algorithm resides in the fact that it extracts and combines 10 non-linear features of complexity instead of single features. It was hypothesized that feeding different machine learning methods, e.g., logistic

⁹ Brain configuration as organization of the functional brain in time and space.

¹⁰ All these non-linear features are thoroughly described in study 4.

regression, decision trees, k-nearest neighbour, with this algorithm to identify brain patterns in each group, would enable an excellent classification performance.

The sample used in study 4 is the same as in a previous publication (Crook-Rumsey, 2020). The study was approved by the Health Research Authority, UK (REC reference: 17/EM/1010), and participants provided informed consent. Participants were divided into four groups depending on their age (i.e., younger adults aged 20-34, older adults aged ≥ 65) and their sleep quality (good vs. bad), as assessed using the global score of the Pittsburg Sleep Quality Inventory (PSQI). Scores range from 0 to 21. Scores > 5 are indicative of poor sleep or significant sleep disturbance (Buysse et al., 1989). None of the participants presented any psychiatric nor neurological disease. To make sure that none of them presented MCI, they were assessed with the Hopkins Verbal Learning Test-Revised (HVLT-R), a test that captures subtle differences in cognition (Benedict et al., 1998). For further detail on the participants, the psychometric characteristics of the scales, the EEG signal processing or the analysis see the method section of study 4.

In the next section the titles of the studies, the state of the manuscript (i.e., submitted to a journal, under review or accepted) and the contribution of the authors and co-authors will be detailed.

1.6. Contribution of authors and co-authors of the studies

Study 1:

Cifre, I*, Miller Flores, M., **Penalba-Sánchez, L.**, Ochab, J.K., and Chialvo, D.R. (2021) Revisiting Nonlinear Functional Brain Co-activations: Directed, Dynamic, and Delayed. *Frontiers in neuroscience*. (October 2021, Vol.15) <https://doi.org/10.3389/fnins.2021.700171>

IC designed, pre-processed, analysed the data and wrote the manuscript, LPS contributed on the analyses, writing and revision, MMF and OJK reviewed the article, DRC designed and supervised all the steps of the study.

Study 2:

Penalba-Sánchez, L*, Oliveira-Silva, P., Sumich, A., Cifre, I. (2022). Increased Functional connectivity patterns in mild Alzheimer's Disease: A rsfMRI study. *Frontiers in Aging Neuroscience*. *Accepted*.

LPS conducted the data preprocessing, analysis and wrote the manuscript. IC and AS contributed in the design of the study. IC provided technical support in the data preprocessing and analysis. IC, AS and POS contributed to manuscript revision, and approved the submitted version.

Study 3:

Cifre, I*., **Penalba-Sanchez, L.**, Ochab, J., Rubido, N., Chialvo, D.R. (2022). The distance-dependent brain functional connectivity is normal in ipsilateral but disturbed between homologous-contralateral regions in Alzheimer disease. *Ready to submit*.

IC and LPS designed the study, pre-processed, analysed the data and wrote the manuscript; JO and NR assisted in writing and reviewing the article; DRC worked on the design of the study and supervised all the steps of the study.

Study 4:

Penalba-Sánchez, L*, Silva, G., Crook-Rumsey, M., Sumich A., Rodrigues, M.P., Oliveira-Silva, P., Cifre, I. (2022). Classification of sleep quality and aging as a function of brain complexity: a multiband non-linear EEG analysis. *Submitted*.

LPS designed the study, organized and pre-processed the data, conducted part of the analysis and wrote the manuscript; GS and PMR proposed the algorithm, helped in the analysis and reviewed the manuscript; MCR collected EEG and sleep self-reported data and helped in the preprocessing; AS, POS and IC supervised all the steps of the study and reviewed the manuscript.

References

- Alexander-Bloch, A., Lambiotte, R., Roberts, B., Giedd, J., Gogtay, N., & Bullmore, E. (2012). The discovery of population differences in network community structure: New methods and applications to brain functional networks in schizophrenia. *NeuroImage*, 59(4), 3889–3900. <https://doi.org/10.1016/j.neuroimage.2011.11.035>
- Badhwar, A. P., Tam, A., Dansereau, C., Orban, P., Hoffstaedter, F., & Bellec, P. (2017). Resting-state network dysfunction in Alzheimer's disease: A systematic review and meta-analysis. *Alzheimer's and Dementia: Diagnosis, Assessment and Disease Monitoring*, 8, 73–85.
- Bandettini, P. A. (2009). What's new in neuroimaging methods? *Annals of the New York Academy of Sciences*, 1156, 260–293. <https://doi.org/10.1111/j.1749-6632.2009.04420.x>
- Benedict RHB, Schretlen D, Groninger L, Brandt J. Hopkins verbal learning test - Revised: Normative data and analysis of inter-form and test-retest reliability. (1998). *Clinical Neuropsychologist*;12(1):43-55. doi:10.1076/clin.12.1.43.1726
- Biswal, B., Zerrin Yetkin, F., Haughton, V.M. and Hyde, J.S. (1995), Functional connectivity in the motor cortex of resting human brain using echo-planar mri. *Magn. Reson. Med.*, 34: 537-541.

- Buysse DJ RC. The Pittsburgh Sleep Quality Index: a new instrument for psychiatric practice and research. (1989). *Psychiatry research Elsevier*. Published online: 193-213.
doi:doi:10.1016/0165-1781(89)90047-4
- Bzdok,D., Ioannidis, J. (2019). Exploration, Inference, and Prediction in Neuroscience and Biomedicine. *Trends in Neurosciences*, (Vol. 42, Issue 4, pp. 251-262).
<https://doi.org/10.1016/j.tins.2019.02.001>.
- Cassani, R., Estarellas, M., San-Martin, R., Fraga, F. J., & Falk, T. H. (2018). Systematic review on resting-state EEG for Alzheimer's disease diagnosis and progression assessment. In *Disease Markers* (Vol. 2018). Hindawi Limited. <https://doi.org/10.1155/2018/5174815>
- Chao-Gan, Y., & Yu-Feng, Z. (2010). DPARSF: A MATLAB Toolbox for "Pipeline" Data Analysis of Resting-State fMRI. *Frontiers in systems neuroscience*, 4, 13.
<https://doi.org/10.3389/fnsys.2010.00013>
- Chen X, Zhang H, Gao Y, Wee CY, Li G, Shen D. (2016). High-order resting-state functional connectivity network for MCI classification. *Hum Brain Mapp* 37:3282–3296.
- Colombo, MA., Wei, Y., Ramautar, JR., Linkenkaer-Hansen, K., Tagliazucchi, E., van Someren, EJW. (2016). More severe insomnia complaints in people with stronger long-range temporal correlations in wake resting-state EEG. *Front Physiol*;7(NOV). doi:10.3389/fphys.2016.00576
- Craddock, C., Benhajali, Y., Chu, C., Chouinard, F., Evans, A., Jakab, A., et al. (2013). The neuro bureau preprocessing initiative: open sharing of preprocessed neuroimaging data and derivatives. *Front. Neuroinformatics* 7:41. doi: 10.3389/conf.fninf.2013.09.00041
- Crook-Rumsey M. (2020). *Neurophysiology of Prospective Memory in Typical and Atypical Ageing*. Nottingham Trent University. ProQuest Dissertations Publishing. 28605687.
- de Lacy N, Doherty D, King BH, Rachakonda S, Calhoun VD. (2017). Disruption to control network function correlates with altered dynamic connectivity in the wider autism spectrum. *Neuroimage Clin* 15:513–524
- D'Atri, A., Scarpelli, S., Gorgoni, M., Truglia, I., Lauri, G., Cordone, S., Ferrara, M., Marra, C., Rossini, P. M., & de Gennaro, L. (2021). EEG alterations during wake and sleep in mild cognitive impairment and Alzheimer's disease. *IScience*, 24(4).
<https://doi.org/10.1016/j.isci.2021.102386>
- Demirtaş M, Tornador C, Falcón C, López-Solà M, Hernández-Ribas R, Pujol J, et al. (2016). Dynamic functional connectivity reveals altered variability in functional connectivity among patients with major depressive disorder. *Hum Brain Mapp* 37:2918–2930

- Dregan A, Armstrong D. Age, cohort and period effects in the prevalence of sleep disturbances among older people: The impact of economic downturn. (2009). *Soc Sci Med*. 69(10):1432-1438. doi: 10.1016/J.SOCSCIMED.2009.08.041
- Dubois, B., Hampel, H., Feldman, H. H., Scheltens, P., Aisen, P., Andrieu, S., Bakardjian, H., Benali, H., Bertram, L., Blennow, K., Broich, K., Cavado, E., Crutch, S., Dartigues, J. F., Duyckaerts, C., Epelbaum, S., Frisoni, G. B., Gauthier, S., Genthon, R., Gouw, A. A. (2016). Proceedings of the Meeting of the International Working Group (IWG) and the American Alzheimer's Association on "The Preclinical State of AD"; July 23, 2015; Washington DC, USA (2016). Preclinical Alzheimer's disease: Definition, natural history, and diagnostic criteria. *Alzheimer's & dementia: the journal of the Alzheimer's Association*, 12(3), 292–323.
<https://doi.org/10.1016/j.jalz.2016.02.002>
- Falahpour M, Thompson WK, Abbott AE, Jahedi A, Mulvey ME, Datko M, et al. (2016). "Underconnected," but not broken? Dynamic fMRI shows underconnectivity in autism is linked to increased intra-individual variability across time. *Brain Connect* 6:403–414
- Faust O, Bairy MG. (2012). Nonlinear analysis of physiological signals: a review. *J Mech Med Biol*. 2012;12. doi:10.1142/S0219519412400155
- Fingelkurts, A. A., Fingelkurts, A. A., & Kähkönen, S. (2005). Functional connectivity in the brain - Is it an elusive concept? In *Neuroscience and Biobehavioral Reviews* (Vol. 28, Issue 8, pp. 827–836). <https://doi.org/10.1016/j.neubiorev.2004.10.009>
- Jeong J, Kim DJ, Kim SY, Chae JH, Go HJ, Kim KS. (2001). Introduction sleep deprivation has been a valuable tool for the study of sleep mechanisms effect of total sleep deprivation on the dimensional complexity of the waking EEG, *Sleep*. Vol 24.
<https://academic.oup.com/sleep/article/24/2/197/2749984>
- Keilholz, S., Caballero-Gaudes, C., Bandettini, P., Deco, G., & Calhoun, V. (2017). Time-Resolved Resting-State Functional Magnetic Resonance Imaging Analysis: Current Status, Challenges, and New Directions. In *Brain Connectivity* (Vol. 7, Issue 8, pp. 465–481). Mary Ann Liebert Inc. <https://doi.org/10.1089/brain.2017.0543>
- Leonardi, N. and Van De Ville, D. (2015). On spurious and real fluctuations of dynamic functional connectivity during rest, *NeuroImage*, 104, pp. 430–436. Available at:
<https://doi.org/10.1016/j.neuroimage.2014.09.007>
- Li X, Zhu D, Jiang X, Jin C, Zhang X, Guo L, et al. (2014). Dynamic functional connectomics signatures for characterization and differentiation of PTSD patients. *Hum Brain Mapp*, 35:1761–1778

- Meguro K, Constans JM, Shimada M, Yamaguchi S, Ishizaki J, Ishii H, et al. (2003). Corpus callosum atrophy, white matter lesions, and frontal executive dysfunction in normal aging and Alzheimer's disease. A community-based study: The Tajiri Project. *International Psychogeriatrics*. 2003;15(1):9-25. 324
- Miller RL, Yaesoubi M, Calhoun VD. (2016). Cross-frequency rs-fMRI network connectivity patterns manifest differently for schizophrenia patients and healthy controls. *IEEE Signal Process Lett*, 23:1076–1080
- Ou J, Lian Z, Xie L, Li X, Wang P, Hao Y, et al. (2014). Atomic dynamic functional interaction patterns for characterization of ADHD. *Hum Brain Mapp* 35:5262–5278
- Oosterman, J.M., Oosterveld, S., Rikkert, M.G.O., Claassen, J.A., Kessels, R.P.C., (2012). Medial temporal lobe atrophy relates to executive dysfunction in Alzheimer's disease. *International Psychogeriatrics*. 326;24(9):1474-82.
- Rashid B, Arbabshirani MR, Damaraju E, Cetin MS, Miller R, Pearlson GD, Calhoun VD. (2016). Classification of schizophrenia and bipolar patients using static and dynamic resting-state fMRI brain connectivity. *Neuroimage* 134:645–657
- Scullin MK. Do Older Adults Need Sleep? A Review of Neuroimaging. (2017). Sleep, and Aging Studies. *Curr Sleep Med Rep*, 3(3):204-214. doi:10.1007/s40675-017-0086-z
- Shen, X., Tokoglu, F., Papademetris, X., & Constable, R. (2013). Groupwise whole-brain parcellation from resting-state fMRI data for network node identification. *NeuroImage*, 82, 403–415. <https://doi.org/10.1016/j.neuroimage.2013.05.081>
- Silva, G., Alves, M., Cunha, R., Bispo, BC., Oliveira-Silva, P., Rodrigues, PM. (2022). Early detection of Alzheimer's and Parkinson's diseases using multiband nonlinear EEG analysis. *Psychol Neurosci*. Published online March 28. doi:10.1037/pne0000287
- Tagliazucchi, E., Balenzuela, P., Fraiman, D., & Chialvo, D. R. (2012). Criticality in large-scale brain fmri dynamics unveiled by a novel point process analysis. *Frontiers in Physiology*, 3 FEB. <https://doi.org/10.3389/fphys.2012.00015>
- Tagliazucchi, E., Siniatchkin, M., Laufs, H., & Chialvo, D. R. (2016). The voxel-wise functional connectome can be efficiently derived from co-activations in a sparse spatio-temporal point-process. *Frontiers in Neuroscience*, 10(AUG). <https://doi.org/10.3389/fnins.2016.00381>
- Tzourio-Mazoyer N, Landeau B, Papathanassiou D, et al. (2002). Automated anatomical labeling of activations in SPM using a macroscopic anatomical parcellation of the MNI MRI single-subject brain. *Neuroimage*;15(1):273-289. doi:10.1006/nimg.2001.0978

Yao, Z., Hu, B., Xie, Y., Moore, P., & Zheng, J. (2015). A review of structural and functional brain networks: small world and atlas. *Brain informatics*, 2(1), 45–52. <https://doi.org/10.1007/s40708-015-0009-z>

Yu Q, Erhardt EB, Sui J, Du Y, He H, Hjelm D, et al. (2015). Assessing dynamic brain graphs of time-varying connectivity in fMRI data: application to healthy controls and patients with schizophrenia. *Neuroimage* 107:345–355.

2. Study 1. Revisiting Nonlinear Functional Brain Co-activations: Directed, Dynamic, and Delayed. (Published)



Revisiting Nonlinear Functional Brain Co-activations: Directed, Dynamic, and Delayed

Ignacio Cifre^{1,2*}, Maria T. Miller Flores², Lucia Penalba¹, Jeremi K. Ochab³ and Dante R. Chialvo^{2,4}

¹ Facultat de Psicologia, Ciències de l'Educació i de l'Esport, Blanquerna, Universitat Ramon Llull, Barcelona, Spain, ² Center for Complex Systems and Brain Sciences (CEMSCS), Escuela de Ciencia y Tecnología, Universidad Nacional de San Martín, Buenos Aires, Argentina, ³ Institute of Theoretical Physics and Mark Kac Center for Complex Systems Research, Jagiellonian University, Krakow, Poland, ⁴ Consejo Nacional de Investigaciones Científicas y Tecnológicas (CONICET), Buenos Aires, Argentina

OPEN ACCESS

Edited by:

Javier Gonzalez-Castillo,
National Institute of Mental Health,
National Institutes of Health (NIH),
United States

Reviewed by:

Michal Ramot,
National Institute of Mental Health,
National Institutes of Health (NIH),
United States
Gopikrishna Deshpande,
Auburn University, United States

*Correspondence:

Ignacio Cifre
ignaciocl@blanquerna.url.edu

Specialty section:

This article was submitted to
Brain Imaging Methods,
a section of the journal
Frontiers in Neuroscience

Received: 25 April 2021

Accepted: 23 August 2021

Published: 12 October 2021

Citation:

Cifre I, Miller Flores MT, Penalba L,
Ochab JK and Chialvo DR (2021)
Revisiting Nonlinear Functional Brain
Co-activations: Directed, Dynamic,
and Delayed.
Front. Neurosci. 15:700171.
doi: 10.3389/fnins.2021.700171

The center stage of neuro-imaging is currently occupied by studies of functional correlations between brain regions. These correlations define the brain functional networks, which are the most frequently used framework to represent and interpret a variety of experimental findings. In the previous study, we first demonstrated that the relatively stronger blood oxygenated level dependent (BOLD) activations contain most of the information relevant to understand functional connectivity, and subsequent work confirmed that a large compression of the original signals can be obtained without significant loss of information. In this study, we revisit the correlation properties of these epochs to define a measure of nonlinear dynamic directed functional connectivity (*nldFC*) across regions of interest. We show that the proposed metric provides at once, without extensive numerical complications, *directed* information of the functional correlations, as well as a measure of *temporal lags* across regions, overall offering a different and complementary perspective in the analysis of brain co-activation patterns. In this study, we provide further details for the computations of these measures and for a proof of concept based on replicating existing results from an Autistic Syndrome database, and discuss the main features and advantages of the proposed strategy for the study of brain functional correlations.

Keywords: fMRI, resting state networks, functional connectivity, dynamic functional connectivity, autism (ASD)

1. INTRODUCTION

The large scale dynamics of the brain exhibits a plethora of spatio-temporal patterns. Since the first description of voxel-wise correlation networks (Eguíluz et al., 2005), there has been a continuous interest in developing better ways to derive brain “networks” from fMRI time series data. Common to all is the identification of functional “nodes” [i.e., fMRI time series extracted from regions of interest (ROI)], functional edges (i.e., the cross-correlations), which allows for the subsequent graph analysis. An important methodological challenge has been always to define an adequate coarse graining of the brain imaging data to compress 1,000 of the so-called blood oxygenated level dependent time series. The usual analysis aims at the identification of bursts of correlated activity across certain regions, which requires extensive computations, complicated in part by the humongous size of the data sets.

In the previous study, we proposed that the timing of the brief epochs of relatively stronger BOLD activations contain a great deal of functional connectivity (FC) information (Tagliazucchi et al., 2011, 2012). The results of subsequent work (Liu and Duyn, 2013; Liu et al., 2013; Petridou et al., 2013; Wu et al., 2013; Amico et al., 2014; Jiang et al., 2014; Li et al., 2014; Allan et al., 2015; Chen et al., 2015; Tagliazucchi et al., 2016) seems to provide ample support to this idea, by confirming the functional relevance of such relatively large amplitude BOLD events under a variety of conditions.

The study goes beyond the analysis of correlations between BOLD time series to explore and define a set of measures of the *nonlinear directed dynamic functional correlation* across ROIs. The use of such measures, despite its simplicity, may help to expand at once the perspective of the usual FC paradigms, such as seed correlation maps and networks, into the realms of nonlinear time-dependent directed correlations.

The study is organized as follows: In the next section, we describe the essence of the method, starting with the basic procedure to define the BOLD-triggered events followed by a description of the available correlation measures that allow a proper definition of the functional connectivity between the events, including a definition of directionality and temporal lag of the events. Section 3 contains the analysis of a simple example as a proof of concept of healthy subject fMRI data set, followed by the replication and further analysis of a voxel-wise published data set from Autism Syndrome in order to show the method features. This study closes with a discussion of the advantages and limitations of the method and potential implications of the results. Derivations and further technical details are condensed in the **Supplementary Material**.

2. METHODS

The analysis to be discussed can use BOLD time series recorded indistinctly from either resting state conditions or during an experiment in which the subject is performing a given task. The most common approach to determine functional connectivity is to compute Pearson's linear correlation between BOLD time series (van den Heuvel and Hulshoff P., 2010; Finn et al., 2015). In contrast, the objective of the present analysis is to determine the relation between relatively large amplitude BOLD activations from a given pair of signals. In this section, it will be discussed: 2.1 how large amplitude events are selected given series of fMRI data; 2.2 correlations computed with the selected events; 2.3 how directionality is understood when working with events; and 2.4 how the dynamic connectivity, understood here as lags between time series, is computed.

2.1. Definition of BOLD-Triggered Events

First, each BOLD time series is z-scored (its mean is subtracted, and it is divided by its SD). Next, a threshold for detecting strong activity is chosen, (typically the results remain unchanged when using a range of 1 – 2 SDs) and for each time series, the timing of each upward threshold crossing is determined (**Figure 1A**). Note that the number of threshold crossings depends on the auto-correlation of the BOLD signals (which stays in the range

0.6–0.85 Ochab et al., 2019) and more generally on the exponent of the $1/f^\alpha$ frequency spectrum. Empirically, for the threshold of 1σ , in a BOLD signal we find on average 8.5 ± 2.8 upward crossings per 4 min of fMRI scan.

The timing is further used to define the *seed* or *source* events. For a given seed voxel or region of interest (ROI), they consist of segments of BOLD time series starting typically 4 – 5 s before and ending 9 – 15s after the crossing (which translates to 2 – 3 TRs before and 4 – 7 TRs after, with $TR = 2.3$ in the data we are using as a proof of concept in this study). This timescale is chosen by the typical duration of these events, which in turn is dictated by the longest timescale of the hemodynamic response function ($\sim 10 - 15$ s).

Finally, for each seed event, the *target* events are extracted from all the other BOLD time series at the exact same times as the seed, see **Figures 1B,C**. The average time courses of the events follow typically a smooth pattern, although they do exhibit variability, for both the seed (see **Figure 1D**) and targets (see **Figures 1E,F**). If the interest of a given experiment is to define an average inter-relation measure between ROIs, then all the seed and target events can be averaged (as shown by red-and-black circles in **Figures 1D–F**), for instance over the entire scan fMRI session.

2.2. Correlations

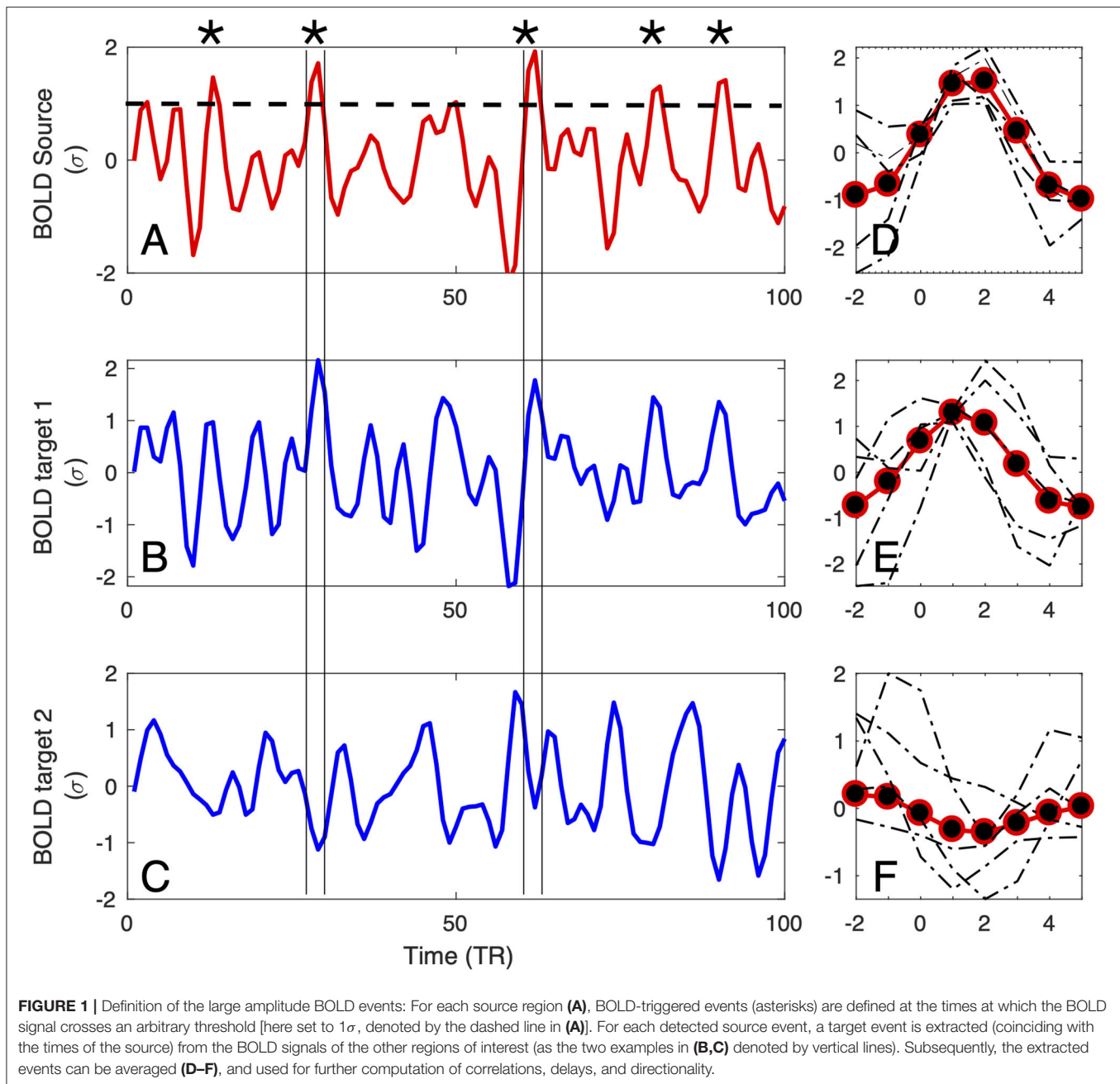
Once the source and the target events are extracted from the BOLD time series, a few options of computing correlations are possible:

1. $r_P(i, j)$ linear Pearson's correlation between the whole time series i and the whole time series j (computed in section III where we perform a proof of concept). This option is not related to events, but in the next section we will compute for comparison purposes,
2. $r_E^{(k)}(i, j)$ linear correlation between a k -th source event in time series i and a respective target event in time series j . This option seems the most plausible when analyzing transient events, for instance localized tics on a motor disease.
3. $\bar{r}_E(i, j) = 1/K \sum_{k=1}^K r_E^{(k)}(i, j)$ average linear correlation between K source events in time series i and respective target events in time series j ,
4. $r_C(i, j)$ linear correlation between concatenated source events in time series i and concatenated respective target event in time series j ,
5. $r_E(i, j)$ linear correlation between an average source event in time series i and an average target event in time series j (computed in section III where we perform a proof of concept).

In this study, we will only use measures defined by 1 and 5. The other choices, 3, 4, are not discussed here, but it is worth considering them in future studies to obtain statistically less biased estimators of correlations.

2.3. Directionality

Given two regions of interest i and j , the linear Pearson correlation between their BOLD time series by definition is symmetric, i.e., $r_P(i, j) = r_P(j, i)$. It is not the case, if the



correlations are computed using events. Then, the distinction between source and target becomes relevant, as shown in **Figure 2A**. The shaded areas in the plots mark the positions of source events of each of the two relatively strongly correlated ROIs. Visibly, the first two events are common for both time series, but for instance the BOLD activations around $TR = 30$ and $TR = 40$ are source events for ROI 2 but not for ROI 1.

Consequently, the set of events over which one computes correlations when ROI 1 is considered the source is different from those observed when ROI 2 is considered the source, as it can be seen in **Figure 2B**. The four plots in **Figure 2B**, shows an example for two ROI's in which (in a matrix format) the sources

as columns and the targets as rows. The top left panels contain the source events of ROI 1 (and its average) and the top right one its target (ROI 2). Similarly, the bottom right panel shows the source events extracted from ROI 2 (and its average) and the left bottom one its target (ROI 1). So even though the BOLD series of both regions are highly correlated, the source and target events are different, and hence, the event correlation is not symmetric $r_E(i,j) \neq r_E(j,i)$.

The asymmetry in the correlations may indicate that on average, the co-activations between regions have a preferred direction. Being cautious about extrapolating these results to neuronal activation, we can estimate and assess a

global correlation asymmetry of the functional connectivity by computing

$$A = \sum_{i,j} (r_E(i,j) - r_E(j,i)), \quad (1)$$

for a given region, or similarly to determine the asymmetry of each ROI, or of each pair of time series i and j . In practice, we computed this metric subtracting the transposed mean correlation matrix from the non-transposed one (see **Supplementary Material 1**).

The directionality can be also computed, in the spirit of analysis of point processes (Tagliazucchi et al., 2012, 2016; Cifre et al., 2020), from the relative number of events occurring simultaneously in two regions. For instance, in **Figure 2**, there are two out of six source events in ROI 1 that are also triggers (i.e., above threshold) in ROI 2, and two out of five in ROI 2 that are also triggers in ROI 1. This approach takes into account event amplitudes, which to a large extent could be also achieved by computing covariance instead of the Pearson correlation between source and target events. Below, we call such ratio event directionality.

2.4. Delays

Several studies (Mitra et al., 2014, 2015a,b; Mitra and Raichle, 2016, 2018) have provided consistent evidence for the presence of very slow (>1 s) fluctuations in the fMRI BOLD signal propagating throughout the neocortex, thalamus, striatum, and cerebellum. More recently, these slow waves of activity were shown to be associated with spontaneous arousal fluctuations that, in turn, can account for the topographic organization of the brain functional connectivity (Raut et al., 2021). This information was gathered by the use of conventional lagged cross-covariance between pairs of BOLD time series $x_i(t)$ and $x_j(t)$ extracted from regions i and j :

$$C_{ij}(\tau) = \frac{1}{T} \sum_{t=1}^T x_i(t + \tau)x_j(t) \quad (2)$$

where τ is the lag (in units of TRs). The value of $\tau(i,j)$ at which $C_{ij}(\tau)$ exhibits an extremum defines the delay between signals x_i and x_j . To improve the resolution beyond multiple integers of TR, a parabolic interpolation of the cross-covariance extremum allows to determine the temporal lags with a finer resolution, as done in Mitra et al. (2014). Since by definition the time delay matrix $\tau(i,j)$ is anti-symmetric, i.e., $\tau(i,j) = -\tau(j,i)$, the information on the cross-covariance value and the lags can be used to determine the structure of the entire spatio-temporal processes.

Here, we propose a different approach to determine temporal delays. Instead of computing (Equation 2) of the entire BOLD time series, we make use of the fact that the BOLD-triggered events have a well-defined timing (see **Figure 3**). Given a source time series $x_i(t)$ and a target time series $x_j(t)$, we obtain a set of k_i source events. For each source event in $x_i(t)$, we find the closest peak in $x_j(t)$ irrespective of its size and whether it occurred before or after the source event. We search for the peak within a

window of $[-6, 8]$ TRs from the source threshold crossing. As shown in **Figure 3**, to obtain a finer timing of both the source and target peak we also use a parabolic fit. The lag $\tau(i,j)$ is then defined as the difference between the timing of the target and the peaks of the source parabola. As a technical side note, when getting a peak value at the left or right edge of the time window we do not perform the parabola peak estimation, which could have unbounded values, but we set the lag to -6 or 6 , respectively. If there is a particular interest, the same approach could be used to search for a negative peak (i.e., a de-activation) following a source event and estimate the activation de-activation delay between specific ROIs.

Since the sets of source (threshold crossing) events of $x_i(t)$ and $x_j(t)$ can be (and usually are) different, the matrix $\tau(i,j)$ is, in general, non-symmetric irrespective of the length of the time series. Additionally, for each i,j pair of ROIs we can obtain a set of delays for each individual source event k : $\tau^{(k)}(i,j)$, an average of these values $\bar{\tau}(i,j)$, or alternatively a delay between average events $\tau(i,j)$ (like the ones in **Figures 1D–F**).

3. RESULTS

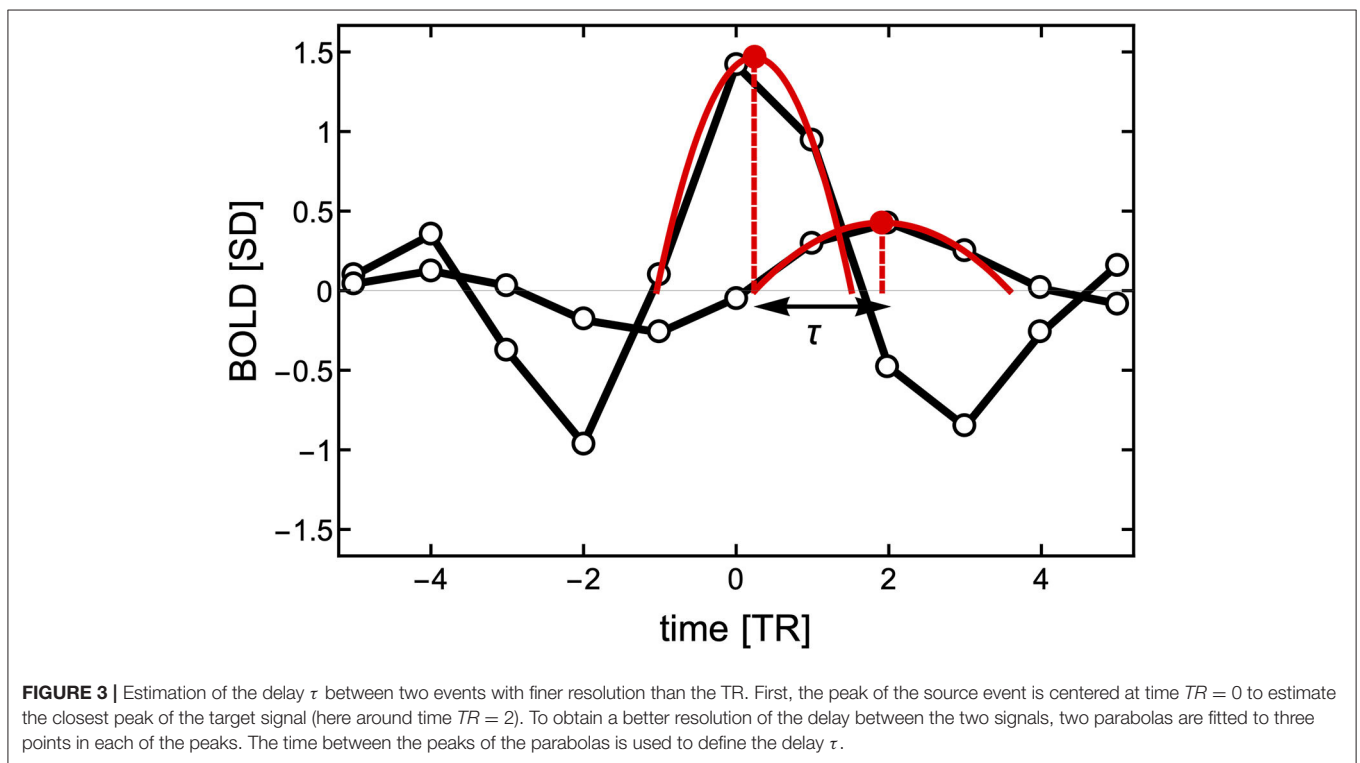
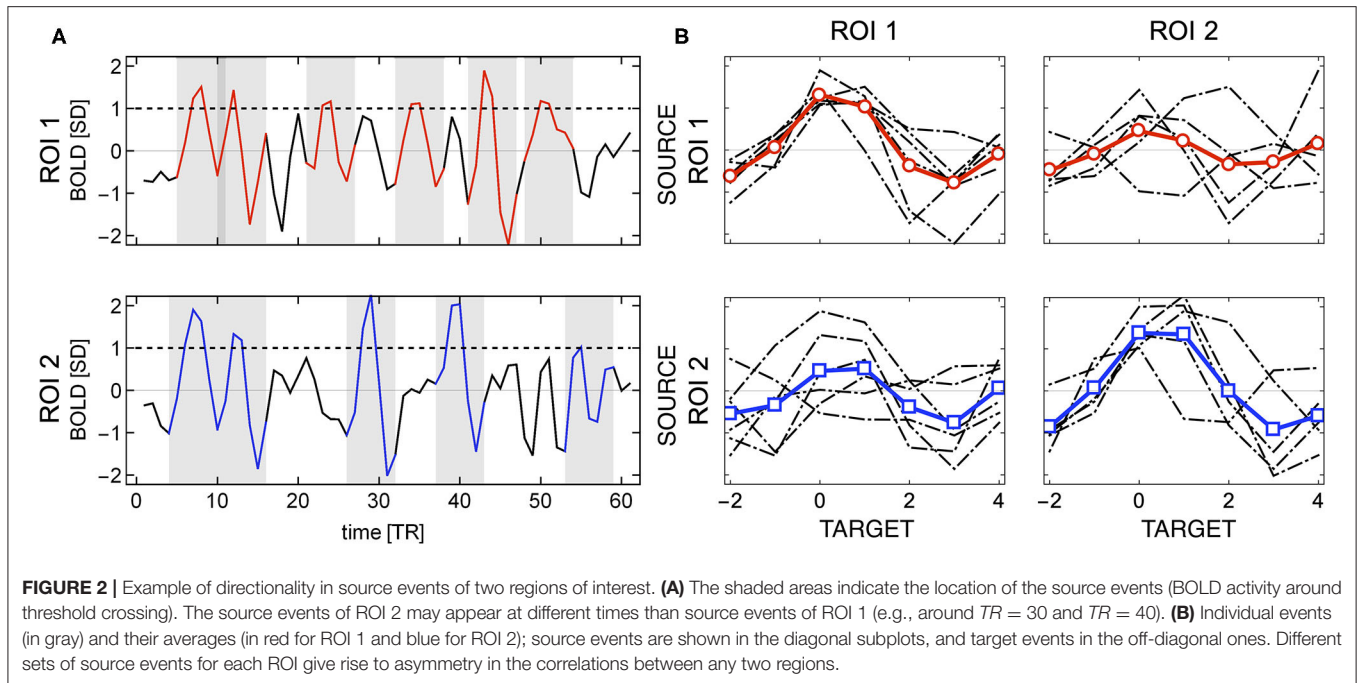
In this section, we will proceed to describe the performance of the method. It will be carried out on two settings: The first (section 3.1) corresponds to the analysis of BOLD time series from 90 ROIs defined by the automated anatomical labelling (AAL) parcellation (Tzourio-Mazoyer et al., 2002), and the second (section 3.2) describes a voxel-wise functional connectivity analysis using both the classical Pearson correlation and our methodology. From the outset, we note that the objective of these comparisons is not to re-interpret or scrutinize the study under replication, but only to illustrate the use and caveats of our method. The validation of our method needs to wait for the use of this approach by others in different settings. To facilitate those enquires, the code is available at the repository <https://github.com/remolek/NFC>.

3.1. Functional Connectivity, Delay, and Directionality Computed From AAL Parceled Time Series

Here, we will provide examples of typical results of the computations explained previously. To that aim, we will use fMRI BOLD data from 32 healthy participants downloaded from the Autism Brain Imaging Data Exchange (ABIDE) database (Craddock et al., 2013). Each dataset comprises 90 AAL preprocessed time series (using Data Processing Assistant for Resting-State fMRI (DPARSF) pipeline). In all cases, the time series are demeaned and normalized to their SD (i.e., z-scored),

Typical results from the computations using both, the standard FC approach and our method are presented in **Figure 4**. For each of the three measures and for both methods, the figure shows a matrix from single subject results, a mean matrix of the whole group and the distributions for each of the computations.

First, **Figure 4A** shows typical results obtained from Pearson's correlations between all the time series, and



note that the distribution exhibits the usual Gaussian shape. This is not the case for the distribution of event correlations (**Figure 4B**) that is expected for the sampling distribution of Pearson's estimator for a small length of time series. This feature is further discussed in **Supplementary Material 3**.

Figure 4C shows the matrix and the distribution of the edges' directionality computed as the proportion of shared events between regions (two leftmost panels) as explained in section 2.3. The alternative measure performed by subtracting the transposed matrix is shown in **Supplementary Material 3**.

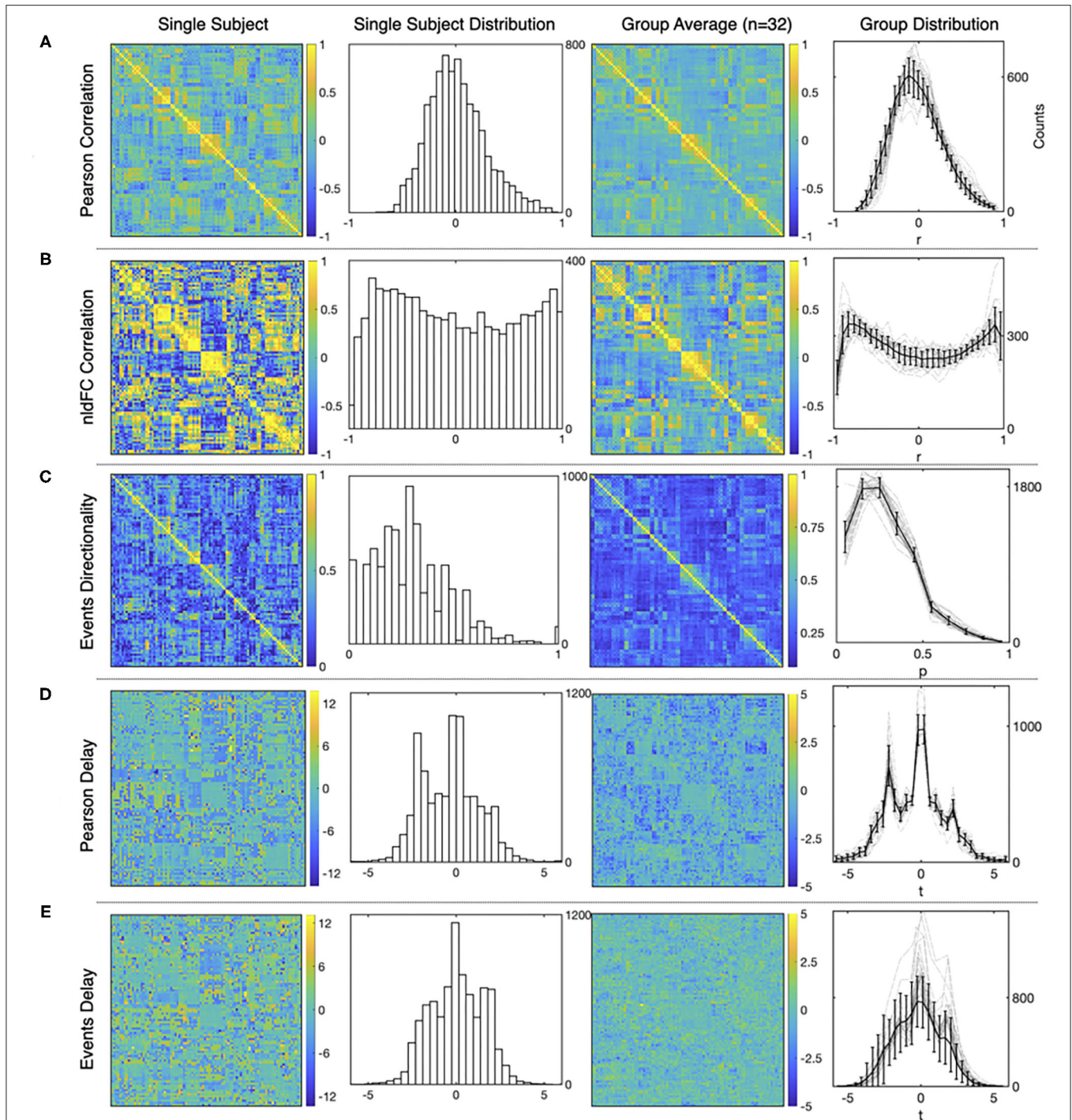
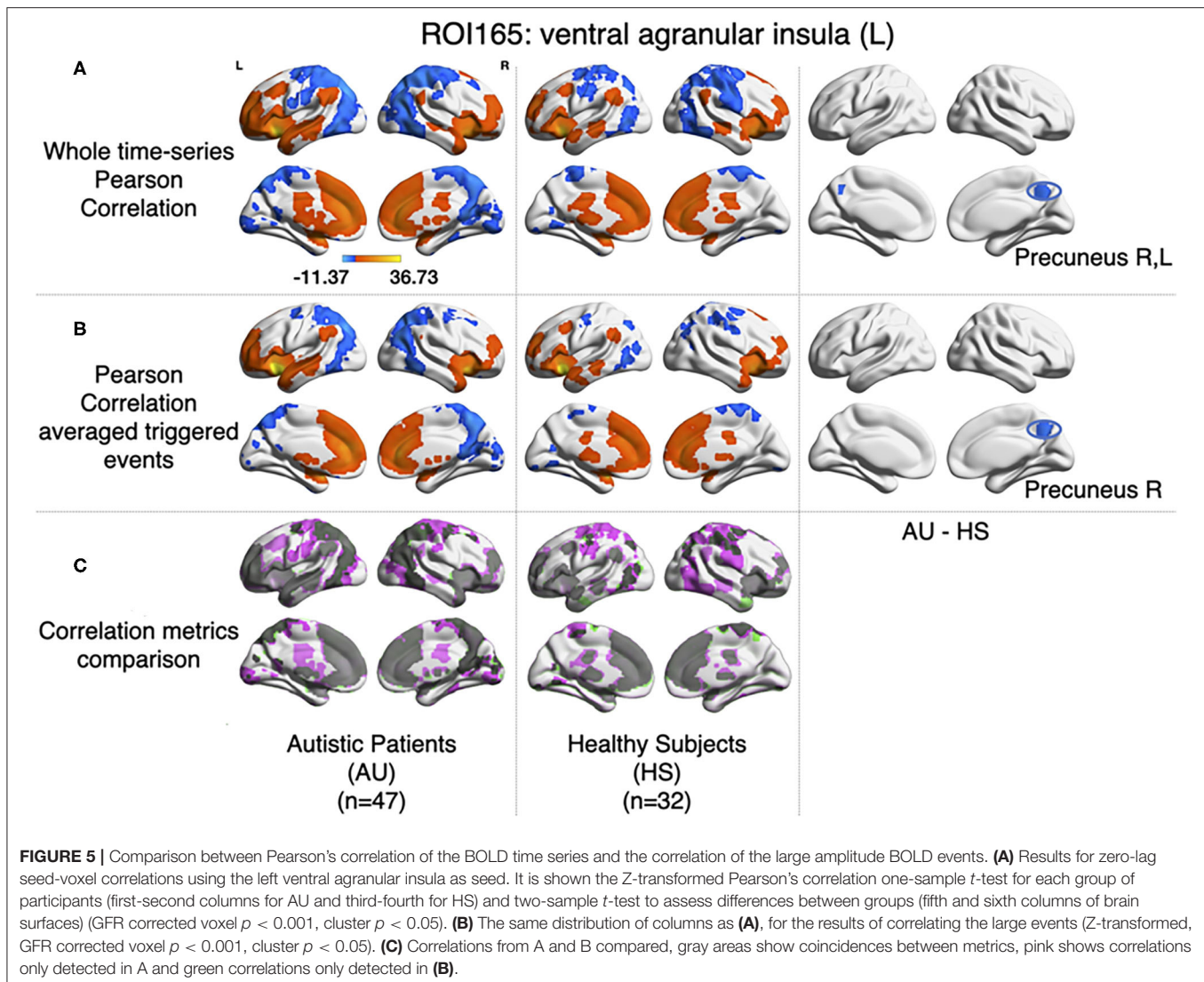


FIGURE 4 | Examples of the matrices and distributions for each calculation performed over a fMRI dataset of 90 time series from the AAL atlas Tzourio-Mazoyer et al. (2002). The first and the second columns corresponds to a single subject statistics, while the average results from a group of healthy subjects ($n = 32$) are shown in the third and the fourth column. **(A–E)** show results for Pearson functional correlations, event correlations, event asymmetry, Pearson's delay, and event delay, respectively. For each measure, the first and the third columns show results in a matrix format, while the second and the fourth columns show the distributions of each measure (mean values and S.D. error bars are used for the group distributions).

Delay between time series is shown in **Figure 4D**, for shifted time series as in Mitra and Raichle (2018) and **Figure 4E**, for delay computed using events. Note that for

Figure 4D, the apparent asymmetry is due to the TRs subtracted at the beginning and end of the signal, to allow the computation, while for **Figure 4E**, the event selection



between target and source, so it is not an artifact of the computation.

To further inspect the behavior of these metrics, we computed average path length and clustering coefficient of the networks given a certain threshold, and it can be seen in **Supplementary Material 2**.

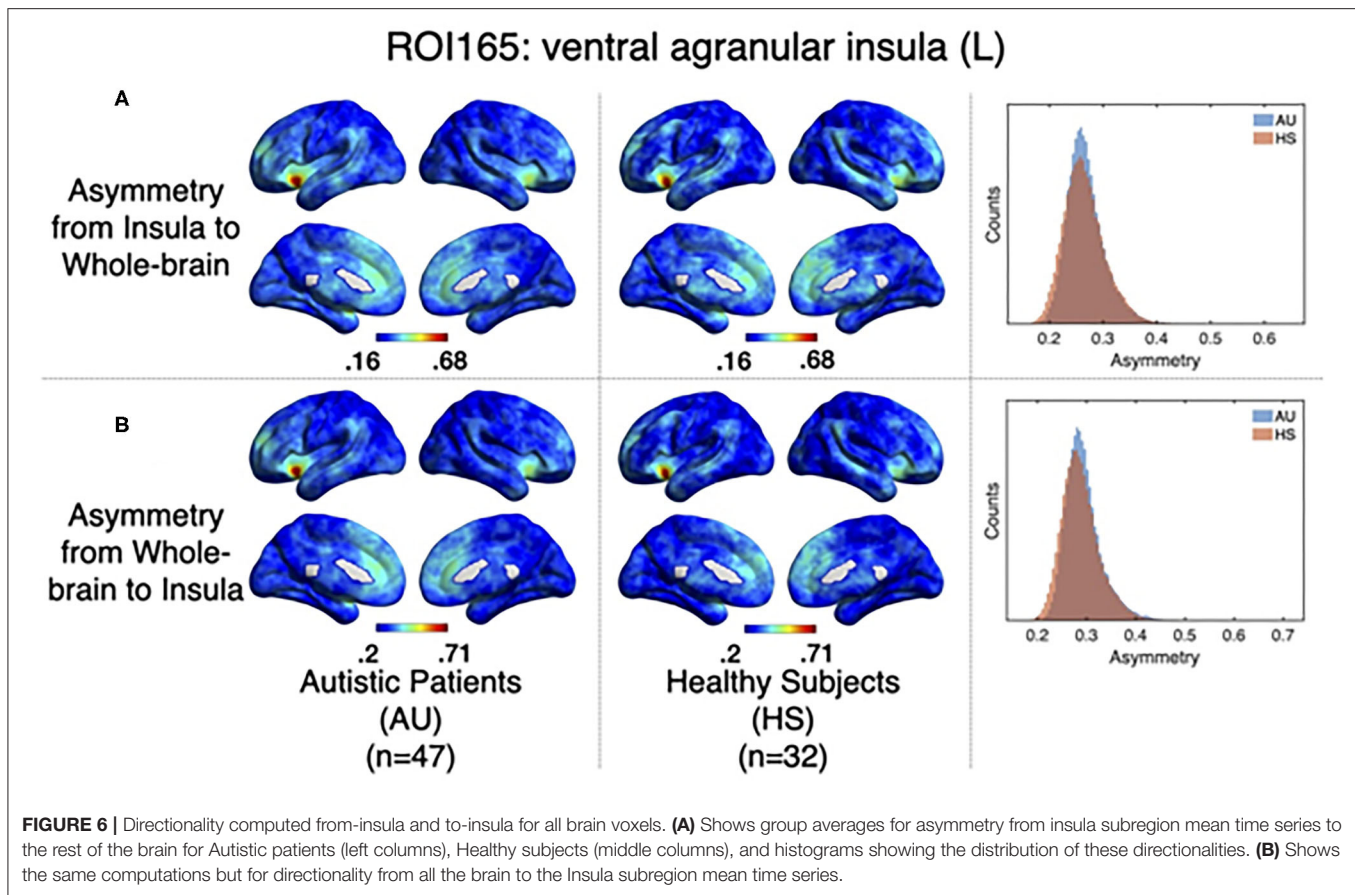
3.2. Replication of Voxel-Wise Functional Connectivity Findings

As a further test of the computations explained above, we have used fMRI data from the ABIDE preprocessed database (Craddock et al., 2013) to replicate recent findings on functional connectivity between insular sub regions on Autism Syndrome patients Xu et al. (2018). ABIDE is an open database with thousands of pre-processed fMRI brain scans of Autism Syndrome patients (AU) and age-matched Healthy subjects (HS) http://preprocessed-connectomes-project.org/abide/quality_assessment.html (Rolls et al., 2016; Zheng

et al., 2016; Dadi et al., 2019). For these computations, we collected a sample of 47 AU and 32 HS. The MRI data acquisition as the preprocessing pipeline used can be accessed here: <http://preprocessed-connectomes-project.org/abide/Pipelines.html>.

3.2.1. Pearson's Correlations

For each subject, the average BOLD time series from six insular subregions (using brainnetome functional atlas, Fan et al., 2016) as extracted and correlated using Pearson's correlation with all the rest of the voxels of the brain (gray matter masked) as in Xu et al. (2018). One-sample *t*-test was computed for each group of participants (AU and HS) to result in the correlation pattern of each insular subregion, obtaining comparable results as in Xu et al. (2018) (**Figure 1**). In this study, we are showing results from the left ventral agranular insula subregion as a proof of replication. As in Xu et al. (2018), HS resulted in higher correlation of this ROI with bilateral precuneus cortex (see **Figure 5**).



3.2.2. Nonlinear Functional Co-activations

Following the method explained in Tagliazucchi et al. (2011), relevant events from the mean time series of left ventral agranular insula subregion were extracted (triggering events where the amplitude is above a 1 S.D. threshold, 2 TR previous to this trigger, and 4 TR after). All time series from all the voxels in the brain (gray matter masking) corresponding to those events were extracted. Then, the correlations between the average source event of the insula and the average target event of each voxel were computed. As it can be observed in Figure 5B, similar results to Pearson's correlation of the whole signal were obtained (note that here we have only taken into account the signal from events, not the whole time series). The same cluster of higher correlation between insula and precuneus cortex in the HS group can be observed by computing a two-sample *t*-test (GFR corrected, p -voxel = 0.001, p -cluster = 0.05).

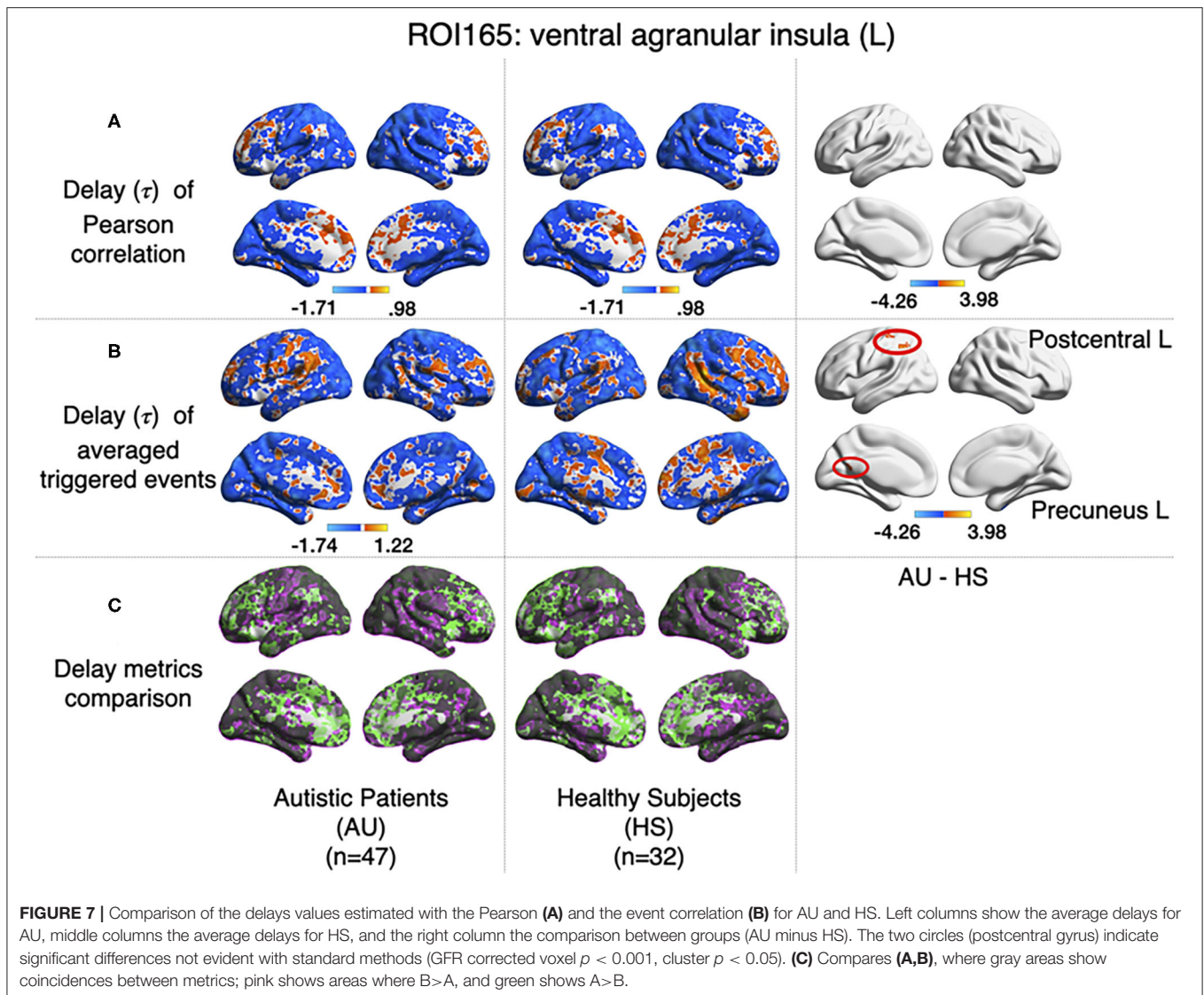
3.2.3. Directionality

As it has been explained above, the correlation value between two signals (i, j) obtained when computing relevant events is not symmetric. The correlation of the source events with its target $r(i, j)$ is not necessarily the same as the correlation of the events of that target, acting as a source, with the original source, acting as a target $r(j, i)$. The difference between this $r(i, j)$ and $r(j, i)$ can be understood in terms of directionality of the

correlations. To test whether the functional activity of the left ventral agranular insula exhibits such property, we computed directionality across the whole brain. Overall, we have observed only very small differences (see histograms in Figure 6) but they are no significant differences between groups in specific areas (Figure 6, GFR corrected all $p > 0.05$). This contrasted with the significant findings we found for the correlation and delay computations (Figures 5, 7). The density distributions shown in Figure 6 (right panels) indicate that in both, HS and AU subjects, the correlations are directed (asymmetric) and that the mode of the directionality is most frequent in the AU subjects (depicted in light blue) than in the HS ($p < 0.01$).

3.2.4. Delay

All previous computations correspond to correlations computed at equal time. In addition, it is straightforward to estimate the average delay between the peak of the source events to the peak of its closest target events. We computed this delay measure from the source events extracted from the left ventral agranular insula in respect to all the rest of the brain voxels. Comparing the delays between the groups, it can be seen that while the left postcentral gyrus and the precuneus cortex exhibit a positive delay in the AU group, the HS subjects show a negative delay (Figure 7). To illustrate these delay differences, Figure 8 shows examples of time



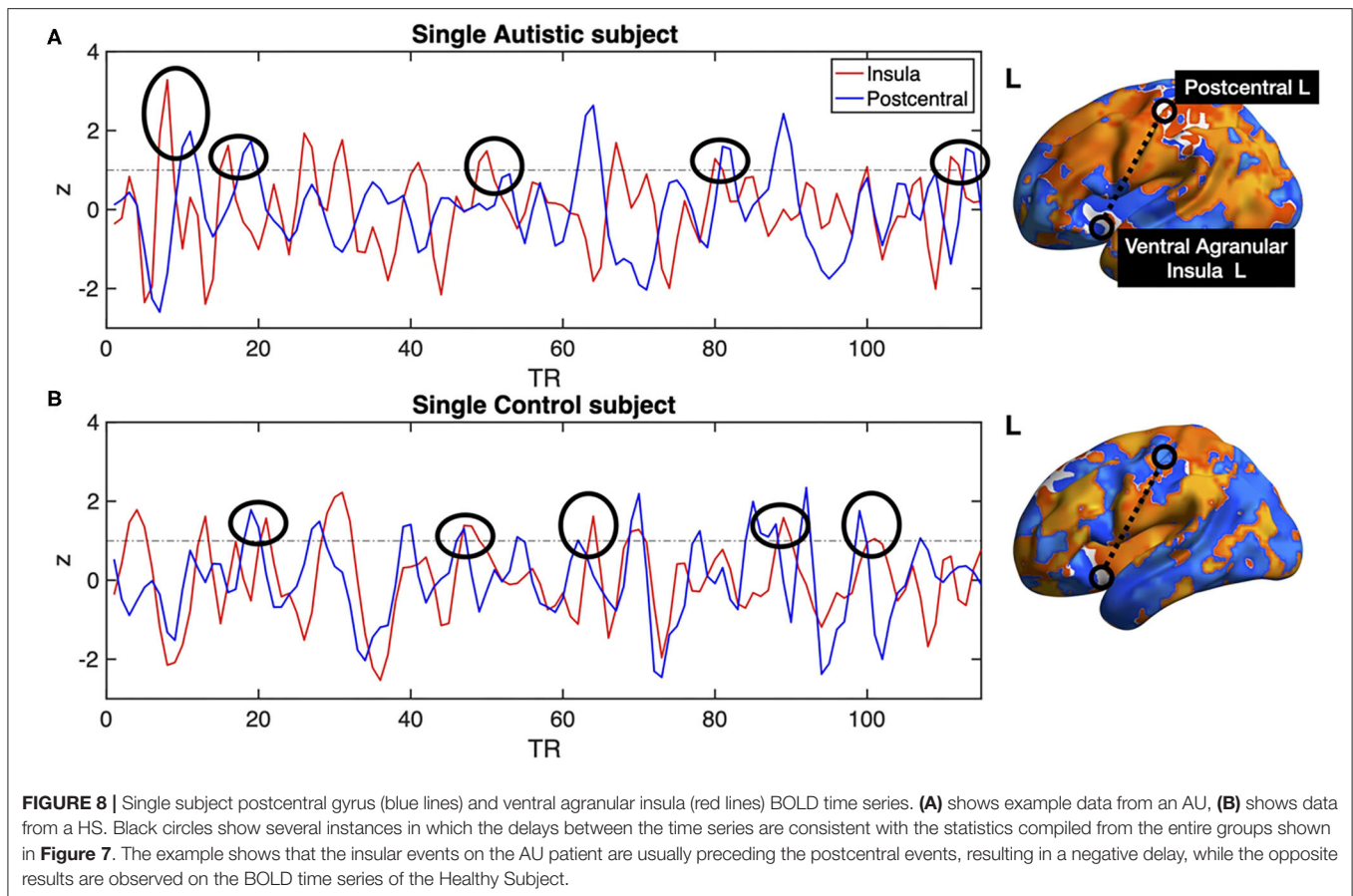
series of the postcentral gyrus and the ventral agranular insula for a single AU subject (**Figure 8A**) and an HS subject (**Figure 8B**).

4. DISCUSSION: FEATURES, ADVANTAGES, AND LIMITATIONS OF THE PROPOSED STRATEGY

Since its introduction, almost a decade ago, it has been suggested that the point process (or its variants) extracted from the large amplitude BOLD deflections contains enough dynamical information (Tagliazucchi et al., 2011, 2012), to identify the timing and the location of epochs of high correlations among brain regions. This identification has acquired relevance in the context of dynamical functional connectivity see, for instance, the reviews by (Keilholz et al., 2017) and (Iraji et al., 2020). In line with this, the recent report of Esfahlani et al. (2020) emphasizes the fact that few events of co-activation can estimate

the functional connectivity architecture of a system, a finding that is in full agreement with our original arguments. Thus, it is important to remark that behind all these reports there is a basic reason why these few points contain most of the information as discussed recently (Cifre et al., 2020).

Emphasizing the relevance of relatively high amplitude BOLD signal while compressing the data motivated the two paradigms we have proposed previously, namely, the point process (Tagliazucchi et al., 2012) and the so-called rBeta technique (Tagliazucchi et al., 2011). Both attempt to capture the spatio-temporal dynamics with the smallest possible sampling with a trade-off between temporal and spatial resolution. The point process compresses in the temporal domain, which implies that to smoothly represent spatio-temporal correlated patterns, one needs to sample more voxels. On the other hand, the rBeta approach uses much fewer voxels, but at the expense of keeping additional temporal information around each threshold crossing. These two variants have demonstrated two main advantages



comparing to the above-mentioned functional connectivity measures, the first one is that they imply a data size reduction and less computational resources to obtain comparable results to full time series analyses, and second, as these are only focusing on relevant high amplitude time-points, or events, non-significant events occurring during the scan are not blurring the computations.

It is important to remind that, in terms of neurophysiology, the observed changes in the BOLD signal can not be simply and exclusively attributed to change in neural responses (Aguirre et al., 1998; Noseworthy et al., 2003; Handwerker et al., 2004; Raut et al., 2021). The HRF variability has been pointed several times as a common confounder in the determination of functional connectivity using Pearson's correlation of the BOLD signals (Rangaprakash et al., 2018; Yan et al., 2018). It has been suggested the need to de-convolve the BOLD signal in order to obtain a confounder-free robust FC [as discussed in Wu et al. (2013) and more recently in Wang et al. (2020)].

In that regard, the present approach explicitly takes into account such variability because the source events extracted from any given ROI represents (by construction) the *local* HRF. This similarity was already noted in Tagliazucchi et al. (2012) by comparing the de-convolved BOLD signal using either a canonical HRF or the source event extracted by our approach (see Figure 1D in Tagliazucchi et al., 2012). The most

recent work of Urunuela et al. (2021) summarizes this point very well: “deconvolution approaches hold a close parallelism to recent methodologies aiming to understand the dynamics of neuronal activations and interactions at short temporal resolution and that focus on extreme events of the fMRI signal (Lindquist et al., 2007).” In that work, the authors provide a very persuasive evidence of such parallelism: “**Figure 6** shows that the innovation- or activity-inducing CAPs computed from deconvolved events in a single resting-state fMRI dataset closely resemble the conventional CAPs computed directly from extreme events of the fMRI signal (Tagliazucchi et al., 2011, 2012, 2016; Liu and Duyn, 2013; Liu et al., 2013, 2021; Cifre et al., 2020; Zhang et al., 2020; Rolls et al., 2021).”

The nonlinear dynamic functional connectivity method we are proposing offers an unexplored and widely different perspective in the analysis of brain co-activation patterns without much numerical complications, since it implies no more than thresholding and the computation of linear correlations, facilitating a simple interpretation of the resulting functional connectivity paths. The fact that the correlations are computed from events identified either as sources or targets allows for a straightforward definition of directed graphs (i.e., asymmetric correlation matrices). These source-target relations may lead to novel approaches to understand brain dynamics, for instance, as in the example of Autism Syndrome in which the computation

of delays between events showed uncovered distinct information. Indeed, the Pearson correlation, computed between left ventral agranular insula and postcentral gyrus, does not show any differences between AU and HS, while it has been reported that postcentral gyrus has a differential connectivity in Autistic Syndrome when analyzing big samples Gu et al. (2015). However, when we computed the delays from insula to other regions, differences between the two groups in Postcentral Gyrus appeared, which leads us to think that this differential connectivity may be expressed on a spatio-temporal domain. Another example is the additional difference we have found between the two groups concerning a weaker functional connectivity between precuneus cortex and ventral agranular insula, which is accompanied by the above-mentioned differences in delay (Figure 7B).

Note two practical advantages provided by the present approach. The results are highly reproducible on correlations asymmetry and delays, being robust to changes in the threshold used to extract the source events. The method is equally applicable to the analysis of fMRI data during a task, by extracting the source events from the task convolved with a HRF function. A similar approach can be used to study dynamic functional connectivity fluctuations possibly due to ongoing cognition, as suggested in Gonzalez-Castillo et al. (2014).

Further testing of the method should be performed to identify more specifically its limitations. For instance, we have not compared the method with results obtained from sliding-window Pearson's correlation, a widely used method to inspect dynamics in functional connectivity (Hutchison et al., 2013; Preti et al., 2017). In further work, we expect that will uncover a relation between this window-based functional connectivity and the information provided from the delays of our method. Another point that deserves to be clarified is the meaning of the peaks in the delay distribution, something already intriguing from previous results obtained using Pearson's correlation delays (see Figure 5 in Mitra et al., 2015a), which was recently related to very slow arousal fluctuations (Raut et al., 2021).

Finally, we shall mention that while here we concentrated on the activation events, i.e., denoted by the BOLD signal upward crossing of a threshold, the same method can be applied without modification to *de-activation* events. In such a way, graphs of regions of interest to are correlated with the deactivation of

regions can be obtained, something that we are not aware was considered before.

In conclusion, we have analyzed undisclosed properties of the previously published rBeta method (Tagliazucchi et al., 2011). Overall, these calculations provide a different kind of information than the usual Pearson correlation of the entire BOLD time series. As a proof of concept, we have used the method to replicate a recently published study of functional connectivity in Autism Syndrome, reproducing their main findings and uncovering additional features. Given that the proposed approach implementation is simple and robust, it is expected that future work can be dedicated to validate and extend the method to other settings and experimental paradigms.

DATA AVAILABILITY STATEMENT

Publicly available datasets were analyzed in this study. This data can be found here: <http://adni.loni.usc.edu/>.

AUTHOR CONTRIBUTIONS

IC, MTM, LP, JO, and DC: contributed on manuscript writing process. IC, LP, JO, and DC: contributed on reviewing the manuscript, results discussion, and data analysis. All authors contributed to the article and approved the submitted version.

FUNDING

This work was supported by the MICINN (Spain) grant PSI2017-82397-R, the National Science Centre (Poland) grant DEC-2015/17/D/ST2/03492 and the Foundation for Polish Science (FNP) project Bio-inspired Artificial Neural Networks grant POIR.04.04.00-00-14DE/18-00, and by CONICET (Argentina) and Escuela de Ciencia y Tecnología, UNSAM. Work conducted under the auspice of the Jagiellonian University-UNSAM Cooperation Agreement.

SUPPLEMENTARY MATERIAL

The Supplementary Material for this article can be found online at: <https://www.frontiersin.org/articles/10.3389/fnins.2021.700171/full#supplementary-material>

REFERENCES

- Aguirre, G. K., Zarahn, E., and D'Esposito, M. (1998). The variability of human, BOLD hemodynamic responses. *Neuroimage* 4, 360–369. doi: 10.1006/nimg.1998.0369
- Allan, T. W., Francis, S. T., Caballero-Gaudes, C., Morris, P. G., Liddle, E. B., Liddle, P. F., et al. (2015). Functional connectivity in MRI is driven by spontaneous BOLD eVENTS. *PLoS ONE* 10:e0124577. doi: 10.1371/journal.pone.0124577
- Amico, E., Gomez, F., Di Perri, C., Vanhauzenhuyse, A., Lesenfants, D., Boveroux, P., et al. (2014). Posterior cingulate cortex-related co-activation patterns: a resting state fMRI study in propofol-induced loss of consciousness. *PLoS ONE* 9:e100012. doi: 10.1371/journal.pone.0100012
- Chen, J. E., Chang, C., Greicius, M. D., and Glover, G. H. (2015). Introducing co-activation pattern metrics to quantify spontaneous brain network dynamics. *Neuroimage* 111, 476–488. doi: 10.1016/j.neuroimage.2015.01.057
- Cifre, I., Zarepour, M., Horovitz, S. G., Cannas, S., and D. R. Chialvo (2020). Further results on why a point process is effective for estimating correlation between brain regions. *Papers Phys.* 12, 120003. doi: 10.4279/pip.120003
- Craddock, C., Benhajali, Y., Chu, C., Chouinard, F., Evans, A., Jakab, A., et al. (2013). The neuro bureau preprocessing initiative: open sharing of preprocessed neuroimaging data and derivatives. *Front. Neuroinformatics* 7:41. doi: 10.3389/conf.fninf.2013.09.00041

- Dadi, K., Rahim, M., Abraham, A., Chyzyk, D., Milham, M., Thirion, B., et al. (2019). Benchmarking functional connectome-based predictive models for resting-state fMRI. *Neuroimage* 192, 115–134. doi: 10.1016/j.neuroimage.2019.02.062
- Eguíluz, V. M., Chialvo, D. R., Cecchi, G. A., Baliki, M., and Apkarian, A. V. (2005). Scale-Free Brain Functional Networks. *Phys. Rev. Lett.* 94, 018102. doi: 10.1103/PhysRevLett.94.018102
- Esfahlani, F.Z., Jo, Y., Faskowitz, J., Byrge, L., Kennedy, D. P., Sporns, O., Betzel, R. F. (2020). High amplitude co-fluctuations in cortical activity drive functional connectivity. *Proc. Natl. Acad. Sci. U.S.A.* 117, 28393–28401. doi: 10.1073/pnas.2005531117
- Fan, L., Chu, C., Li, H., Chen, L., Xie, S., Zhang, Y., et al. (2016). The Human brainnetome atlas: a new brain atlas based on connectonal architecture. *Cereb. Cortex* 26, 3508–3526. doi: 10.1093/cercor/bhw157
- Finn, E. S., Shen, X., Scheinost, D., Rosenberg, M. D., Huang, J., Chun, M. M., et al. (2015). Functional connectome fingerprinting: Identifying individuals using patterns of brain connectivity. *Nat. Neurosci.* 18, 1664–1671. doi: 10.1038/nn.4135
- Gonzalez-Castillo, J., Handwerker, D. A., Robinson, M. E., Hoy, C. W., Buchanan, L. C., Saad, Z. S., et al. (2014). The spatial structure of resting state connectivity stability on the scale of minutes. *Front. Neurosci.* 8:138. doi: 10.3389/fnins.2014.00138
- Gu, H., Zhang, J., Rolls, E. T., Feng, J., and Cheng, W. (2015). Autism: reduced connectivity between cortical areas involved in face expression, theory of mind, and the sense of self. *Brain* 138, 1382–1393. doi: 10.1093/brain/awv051
- Handwerker, D. A., Ollinger, J. M., and D'Esposito, M. (2004). Variation of BOLD hemodynamic responses across subjects and brain regions and their effects on statistical analyses. *NeuroImage* 4, 1639–1651. doi: 10.1016/j.neuroimage.2003.11.029
- Hutchison, R. M., Womelsdorf, T., Allen, E. A., Bandettini, P. A., Calhoun, V. D., Corbetta, M., et al. (2013). Dynamic functional connectivity: Promise, issues, and interpretations. *NeuroImage* 80, 360–378. doi: 10.1016/j.neuroimage.2013.05.079
- Iraji, A., Faghiri, A., Lewis, N., Fu, Z., Rachakonda, S., and Calhoun, V. D. (2020). Tools of the trade: estimating time-varying connectivity patterns from fMRI data. *PsyArXiv*.
- Jiang, X., Lv, J., Zhu, D., Zhang, T., Hu, X., Guo, L., et al. (2014). “Integrating group-wise functional brain activities via point processes,” in *2014 IEEE 11th International Symposium on Biomedical Imaging (ISBI)* (Beijing: IEEE), 669–672.
- Keilholz, S., Caballero-Gaudes, C., Bandettini, P., Deco, G., and Calhoun, V. (2017). Time-resolved resting-state functional magnetic resonance imaging analysis: current status, challenges, and new directions. *Brain Connect.* 7, 465. doi: 10.1089/brain.2017.0543
- Li, W., Li, Y., Hu, C., Chen, X., and Dai, H. (2014). Point process analysis in brain networks of patients with diabetes. *Neurocomputing* 145, 182–189. doi: 10.1016/j.neucom.2014.05.045
- Lindquist, M. A., Waugh, C., Wager, T. D. (2007). Modeling state-related fMRI activity using change-point theory. *NeuroImage* 35, 1125–1141. doi: 10.1016/j.neuroimage.2007.01.004
- Liu, X., Chang, C., and Duyn, J. H. (2013). Decomposition of spontaneous brain activity into distinct fMRI co-activation patterns. *Front. Syst. Neurosci.* 7:101. doi: 10.3389/fnsys.2013.00101
- Liu, X., and Duyn, J. H. (2013). Time-varying functional network information extracted from brief instances of spontaneous brain activity. *Proc. Natl. Acad. Sci. U.S.A.* 110, 4392–4397. doi: 10.1073/pnas.1216856110
- Liu, X., Zhang, N., Chang, C., and Duyn, J. H. (2021). Co-activation patterns in resting-state fMRI signals. *Hum. Brain Mapp.* 42, 2790–2801. doi: 10.1016/j.neuroimage.2018.01.041
- Mitra, A., and Raichle, M. E. (2016). How networks communicate: propagation patterns in spontaneous brain activity. *Philos. Trans. R. Soc. B Biol. Sci.* 371, 20150546. doi: 10.1098/rstb.2015.0546
- Mitra, A., and Raichle, M. E. (2018). Principles of cross-network communication in human resting state fMRI. *Scand. J. Psychol.* 59, 83–90. doi: 10.1111/sjop.12422
- Mitra, A., Snyder, A. Z., Blazey, T., and Raichle, M. E. (2015a). Lag threads organize the brain's intrinsic activity. *Proc. Natl. Acad. Sci. U.S.A.* 112, E2235–E2244. doi: 10.1073/PNAS.1503960112
- Mitra, A., Snyder, A. Z., Constantino, J. N., and Raichle, M. E. (2015b). The lag structure of intrinsic activity is focally altered in high functioning adults with autism. *Cereb. Cortex* 27, 1083–1093. doi: 10.1093/cercor/bhv294
- Mitra, A., Snyder, A. Z., Hacker, C. D., and Raichle, M. E. (2014). Lag structure in resting-state fMRI. *J. Neurophysiol.* 111, 2374–2391. doi: 10.1152/jn.00804.2013
- Noseworthy, M. D., Alfonsi, J., and Bells, S. (2003). Attenuation of brain BOLD response following lipid ingestion. *Hum. Brain Mapp.* 2, 116–121. doi: 10.1002/hbm.10131
- Ochab, J. K., Tarnowski, W., Nowak, M. A., and Chialvo, D. R. (2019). On the pros and cons of using temporal derivatives to assess brain functional connectivity. *NeuroImage* 184, 577–585. doi: 10.1016/j.neuroimage.2018.09.063
- Petridou, N., Gaudes, C. C., Dryden, I. L., Francis, S. T., and Gowland, P. A. (2013). Periods of rest in fMRI contain individual spontaneous events which are related to slowly fluctuating spontaneous activity. *Hum. Brain Mapp.* 34, 1319–1329. doi: 10.1002/hbm.21513
- Preti, M. G., Bolton, T. A., and Van De Ville, D. (2017). The dynamic functional connectome: State-of-the-art and perspectives. *NeuroImage* 160, 41–54. doi: 10.1016/j.neuroimage.2016.12.061
- Rangaprakash, D., Wu, G. R., Marinazzo, D., Hu, X., and Deshpande, G. (2018). Hemodynamic response function (HRF) variability confounds resting-state fMRI functional connectivity. *Magn. Reson. Med.* 4, 1697–1713. doi: 10.1002/mrm.27146
- Raut, R. V., Snyder, A. Z., Mitra, A., Yellin, D., Fujii, N., Malach, R., et al. (2021). Global waves synchronize the brain's functional systems with fluctuating arousal. *Sci. Adv.* 30:eabf2709. doi: 10.1126/sciadv.abf2709
- Rolls, E. T., Cheng, W., and Feng, J. (2021). Brain dynamics: synchronous peaks, functional connectivity, and its temporal variability. *Hum. Brain Mapp.* 42, 2790–2801. doi: 10.1002/hbm.25404
- Rolls, E. T., Zhang, J., Feng, J., Wan, L., Cheng, W., Luo, Q., et al. (2016). Functional connectivity decreases in autism in emotion, self, and face circuits identified by Knowledge-based enrichment analysis. *NeuroImage* 148, 169–178. doi: 10.1016/j.neuroimage.2016.12.068
- Tagliazucchi, E., Balenzuela, P., Fraiman, D., and Chialvo, D. R. (2012). Criticality in large-scale brain fMRI dynamics unveiled by a novel point process analysis. *Front. Physiol.* 3:15. doi: 10.3389/fphys.2012.00015
- Tagliazucchi, E., Balenzuela, P., Fraiman, D., Montoya, P., and Chialvo, D. R. (2011). Spontaneous BOLD event triggered averages for estimating functional connectivity at resting state. *Neurosci. Lett.* 488, 158–163. doi: 10.1016/j.neulet.2010.11.020
- Tagliazucchi, E., Siniatchkin, M., Laufs, H., and Chialvo, D. R. (2016). The voxel-wise functional connectome can be efficiently derived from co-activations in a sparse spatio-temporal point-process. *Front. Neurosci.* 10:381. doi: 10.3389/fnins.2016.00381
- Tzourio-Mazoyer, N., Landeau, B., Papathanassiou, D., Crivello, F., Etard, O., Delcroix, N., et al. (2002). Automated anatomical labeling of activations in spm using a macroscopic anatomical parcellation of the MNI MRI single-subject brain. *NeuroImage* 15, 273–289. doi: 10.1006/NIMG.2001.0978
- Uruñuela, E., Bolton, T. A. W., Van De Ville, D., and Caballero-Gaudes, C. (2021). Hemodynamic deconvolution demystified: sparsity-driven regularization at work. *arXiv*
- van den Heuvel, M. P., and Hulshoff P., H. E. (2010). Exploring the brain network: a review on resting-state fMRI functional connectivity. *Eur. Neuropsychopharmacol.* 20, 519–534. doi: 10.1016/j.euroneuro.2010.03.008
- Wang, T., Wilkes, D. M., Li, M., Wu, X., Gore, J. C., and Ding, Z. (2020). Hemodynamic response function in brain white matter in a resting state. *Cereb. Cortex Commun.* 1, 1–13. doi: 10.1093/texcom/tgaa056
- Wu, G.-R., Liao, W., Stramaglia, S., Ding, J.-R., Chen, H., and Marinazzo, D. (2013). A blind deconvolution approach to recover effective connectivity brain networks from resting state fMRI data. *Med. Image Anal.* 17, 365–374. doi: 10.1016/J.MEDIA.2013.01.003
- Xu, J., Wang, H., Zhang, L., Xu, Z., Li, T., Zhou, Z., et al. (2018). Both hypo-connectivity and hyper-connectivity of the insular subregions associated with severity in children with autism spectrum disorders. *Front. Neurosci.* 12:234. doi: 10.3389/fnins.2018.00234

- Yan, W., Rangaprakash, D., and Deshpande, G. (2018). Aberrant hemodynamic responses in autism: implications for resting state fMRI functional connectivity studies. *Neuroimage Clin.* 19, 320–330. doi: 10.1016/j.nicl.2018.04.013
- Zhang, X., Pan, W. J., and Keilholz, S. D. (2020). The relationship between bold and neural activity arises from temporally sparse events. *Neuroimage* 207:116390. doi: 10.1016/j.neuroimage.2019.116390
- Zheng, F., Xie, Y., Chen, X., Yao, Z., Zheng, W., Liu, G., et al. (2016). Resting-state time-varying analysis reveals aberrant variations of functional connectivity in autism. *Front. Hum. Neurosci.* 10:463. doi: 10.3389/fnhum.2016.00463

Conflict of Interest: The authors declare that the research was conducted in the absence of any commercial or financial relationships that could be construed as a potential conflict of interest.

Publisher's Note: All claims expressed in this article are solely those of the authors and do not necessarily represent those of their affiliated organizations, or those of the publisher, the editors and the reviewers. Any product that may be evaluated in this article, or claim that may be made by its manufacturer, is not guaranteed or endorsed by the publisher.

Copyright © 2021 Cifre, Miller Flores, Penalba, Ochoa and Chialvo. This is an open-access article distributed under the terms of the Creative Commons Attribution License (CC BY). The use, distribution or reproduction in other forums is permitted, provided the original author(s) and the copyright owner(s) are credited and that the original publication in this journal is cited, in accordance with accepted academic practice. No use, distribution or reproduction is permitted which does not comply with these terms.

- 3. Study 2. Increased Functional connectivity patterns in mild Alzheimer's Disease:
A rsfMRI study (*Accepted*)**

Increased Functional connectivity patterns in mild Alzheimer's Disease: A rsfMRI study

Lucía Penalba^{1,2,3*}, Patrícia-Oliveira Silva², Alexander Sumich³, Ignacio Cifre¹

¹ Facultat de Psicologia, Ciències de l'educació i de l'Esport, Blanquerna, Universitat Ramon Llull, Barcelona, Spain

² Human Neurobehavioral Laboratory (HNL), Research Centre for Human Development (CEDH), Faculdade de Educação e Psicologia, Universidade Católica Portuguesa, Porto, Portugal;

³ NTU Psychology, School of Social Sciences, Nottingham Trent University

* Correspondence:

Corresponding Author

luciaps@blanquerna.url.edu

Keywords: Alzheimer's disease, Mild Cognitive Impairment, Functional connectivity, dynamic functional connectivity, point process analysis, resting state fMRI

ABSTRACT

Background: Alzheimer's disease (AD) is the most common age-related neurodegenerative disorder. In view of our rapidly aging population, there is an urgent need to identify Alzheimer's Disease (AD) at an early stage. A potential way to do so is by assessing the functional connectivity (FC), i.e., the statistical dependency between two or more brain regions, through novel analysis techniques. *Methods:* In the present study, we assessed the static and dynamic FC using different approaches. A resting state (rs)fMRI dataset from the Alzheimer's disease neuroimaging initiative (ADNI) was used (n= 128). The blood oxygen level dependent (BOLD) signals of 116 regions of 4 groups of participants, i.e., healthy controls (HC) (n=35), early mild cognitive impairment (EMCI) (n= 29), late mild cognitive impairment (LMCI) (n= 30) and Alzheimer's disease (AD) (n= 34) were extracted and analyzed. FC and dynamic FC were extracted using Pearson's correlation, sliding-windows correlation analysis (SWA) and the Point Process analysis (PPA). Additionally, graph theory measures to explore network segregation and integration were computed. *Results:* Our results showed a longer characteristic path length and a decreased degree in EMCI in comparison to the other groups. Additionally, an increased FC in several regions in LMCI and AD in contrast to HC and EMCI was detected. These results suggest a maladaptive short-term mechanism to maintain cognition. *Conclusion:* The increased pattern of FC in several regions in LMCI and AD is observable in all the analysis, however, the PPA enabled us to reduce the computational demands and offered new specific dynamic FC findings.

1. INTRODUCTION

Alzheimer's disease (AD) is the most prevalent progressive neurodegenerative disease associated with age. It typically starts with a preclinical stage and progresses through mild cognitive impairment (MCI) to clinically relevant AD (i.e., dementia type AD). Although great effort has been made to identify AD biomarkers, AD remains a clinical diagnosis. Early and accurate prediction of the disease remains limited. To address the increasing burden of AD, the dynamic brain changes associated with shifts in cognitive function that underpin what causes dementia must be understood. Abnormal brain connectivity has been observed 20 years prior to the onset of brain atrophy and clinically relevant symptoms of AD (Ashraf et al., 2015; Nakamura et al., 2017). Thus, relative risk of development of

Increased Functional Connectivity in Alzheimer's

MCI and dementia might be determined based on resting state functional connectivity (FC). It is therefore critical to thoroughly understand aberrant FC at each stage of the disease in order to improve strategies for early intervention.

Resting state functional magnetic resonance imaging (rsfMRI) data, acquired while the participants are awake without performing any task, can be used to assess intrinsic brain functional connectivity. By means of this high spatial resolution neuroimaging technique, the Blood Oxygen Level Dependent (BOLD) signal across brain regions is quantified (Yamasaki et al., 2012; Sporns, 2013; Liu et al., 2015; Xue et al., 2019;). Some investigators have analysed the BOLD signals using graph analytical methods to explore the network's topological features of patients with AD (Toussaint et al., 2014; Jie et al., 2016; Bhuvaneshwari and Kavitha, 2017; Xu et al., 2020). For instance, the characteristic path length supposedly reflects functional integration of brain networks. Hence, a shorter path length indicates efficient communication between regions. On the other hand, the clustering or modular coefficients provides information regarding the segregation of the networks, i.e., degree of specialization of brain regions. Seminal research revealed a decreased path length and clustering coefficients in AD in comparison to healthy patients (Supekar et al., 2008; Krienen and Buckner, 2009). Other studies reported a decrease in clustering degree and modularity in AD (Brier *et al.*, 2014) and MCI (Seo *et al.*, 2013) but a similar characteristic path length relative to individuals without MCI or AD.

FC and dynamic functional connectivity (dFC) are measures of signal synchronicity that allow researchers to analyse the gradual and continuous changes of the BOLD signal, which are represented by signal correlations of the whole signal or selected windows, respectively (for a detailed technical description see: (Chen et al., 2017; Keilholz et al., 2017a; Scarapicchia et al., 2018; Zhang et al., 2020). Three meta-analyses (Li et al., 2015; Jacobs et al., 2013; Badhwar et al., 2017) and another study (Kim *et al.*, 2016) using FC revealed a decrease in default mode network (DMN) connectivity in AD, mostly involving the precuneus (PCu) and the posterior cingulate cortex (PCC). These areas are implicated in episodic memory and attentional processing and are typically affected in AD (Jacobs *et al.*, 2013). In MCI, results are less consistent. Some studies have found an increase in FC in the mentioned regions, while others have found the opposite. Additionally, increased limbic connectivity has been seen in MCI (Badhwar et al., 2017) and increased connectivity of the salience network (SAL) has been observed in both MCI and AD (J. Wang et al., 2013; Thomas et al., 2014). Such inconsistent findings in FC may reflect the heterogeneity of MCI subtypes, which might be differentiated, for example, by symptoms and extent of illness progression (Badhwar *et al.*, 2017).

Additionally, seminal researchers have been discussing that an increase in functional connectivity between brain regions in MCI and early stages of AD has been seen to take place when the communication between specific brain regions is impaired. This has been interpreted as reflecting recruitment of alternative paths within the system. (Hillary and Grafman, 2017; Marek and Dosenbach, 2018), (Oldham and Fornito, 2019). The DMN, SAL and frontoparietal network (FPN) are networks that have been reported to become hyperconnected at some stage during disease progression. These multimodal networks connect several regions and integrate information processing, providing high-value at a high-cost (Hillary and Grafman, 2017; Marek and Dosenbach, 2018). An increase in FC between alternative paths is efficient and adaptive in the short term. However, rich hubs are a perfect place for beta-amyloid deposition, which can lead to secondary damage caused by metabolic stress and eventual breakdown of the system (Hillary and Grafman, 2017). Thus, hyperconnectivity that takes place at the beginning of many neurodegenerative diseases may be followed by hypoconnectivity between these recruited paths and cognitive decline, as the illness progresses (Marek and Dosenbach, 2018).

Increased Functional Connectivity in Alzheimer's

A further source of inconsistent FC findings in MCI and AD may be the use of different methods and parameters. For instance, preprocessing steps, parcellation methods, window size used, p values, number of samples or inclusion and exclusion criteria (Tam et al., 2015; Badhwar et al., 2017). With regards to samples, studies that used exploration methods (e.g., correlation, clustering algorithms, or matrix decomposition) and other statistical methods (e.g., t -test, ANOVA, Bayesian inference) typically do not compare across the finer stages of illness (e.g., HC, EMCI, LMCI and AD), although some machine learning studies have done so. There have, however, been comparisons of HC, MCI, and AD (Zhang *et al.*, 2020); HC, EMCI and LMCI (Cai et al., 2015; Lee et al., 2016); HC with AD (Zheng *et al.*, 2017), HC with EMCI (Zamani et al., 2021), HC with amnesic MCI (L. Wang et al., 2013; Jie et al., 2016); HC with amnesic vs non amnesic MCI. Nevertheless, the precise trajectory for FC from HC to AD remains unclear.

One of the limitations of traditional FC approaches is the high demand on computational processing and sensitivity to residual noise. As the BOLD signal usually presents the same stereotypical pattern, larger amplitude BOLD signal peaks likely provide the most critical information, i.e., neural events (Aguirre et al., 1998; Cifre et al., 2020;). Several studies suggest that patients with neurological and psychiatric diseases present greater variability in the BOLD signal over the scan session (Keilholz et al., 2017). Hence, these peaks might be highly useful in these cases as they might reveal key intrinsic brain connectivity that can only be detected when assessing the amplitude of the signals (Keilholz et al., 2017). In fact, a higher recognition accuracy between healthy participants and patients with autism has already been detected in our previous work (Cifre et al., 2021) using a Point Process Analysis (PPA), a method that captures these relevant events. Other researchers obtained similar results, thereby successfully differentiating across groups, when applying the PPA to patients with diabetes (Li *et al.*, 2014).

Using the PPA method, local peaks of the BOLD time series are selected to generate a co-activation matrix that defines the co-occurrence of points. Apart from reducing noise, the bursts of correlated activity between regions are not required when using the PPA. This phenomenon occurs because the assumption behind this method is that those events with a higher amplitude, i.e., peaks, contain avalanches of neural information that are the consequence of intrinsic activity between communities of neurons (Cifre et al., 2021). Previous work exploring the BOLD activation showed similar results when using a seed-based approach and a PPA, i.e., the activation maps when using a seed-based approach, selecting all the time points (between 140 to 240) in comparison to when using a PPA, selecting just those time points that surpass 1 SD of the BOLD signal, (between 4 and 8 points) were similar. Additionally, when exploring the changes in brain integration or connectivity, the PPA is more sensitive to capturing changes across groups (Tagliazucchi et al., 2011; Tagliazucchi et al., 2012; Hutchison et al., 2013; Cifre et al., 2020; Cifre et al., 2021). To our knowledge, PPA has never been applied to rsfMRI datasets of patients with AD and MCI. This method might offer an efficient way to manage big data sets and to better understand the changes in the FC dynamics across the different stages of the disease.

The main goal of this present study was to explore FC and dFC across groups. A PPA was applied to a dataset of patients with AD, LMCI, EMCI and age and sex-matched healthy individuals (HC). Additionally, to compare findings with other classical methods, pairwise correlations of the whole BOLD signal, graph theory measures and a SWA were applied. In line with previous literature, it was expected to find [1] differences across the four groups in FC and variability within and between the DMN, SAL, visual networks (VS) and CEN; [2] an increased FC in EMCI and LMCI and a slightly decreased FC in AD in several networks in contrast to the other groups and [3] more subtle differences across groups when using the PPA in comparison to the other methods.

2. MATERIALS AND METHODS

Participants:

All rsfMRI, T1 MRI and demographic data from participants were downloaded from the Alzheimer's Disease Neuroimaging Initiative (ADNI) (<http://adni.loni.usc.edu/>) (Franzmeier *et al.*, 2017). 36 HC age and sex matched, 29 with EMCI, 30 with LMCI group, and 34 with AD. All the images correspond to the screening visit, which are coded in ADNI2 as Screening MRI-New Pt (V02). Between groups, there were no differences in age, sex, and years of education. Patients with AD presented significantly lower scores in the screening assessment cognitive test Mini Mental State Examination (MMSE) in comparison with the three other groups. Expectedly, there were no differences between groups in episodic memory measured by the Scale Logical Memory II (delayed paragraph A recall) from the Wechsler Memory Scale) cognitive tests (see **Table 1**). A participant from the HC group was eliminated before the analysis because some time series were missing. Further inclusion and exclusion criteria is exposed in detail in the "ADNI 2 Procedures manual" (pages 27-30); access is available through this link: (<http://adni.loni.usc.edu/wp-content/uploads/2008/07/adni2-procedures-manual.pdf>). Data access was approved by contacting the ADNI Ethics Committee (<http://adni.loni.usc.edu/data-samples/access-data/>) and sending a request with a proposed analysis and the name of the principal investigators.

Data acquisition:

T1 and fMRI images were acquired using Philips Medical Systems Scanners and underwent control at Mayo Clinic. The fMRI images were obtained with a field strength of 3.0 tesla, with a repetition time of 3s, an echo time of 30ms, a flip angle of 80 degrees, matrix 64 x 64, 140 volumes, 48 slices per volume and a slice thickness of 3.3 mm. The voxel size was 3.3 x 3.3 x 3.3 mm³. For further details on MRI acquisitions see the "MRI scanner protocol" at (http://adni.loni.usc.edu/wp-content/uploads/2010/05/ADNI2_MRI_Training_Manual_FINAL.pdf).

Data preprocessing

The MATLAB toolbox "Data Processing Assistant for Resting-State fMRI" (DPARSF) (Yan and Zang, 2010) was used to preprocess the data. First, slice timing and head motion correction were applied. No subjects with a mean movement on translation or rotation over 2 mm were found. Then, registration was performed to the corrected fMRI image. Last, normalization using the Montreal Neurological Institute (MNI) space, spatial smoothing (with an 8 mm full-width half maximum Gaussian Kernel) and bandpass filtering (0.001-0.1Hz) to remove low-frequency scanner drift and physiological noise of the fMRI images were applied.

The automated anatomical labelling (AAL) atlas (Tzourio-Mazoyer *et al.*, 2002) was used to extract 116 Regions-Of-Interest (ROIs) of the preprocessed rsfMRI dataset. This parcellation method has been shown to be optimal to understand the FC between brain regions (Arslan *et al.*, 2018). The voxels within each ROI were averaged to obtain a time series per ROI. Each time series contains 140 timepoints (3seconds TR, i.e., 420 seconds in total).

All the analysis described in the following subsections (see **Figure 1**) were performed using MATLAB ver. R2018a.

Increased Functional Connectivity in Alzheimer's

Static FC analysis with Pearson's correlation:

The Pearson's correlation coefficient (PCC) between entire timeseries was computed to extract the FC in a pairwise manner (ROI to ROI correlation) per participant. Hence, correlation matrices of 116 x 116 (ROI * ROI) were obtained per each subject. Then, a one-way analysis of variance (ANOVA) and post hoc comparisons were conducted to explore differences between groups. Those regions that presented differences in FC across groups were checked for outliers; more specifically, whether the FC was three scaled median absolute deviations (MAD) away from the median, for each participant in each group was explored. Then the FC was computed again after removing these participants.

Graph theory measures:

To explore some characteristics of the brain networks, such as the integration and segregation, several graph theory measures were computed (Rubinov and Sporns, 2010). More specifically, we computed the clustering coefficient to measure local connectivity and segregation, the global path length to measure the average shortest path between two nodes, to reveal how efficient communication between regions or how integrated the brain is, and last, the mean degree, to quantify the mean number of edges connected to a node, i.e., mean of all node degrees. These measures were computed by converting the FC matrices into binary graph matrices that represent nodes and edges.

The brain is a highly centralized network, often called a scale free or power law network (Sporns et al., 2004; Haimovici et al., 2013). This type of structure shows an exponential or power relationship between the degree of connectivity of a node and its frequency of occurrence, more specifically, the brain contains a few rich hubs or nodes that connect to several regions and many nodes connected to just a few regions, i.e., the majority of nodes present a low degree. Taking this fact into consideration, to satisfy small worldness or scale freeness of features, different thresholds were used to binarize the static FC matrices before performing graph theory measures, i.e., raw FC values (PCC), from 0.1 to 0.5 at intervals of 0.01. A threshold of 0.3 was selected. Hence, those ROI-to-ROI connections that exceeded a threshold of 0.3 (PCC value) were set to 1, whilst those below 0.3 were set to 0 (note that the possible FC values range was $-1 \sim 1$, absolute values were not used). This threshold apart from ensuring scale freeness, enables one to better differentiate among groups (see **Supplementary material**). Other researchers using rsfMRI datasets, concluded that a threshold between 0.21 to 0.4 is optimal to enable differentiation of groups (Aurich et al., 2015; Ahmadi et al., 2021; Ye et al., 2015; Ng et al., 2021). Graph theory measures were performed using the brain connectivity toolbox: (<https://sites.google.com/site/bctnet/>).

After extracting the brain network features, a one-way analysis of variance (ANOVA) and post hoc comparisons were conducted to explore differences between pairs of groups.

Temporal variability of FC by means of Sliding window correlation (SWA) and standard deviation:

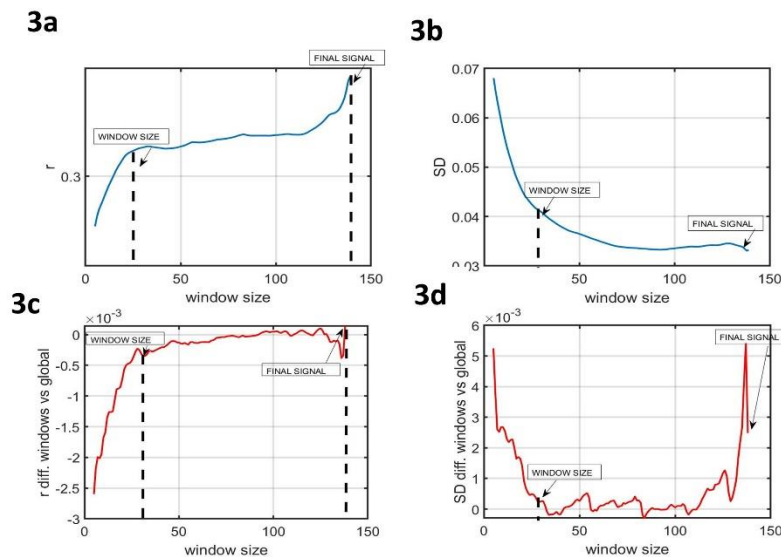
A SWA was used to explore the dFC of our samples, more specifically the temporal variability of FC. In order to use a window length that captured fast changes in the signal while also keeping an optimal level of robustness, a window size assessment was performed prior to the analysis (Leonardi and Van De Ville, 2015). This trade-off between sensitivity and specificity was examined by computing the mean correlation of the mean of all ROI-to-ROI correlations and exploring how the mean FC value varied as a function of window size (see **Figure 2**). The same procedure was used to explore the mean of the standard deviation (*SD*) of each window matrix as a function of window size. The length window assessment was performed for overlapping windows from 5 to 140 time points (i.e., from 15 to 420 seconds), with an increment of one time point (Mokhtari *et al.*, 2019).

Increased Functional Connectivity in Alzheimer's

Once the optimal window size was selected, SWA was performed. First, the FC between each pair of regions was computed for each window, obtaining as many connectivity matrices as windows. Then, the variability (i.e., standard deviation of FC across windows for each ROI-to-ROI) was computed, obtaining one covariance matrix per group.

A one-way analysis of variance (ANOVA) and post hoc comparisons were conducted to explore differences between pairs of groups.

Figure 2



Point Process Analysis, PPA:

The main difference between the static functional connectivity and PPA is that the former keeps all the timepoints for the analysis while the latter one just includes those points that surpass a threshold of 1σ (Cifre et al., 2020; Cifre, Flores, et al., 2021; Tagliazucchi et al., 2012). The steps conducted in the PPA consisted of first thresholding the timeseries of each ROI considering the amplitude of the BOLD signal. Only those events or peaks that surpass 1σ were selected (see Tagliazucchi et al., 2012). Empirically, for the threshold of 1σ in a BOLD signal, we find on average 8.5 ± 2.8 upward crossings per 4 min of fMRI scan. This number of points has been proven to be sufficient by other authors (Tagliazucchi *et al.*, 2012). This is because the BOLD signals that are upward situated are non-linear events that contain the most relevant information and follow a power law. Second, all those points of the timeseries that surpassed $1SD$ of the BOLD signal were selected as relevant. Co-activation binary matrices for each timepoint were generated, e.g., in timepoint 1 FC between ROI 1 and ROI 2 the signal is relevant (both surpass $1SD$), in timepoint 1 ROI 1 and ROI 3 in time 1 signal is not relevant ($<1SD$...). This is conducted for all the 140 timepoints for each 116 pairs or ROIs. Finally, a matrix of addition was computed for each pair of ROIs per participant, e.g., connectivity between ROI 1 and ROI 2 in PPA was acquired by adding all the timepoints that were relevant throughout the time series. This is similar to the correlation matrix obtained in the classic FC, but in the PPA instead of computing the correlation between pairs of regions, the summation of the number of relevant points is obtained (see Supplementary material).

A one-way analysis of variance (ANOVA) and post hoc comparisons were conducted to explore differences between pairs of groups.

Increased Functional Connectivity in Alzheimer's

Statistical analysis:

A one-way analysis of variance (one-way-ANOVA) and multiple comparison tests corrected with Bonferroni correction at $p < .05$ were used to compare results across groups in all the analysis conducted, i.e., FC, graph theory measures, SWA and PPA. This method for multiple comparisons is one of the most commonly used for rsfMRI analysis (Lindquist and Mejia, 2015).

3. RESULTS

Static Functional Connectivity (FC)

The results showed an increased in FC between several ROIs in LMCI and AD in comparison to HC and EMCI (see **Table 2**). More specifically, the AD presented an increased FC between the angular gyrus (left) and cerebellum crus II (left) in contrast to the EMCI and between the superior occipital gyrus (right) and calcarine fissure (left). Relative to HC, AD also presented an increase in FC between the thalamus and the inferior frontal gyrus (left), between the middle temporal gyrus (left) and the caudate nucleus (left), between the vermis 9 and the occipital superior (left) and between the caudate (right) and the frontal inferior gyrus (left). The only regions that presented a decreased FC in AD in comparison to HC were the middle temporal gyrus (right) and the superior occipital gyrus (left).

To explore whether this pattern of connectivity was also present globally, the mean FC of all ROI-to-ROI correlations of each group was conducted. Results did not show a significant difference across groups (see **Figure 3**).

Graph theory measures

Additionally, the clustering coefficient, degree, and global characteristic path length network measures were computed.

Patients with EMCI presented a significant longer characteristic path length and a shorter mean degree in comparison to LMCI, AD and HC. Results in mean clustering coefficient did not show significant differences amongst groups (see **Table 3**).

Sliding window correlation analysis

As expected, the variability when computing SD across windows using short windows, i.e., from 1 to 20 time points (3 to 60 seconds), was substantially higher and the correlation was lower than when computing it for longer windows, i.e., 120 to 139 time points. Window lengths from 30 to 120 TR showed increased stability. Hence, the time series were divided into overlapping windows of 30 time points, i.e., 90 seconds to have as many windows as possible to ensure a good trade-off between sensitivity and robustness. Our windows are short enough not to miss FC fluctuations in our BOLD data and long enough to be robust and only real fluctuations. Previous studies also indicated enough variability and robustness in windows between 30 to 60 time points in rsfMRI studies (considering the frequency of the BOLD signal being 0.1-0.001 Hz) (Esposito *et al.*, 2019).

Greater differences in variability across groups were detected between several areas of the DMN and the attentional networks (executive and dorsal), between the left auditory cortex and the right dorsolateral frontal cortex as well as, between the right cerebellum right and the left sensory motor cortex and between areas within the right cerebellum (see **Table 4**). Expectedly, the group that showed

Increased Functional Connectivity in Alzheimer's

more variability in FC amongst windows is the EMCI group that showed a decrease in the static FC (analysis explained in the subsection above). Moreover, the AD showed a decrease in variability and presented an increase in sFC.

PPA

Some overlap in the results of the static FC and the PPA was detected (see **Table 5**). The LMCI and AD presented an increased FC between several brain regions in comparison to the HC and the EMCI. Specifically, the AD group, when compared with the LMCI, presented a higher FC between the cerebellum crus I (left) and the angular gyrus (left); an increased FC when compared with the EMCI, between the caudate (left) and the frontal gyrus (triangularis part) and also increased FC in comparison to HC between the insula (left) and the middle frontal gyrus (left), between the parahippocampus (right) and the insula (left), between the insula (left) and the inferior frontal triangular part (right) and between the thalamus (right) and the frontal inferior triangular part (left). The AD only presented a decrease in FC in contrast to LMCI between the cerebellum (right) and the amygdala (right).

The LMCI presented a higher FC in comparison to EMCI between the cerebellum (right) and the basal ganglia) and between the superior frontal gyrus medial (left) and the inferior frontal triangular part (right). The LMCI also presented a higher FC compared to HC between the parietal superior gyrus (right) and the orbital medial gyrus (right). The LMCI only presented a decrease in FC between the precuneus (right) and the middle occipital gyrus (right) in comparison to HC.

To summarize, **Figure 4** displays a general view of the results obtained using FC, PPA and SWA. As shown in the images, both the static FC and the PPA results showed an increase in connectivity between specific regions in the AD and the LMCI and a decrease in connectivity in EMCI. Additionally, the SWA results showed that variability in FC between brain regions across time is higher in the EMCI, which is statistically coherent with the fact that correlation, or FC between regions is reduced in this group. The PPA was more sensitive in detecting changes across groups.

4. DISCUSSION

This study aimed to explore FC across stages of AD using the PPA and other classical methods. It was hypothesized that the connectivity in and between the DMN, SN, CEN and VN would be altered in MCI and AD. Our results showed several differences across groups within and between the mentioned networks and other additional networks. Moreover, it was expected that there would be an increase in FC for EMCI but a decrease in AD for the mentioned networks. Unexpectedly, an increase in connectivity in LMCI and AD and a slight decrease in EMCI in contrast to the other groups was found. Last, as expected, the PPA was the most sensitive method when capturing differences in FC across groups. A discussion of the results obtained using the different methods is provided below.

4.1. Static FC and PPA: an increased FC in LMCI and AD

A reduction in mean functional connectivity between several brain regions, mostly in posterior and medial areas, as well as an increase in the FC variability across windows of time was expected in AD in comparison to EMCI and LMCI. However, our results showed a higher FC in LMCI and AD, but a decrease in EMCI in comparison to the other groups between several brain regions. This suggests a non-linear connectivity pattern that begins with an optimal connectivity in HC, followed by a slightly decrease in EMCI, and then by an enhancement of FC between several regions in LMCI and mild AD.

Some researchers used rsEEG (Bonanni *et al.*, 2021) and rsfMRI and reported an increase in FC between multiple brain regions in prodromic AD and a decrease in AD. This mechanism is

Increased Functional Connectivity in Alzheimer's

hypothesized by the authors to be caused due to a GABAergic-glutamatergic dysregulation. Additionally, a post-mortem study (Snowden *et al.*, 2019) that analysed brain tissue found that patients with AD presented a GABAergic increase and a glutamate decrease in AD in the inferior temporal gyrus, the most vulnerable region to accumulate TAU tangles. Consequently, an inhibitory environment and decrease of action potentials takes place. Taken together, we would expect to observe an increase in connectivity in prodromic AD and MCI followed by a decreased FC in AD. In our study, however, a decreased FC was only observed in EMCI followed by an increased FC in LMCI and AD. The exception to this was for a pair of posterior regions that presented a decreased in connectivity in AD, i.e., right middle temporal gyrus and right superior occipital gyrus. This increased FC in LMCI and AD was only seen in the current study by differentiating EMCI and LMCI, not often done in previous work. Moreover, in a post-mortem study, patients with AD were older and presented moderate or severe AD, where decreased connectivity is more expected due to an increase of cellular death and atrophy. Furthermore, it is well established that a high release of glutamate is neurotoxic and might be one of the causes of neuronal death (Maragos *et al.*, 1987). Here, it can be hypothesized that the increased FC observed in LMCI and AD groups could be enhanced by a low GABAergic or inhibitory activity along with a high or excitatory activity in areas where TAU is not yet installed (e.g., thalamus, caudate and/or cerebellum). On the other hand, early pathologic damage might explain the decreased FC in AD between the right middle temporal gyrus and the right superior occipital gyrus.

An increased FC has also been associated with mal(adaptive) rewiring of the brain after pathologic damage occurs. This idea is not mutually exclusive to the neurotransmitter dysregulation hypothesis and the two mechanisms might co-occur in an additive fashion. Some authors have distinguished two types of hyperconnectivity rewiring after brain damage: a local hyperconnectivity and a global hyperconnectivity (Snowden *et al.*, 2019). The former states that local alternative paths close to damaged brain areas are used to ensure that communication between networks is possible to preserve function. The latter refers to the brain using multimodal or rich nodes, independently to the localization of the brain damage, in order to ensure the maintenance of cognitive function. Following the popular stages of AD degradation as proposed by Braak and Braak's (1995) research, the first areas damaged in AD (stages I and II) due to TAU deposition are the posterior ones, more specifically, the brain stem followed by the entorhinal. These areas are then followed by the limbic and whole neocortex in more advanced stages (III-IV), and then the hippocampus and anterodorsal thalamic nucleus. As the participants of our study present mild AD, this sign of increased FC in some posterior areas might indicate that certain regions of the posterior cortex could be affected but other areas are still preserved and can be recruited. A study showed increased correlations between occipital regions. Some investigators presented the same results regarding hyperactivity in AD in the middle occipital gyrus, lingual gyrus and visual cortex and explained the finding as an adaptation of the brain networks in response to disease (Wang *et al.*, 2019).

Although several researchers have justified an increased FC in neurodegenerative diseases as an adaptive mechanism of neuroplasticity to protect behaviour and cognition against brain damage, the mechanisms behind FC and its relationship with cognition and behaviour are not well understood yet. Multiple factors play a role in FC and at the time of writing there is a lack of understanding of what is really causing a specific pattern of FC, i.e., what factors can explain an increased or decreased FC. Currently, interpretations of results in FC have been speculative. Could, for instance an increase in FC in several areas be explained simply by structural disconnection and not by compensatory mechanisms? A study conducted by Patel *et al.* (2018) revealed that structural disconnection in patients with multiple sclerosis could explain an increase in rsfMRI (Wang *et al.*, 2019). Whether this increased in FC is due to neural compensatory mechanisms or not needs to be further investigated using multimodal neuroimaging techniques.

Increased Functional Connectivity in Alzheimer's

4.2. Additional measures performed: Graph theory measures

Patients with EMCI showed a longer characteristic path length in contrast to the patients with LMCI and AD, probably reflecting a need in EMCI to connect interregionally due to local damage. In comparison, in LMCI and AD there might be more widespread pathology, more areas connected in a more disorganized way and presenting shorter paths. A shorter characteristic path length in HC is probably a sign of efficiency in connectivity between long distant areas, while in AD shorter paths might mean disrupted connectivity and the whole brain is more connected but in a disorganized manner, i.e., a decrease in metastability. A study reported a disrupted global metastability in AD (Córdova-Palomera et al., 2017). Other studies reported longer mean characteristic path lengths in MCI (J. Wang *et al.*, 2013).

It can be speculated that in LMCI and at the beginning of AD the brain might be rewiring in a widespread manner, finding local and global alternative paths to maintain cognitive functioning. This adaptive and short-term solution might incur, however, a high cost for the network, as usually any alternative paths that involve rich hubs generate the proper environment to facilitate the formation and accumulation of TAU protein tangles (Bonanni et al., 2021).

4.3. Sliding windows correlation analysis (variability among windows)

It has been reported that patients with pathology might present more variability in the BOLD signal over time. The *SD* of the correlation metrics across windows allowed us to see the variability in FC between pairs of regions. Usually, regions with a greater variability imply a lower correlation (Rolls, Cheng and Feng, 2021) .

Significant differences in variability across windows were found between groups. Results showed that the EMCI presented a greater variability over time in most connections. This finding is aligned with the static FC results that showed a decreased correlation between several brain regions. Most of the ROIs detected are similar for static FC and PPA analysis.

4.4. Specific brain regions affected in AD and LMCI with decrease FC (Static FC analysis, SWA and PPA)

Besides this decrease-increase in FC patterns, the specific brain regions that presented a sharp abnormal connectivity show consistency with other studies. For instance, several studies have reported a decrease in FC in EMCI between thalamus (left/right) and frontal gyrus and between the temporal and occipital gyrus (Cai *et al.*, 2015). Additionally, a study showed that AD participants presented a larger caudate nucleus volume in AD, probably reflecting a compensation mechanism of damage in the closest areas such as the hippocampus. Pathology in the hippocampus could explain an increasing stimulation of the caudate nucleus, causing an increase in volume and FC between it and cortical brain regions (Persson *et al.*, 2018).

On the other hand, the cerebellum was classically thought to be unaffected in MCI and AD (Chételat *et al.*, 2008). However, grey matter atrophy in the cerebellum, and pathological changes, such as betamyloid deposits and neurofibrillary tangles have been observed (Ciavardelli et al., 2010; Córdova et al., 2017). The current results showed abnormal connectivity in the cerebellum and between the cerebellum and other regions (cerebellum crus II and DMN, sensory motor and cerebellum VII, cerebellum 8 and cerebellum 7b). Other studies also found aberrant FC within the cerebellum (Cai et al., 2015) and between the Crus II and the DMN (Toussaint et al., 2014).

The precuneus, a specific region of the DMN, is a relevant hub that enhances connectivity between several brain regions. A decreased FC between this and other regions has been associated with changes in the brain's vulnerability of early Alzheimer's disease. Our PPA results showed a decreased FC in

Increased Functional Connectivity in Alzheimer's

LMCI in contrast with HC (Nelson et al., 2010; Yokoi et al., 2018). A decreased FC of the precuneus might be the cause of increased FC in regions next to this region (local hyperconnectivity hypothesis) and far from this region (global hyperconnectivity hypothesis).

4.5. Added value of SWA and the PPA to the static FC

Although our results showed some overlap or complementarity across methods, for instance areas or networks, there were also differences across methods. It is worth noting that the PPA was able to detect more changes across groups.

Some areas that showed aberrant FC detected by means of the SWA and the PPA were not detected in the static FC. For instance, the AD presented less variability and more synchronicity between the auditory and middle frontal gyrus in comparison to the HC and the EMCI. In addition, the AD group, in contrast to the HC and the EMCI, presented increased FC and decreased variability between regions of the auditory network, e.g., insula, superior temporal and the dorsal (right), such as the inferior frontal triangular part, middle frontal gyrus. Finally, the EMCI presented a decreased connectivity in contrast to the LMCI between the executive function network and the dorsal.

When comparing the SWA and the PPA, a higher variability from the SWA was obtained in the EMCI in comparison to the HC between a region in the executive function network and the dorsal, and in the PPA a higher correlation in the LMCI than in the EMCI. These couple of findings made us hypothesize that there is a stronger synchronicity between these areas in LMCI and HC and less in EMCI. Without performing the PPA we could not have seen the difference in FC between these regions.

Last, the PPA was the method that allowed us to have a more comprehensive or complete view of the aberrant connectivity across the different stages of the disease. That is to say, we could gauge the subtle changes across groups like an increase in LMCI in comparison to EMCI between the dorsal network and the CEN, as well as an increase and decrease in FC between some ROIS of the cerebellum and the basal ganglia in LMCI and AD.

This study presents some limitations. First, the optimization of window parameters to conduct the SWA as well as the threshold to binarize the FC matrix and extract graph measures, were carefully selected after a literature revision and a variability and correlation assessment for each window size, nonetheless the optimization of parameters in FC research is an issue that should be further investigated with novel analysis. Second, the structural parcellation method used in the present study, the AAL, is commonly used for task and rsfMRI studies. Although some studies have used connectivity-driven parcellations and they have shown more consistency with the subjacent resting state connectivity, anatomical parcellations yield the same or even better delimitation of cortical areas which is relevant for network analysis. Given these claims, the selection of a specific parcellation over others will not impact many of the results. As suggested by Arslan and colleagues (2018) in their systematic comparison of parcellation methods, researchers performing network analysis should use any parcellation method available. Third, the participants with eMCI, LMCI or AD, presented a clinical diagnosis and their memory was objectively affected. However, a biological characterization of the participants was not conducted and would enable generalization of findings.

Comparing results across methods was a difficult task because some results were similar across methods, but several differences could also be found. This happened because the methods used measured different FC constructs: static FC, variability in FC and dFC. Hence, expecting similar global results in terms of differences between some networks or patterns of increased or decreased connectivity in several brain regions at a specific stage of the disease was logical, however expecting similar findings across methods, at a finer scale, i.e., small regions was not achievable.

Increased Functional Connectivity in Alzheimer's

CONCLUSION

Our results showed that the EMCI presented a similar but slightly decreased FC to HC in several brain areas, while the LMCI and mild AD presented an increased FC in several regions. These results suggest that the pathology is less dispersed in EMCI and the brain configuration is similar to the HC. When the pathology advances in LMCI and AD, the brain might react by compensating through using the available resources such as the recruitment of alternative paths. This might enhance a high glutamate and low gabaergic activity next to regions where pathologic proteins are installed and in rich hubs such as the thalamus. The analysis performed provided some overlap in the results. For instance, they showed an increased FC in LMCI and AD involving a specific frontal region, i.e., the frontal inferior triangular (left) and posterior regions mostly within the visual network, the DMN, the auditory, cerebellum, basal ganglia, and thalamus. However, and as expected, results also show differences in the areas affected when applying the different methods. This was expected as the literature review shows this heterogeneity because what we are measuring across methods fits under the same "FC" umbrella, but it is not the same, i.e., static FC, variability and dFC are different measures. To end, SWA and PPA added new results and this last method is the most efficient when dealing with datasets and sensitive differentiating changes across the stages of the disease.

Future studies should include a larger sample and diverse AD groups that reflect all the stages of the disease, i.e. amnesic EMCI, amnesic LMCI, mild AD, moderate AD and severe AD. Additionally, longitudinal studies that track the connectivity across years, as well as post mortem studies to explore the brain tissue of different patients that died at different stages of the disease would be highly useful to understand the relationship between neurotransmitters, pathological protein and FC at the different stages of AD. Finally, novel machine learning approaches could be used to compare and integrate findings.

ACKNOWLEDGEMENTS

Financial support was provided by the MICINN (Spain) grant PID2021-125534OB-I00
PID2021-125534OB-I00

Data used for this study was funded by the Alzheimer's Disease Neuroimaging Initiative (ADNI) (National Institutes of Health Grant U01 AG024904) and DOD ADNI (Department of Defense award number W81XWH-12-2-0012). ADNI is funded by the National Institute on Aging, the National Institute of Biomedical Imaging and Bioengineering, and through generous contributions from the following: AbbVie, Alzheimer's Association; Alzheimer's Drug Discovery Foundation; Araclon Biotech; BioClinica, Inc.; Biogen; Bristol-Myers Squibb Company; CereSpir, Inc.; Cogstate; Eisai Inc.; Elan Pharmaceuticals, Inc.; Eli Lilly and Company; EuroImmun; F. Hoffmann-La Roche Ltd and its affiliated company Genentech, Inc.; Fujirebio; GE Healthcare; IXICO Ltd.; Janssen Alzheimer Immunotherapy Research & Development, LLC.; Johnson & Johnson Pharmaceutical Research & Development LLC.; Lumosity; Lundbeck; Merck & Co., Inc.; Meso Scale Diagnostics, LLC.; NeuroRx Research; Neurotrack Technologies; Novartis Pharmaceuticals Corporation; Pfizer Inc.; Piramal Imaging; Servier; Takeda Pharmaceutical Company; and Transition Therapeutics. The Canadian Institutes of Health Research is providing funds to support ADNI clinical sites in Canada. Private sector contributions are facilitated by the Foundation for the National Institutes of Health (www.fnih.org). The grantee organization is the Northern California Institute for Research and Education, and the study is coordinated by the Alzheimer's Therapeutic Research Institute at the University of Southern California. ADNI data are disseminated by the Laboratory for Neuro Imaging at the University of Southern California.

Increased Functional Connectivity in Alzheimer's

The authors thank Alvin Synarong for his contribution in editing the manuscript.

REFERENCES

- Aguirre, G.K., Zarahn, E. and D'Esposito, M. (1998). The variability of human, BOLD hemodynamic responses', *NeuroImage*, 8(4), pp. 360–369. <https://doi.org/10.1006/nimg.1998.0369>.
- Ahmadi, H., Fatemizadeh, E. and Motie-nasrabadi, A. (2021). fMRI functional connectivity evaluation in Alzheimer ' s s tages : Linear and Non-linear approaches, *Research Square*, pp. 1–17.
- Arslan, S., Ktena, S.I., Makropoulos, A., Robinson, E.C., Rueckert, D. and Parisot, S. (2018). Human brain mapping: A systematic comparison of parcellation methods for the human cerebral cortex, *NeuroImage*, 170(April 2017), pp. 5–30. Available at: <https://doi.org/10.1016/j.neuroimage.2017.04.014>.
- Ashraf, A., Fan, Z., Brooks, D.J. and Edison, P. (2015). Cortical hypermetabolism in MCI subjects: a compensatory mechanism?, *European Journal of Nuclear Medicine and Molecular Imaging*, 42(3), pp. 447–458. <https://doi.org/10.1007/s00259-014-2919-z>.
- Badhwar, A.P., Tam, A., Dansereau, C., Orban, P., Hoffstaedter, F. and Bellec, P. (2017). Resting-state network dysfunction in Alzheimer's disease: A systematic review and meta-analysis, *Alzheimer's and Dementia: Diagnosis, Assessment and Disease Monitoring*, 8, pp. 73–85. <https://doi.org/10.1016/j.dadm.2017.03.007>.
- Bhuvaneshwari, B., & Kavitha, A. (2017). Investigations on the brain connectivity patterns in progression of Alzheimer's disease using functional MR imaging and graph theoretical measures. 2017 IEEE 16th International Conference on Cognitive Informatics & Cognitive Computing (ICCI*CC). <https://doi.org/10.1109/icci-cc.2017.8109744>
- Bonanni, L., Moretti, D., Benussi, A., Ferri, L., Russo, M., Carrarini, C., Barbone, F., Arnaldi, D., Falasca, N.W., Koch, G., Cagnin, A., Nobili, F., Babiloni, C., Borroni, B., Padovani, A., Onofri, M. and Franciotti, R. (2021). Hyperconnectivity in Dementia Is Early and Focal and Wanes with Progression, *Cerebral Cortex*, 31(1), pp. 97–105. <https://doi.org/10.1093/cercor/bhaa209>.
- Brier, M.R., Thomas, J.B., Fagan, A.M., Hassenstab, J., Holtzman, D.M., Benzinger, T.L., Morris, J.C. and Ances, B.M. (2014). Functional connectivity and graph theory in preclinical Alzheimer's disease, *Neurobiology of Aging*, 35(4), pp. 757–768. <https://doi.org/10.1016/j.neurobiolaging.2013.10.081>.
- Cai, S., Huang, L., Zou, J., Jing, L., Zhai, B., Ji, G., Von Deneen, K.M., Ren, J., Ren, A. and Alzheimer's Disease Neuroimaging Initiative (2015). Changes in thalamic connectivity in the early and late stages of amnesic mild cognitive impairment: A resting-state functional magnetic resonance study from ADNI, *PLoS ONE*, 10(2). <https://doi.org/10.1371/journal.pone.0115573>.
- Chen, J.E., Rubinov, M. and Chang, C. (2017). Methods and Considerations for Dynamic Analysis of Functional MR Imaging Data, *Neuroimaging Clinics of North America*, 27(4), pp. 547–560. <https://doi.org/10.1016/j.nic.2017.06.009>.

Increased Functional Connectivity in Alzheimer's

Chételat, G., Desgranges, B., Landeau, B., Mézenge, F., Poline, J.B., De La Sayette, V., Viader, F., Eustache, F. and Baron, J.C. (2008). Direct voxel-based comparison between grey matter hypometabolism and atrophy in Alzheimer's disease, *Brain*, 131(1), pp. 60–71. <https://doi.org/10.1093/brain/awm288>.

Ciavardelli, D., Silvestri, E., Del Viscovo, A., Bomba, M., De Gregorio, D., Moreno, M., Di Ilio, C., Goglia, F., Canzoniero, L.M.T. and Sensi, S.L. (2010). Alterations of brain and cerebellar proteomes linked to A β and tau pathology in a female triple-transgenic murine model of Alzheimer's disease, *Cell Death and Disease*, 1(10), pp. 1–11. <https://doi.org/10.1038/cddis.2010.68>.

Cifre, I., Miller Flores, M.T., Penalba, L., Ochab, J.K. and Chialvo, D.R. (2021). Revisiting Nonlinear Functional Brain Co-activations: Directed, Dynamic, and Delayed, *Frontiers in Neuroscience*, 15. <https://doi.org/10.3389/fnins.2021.700171>.

Cifre, I., Zarepour, M., Horowitz, S.G., Cannas, S.A. and Chialvo, D.R. (2020). Further results on why a point process is effective for estimating correlation between brain regions, *Papers in Physics*, 12(June), pp. 1–8. <https://doi.org/10.4279/pip.120003>.

Córdova-Palomera, A., Kaufmann, T., Persson, K., Alnæs, D., Doan, N.T., Moberget, T., Lund, M.J., Barca, M.L., Engvig, A., Brækhus, A., Engedal, K., Andreassen, Ole A., Selbæk, G. and Westlye, L.T. (2017). Disrupted global metastability and static and dynamic brain connectivity across individuals in the Alzheimer's disease continuum, *Scientific Reports*, 7(1), p. 40268. <https://doi.org/10.1038/srep40268>.

Esposito, R., Ospedali, A.O., Shen, H., Rocca, M.A., Valsasina, P., Hidalgo De La Cruz, M. and Filippi, M. (2019). Characterizing Rapid Fluctuations of Resting State Functional Connectivity in Demyelinating, Neurodegenerative, and Psychiatric Conditions: From Static to Time-Varying Analysis, *Frontiers in Neuroscience* / www.frontiersin.org, 1, p. 618. <https://doi.org/10.3389/fnins.2019.00618>.

Franzmeier, N., Duering, M., Weiner, M., Dichgans, M., & Ewers, M. (2017). Left frontal cortex connectivity underlies cognitive reserve in prodromal Alzheimer disease. *Neurology*, 88(11), 1054–1061. <https://doi.org/10.1212/wnl.0000000000003711>

Haimovici, A., Tagliazucchi, E., Balenzuela, P. and Chialvo, D.R. (2013). Brain Organization into Resting State Networks Emerges at Criticality on a Model of the Human Connectome, *Physical Review Letters*, 110(17), p. 178101. <https://doi.org/10.1103/PhysRevLett.110.178101>.

Hillary, F.G. and Grafman, J.H. (2017). Injured Brains and Adaptive Networks: The Benefits and Costs of Hyperconnectivity, *Trends in Cognitive Sciences*, 21(5), pp. 385–401. <https://doi.org/10.1016/j.tics.2017.03.003>.

Hutchison, R.M., Womelsdorf, T., Allen, E.A., Bandettini, P.A., Calhoun, V.D., Corbetta, M., Della Penna, S., Duyn, J.H., Glover, G.H., Gonzalez-Castillo, J., Handwerker, D.A., Keilholz, S., Kiviniemi, V., Leopold, D.A., de Pasquale, F., Sporns, O., Walter, M. and Chang, C. (2013). Dynamic functional connectivity: Promise, issues, and interpretations, *NeuroImage*, 80, pp. 360–378. <https://doi.org/10.1016/j.neuroimage.2013.05.079>.

Increased Functional Connectivity in Alzheimer's

Jacobs, H.I.L., Radua, J., Lückmann, H.C. and Sack, A.T. (2013). Meta-analysis of functional network alterations in Alzheimer's disease: Toward a network biomarker, *Neuroscience and Biobehavioral Reviews*, 37(5), pp. 753–765. <https://doi.org/10.1016/j.neubiorev.2013.03.009>.

Jie, B., Wee, C.Y., Shen, D. and Zhang, D. (2016). Hyper-connectivity of functional networks for brain disease diagnosis. *Medical Image Analysis*, 32, pp. 84–100. <https://doi.org/10.1016/j.media.2016.03.003>.

Keilholz, S., Caballero-Gaudes, C., Bandettini, P., Deco, G. and Calhoun, V. (2017). Time-Resolved Resting-State Functional Magnetic Resonance Imaging Analysis: Current Status, Challenges, and New Directions, *Brain Connectivity*. Mary Ann Liebert Inc., pp. 465–481. <https://doi.org/10.1089/brain.2017.0543>.

Kim, H.J., Cha, J., Lee, J.M., Shin, J.S., Jung, N.Y., Kim, Y.J., Choe, Y.S., Lee, K.H., Kim, S.T., Kim, J.S., Lee, J.H., Na, D.L. and Seo, S.W. (2016). Distinctive Resting State Network Disruptions among Alzheimer's Disease, Subcortical Vascular Dementia, and Mixed Dementia Patients, *Journal of Alzheimer's Disease*, 50(3), pp. 709–718. <https://doi.org/10.3233/JAD-150637>.

Krienen, F.M. and Buckner, R.L. (2009). Segregated fronto-cerebellar circuits revealed by intrinsic functional connectivity, *Cerebral Cortex*, 19(10), pp. 2485–2497. <https://doi.org/10.1093/cercor/bhp135>.

Lee, E.S., Yoo, K., Lee, Y.B., Chung, J., Lim, J.E., Yoon, B. and Jeong, Y. (2016). Default Mode Network Functional Connectivity in Early and Late Mild Cognitive Impairment: Results from the Alzheimer's Disease Neuroimaging Initiative, *Alzheimer Disease and Associated Disorders*, 30(4), pp. 289–296. Available at: <https://doi.org/10.1097/WAD.000000000000143>.

Leonardi, N. and Van De Ville, D. (2015). On spurious and real fluctuations of dynamic functional connectivity during rest, *NeuroImage*, 104, pp. 430–436. <https://doi.org/10.1016/j.neuroimage.2014.09.007>.

Li, H.J., Hou, X.H., Liu, H.H., Yue, C.L., He, Y. and Zuo, X.N. (2015). Toward systems neuroscience in mild cognitive impairment and Alzheimer's disease: A meta-analysis of 75 fMRI studies, *Human Brain Mapping*, 36(3), pp. 1217–1232. <https://doi.org/10.1002/hbm.22689>.

Li, W., Li, Y., Hu, C., Chen, X. and Dai, H. (2014). Point process analysis in brain networks of patients with diabetes, *Neurocomputing*, 145, pp. 182–189. <https://doi.org/10.1016/j.neucom.2014.05.045>.

Lindquist, M.A. and Mejia, A. (2015). Zen and the art of multiple comparisons, *Psychosomatic Medicine*, 77(2), pp. 114–125. <https://doi.org/10.1097/PSY.000000000000148>.

Liu, Sidong, Cai, W., Liu, Siqu, Zhang, F., Fulham, M., Feng, D., Pujol, S. and Kikinis, R. (2015). Multimodal neuroimaging computing: the workflows, methods, and platforms, *Brain Informatics*, 2(3), pp. 181–195. <https://doi.org/10.1007/s40708-015-0020-4>.

Maragos, W.F., Greenamyre, J.T., Penney, J.B. and Young, A.B. (1987). Glutamate dysfunction in Alzheimer's disease: a hypothesis, *Trends in Neurosciences*, 10(2), pp. 65–68. [https://doi.org/10.1016/0166-2236\(87\)90025-7](https://doi.org/10.1016/0166-2236(87)90025-7).

Increased Functional Connectivity in Alzheimer's

Marek, S. and Dosenbach, N.U.F. (2018). The frontoparietal network: Function, electrophysiology, and importance of individual precision mapping, *Dialogues in Clinical Neuroscience*, 20(2), pp. 133–141. <https://doi.org/10.31887/dcms.2018.20.2/smarek>.

Mokhtari, F., Akhlaghi, M. I., Simpson, S. L., Wu, G., & Laurienti, P. J. (2019). Sliding window correlation analysis: Modulating window shape for dynamic brain connectivity in resting state. *NeuroImage*, 189, 655–666. <https://doi.org/10.1016/j.neuroimage.2019.02.001>

Nakamura, A., Cuesta, P., Kato, T., Arahata, Y., Iwata, K., Yamagishi, M., Kuratsubo, I., Kato, K., Bundo, M., Diers, K., Fernández, A., Maestú, F. and Ito, K. (2017). Early functional network alterations in asymptomatic elders at risk for Alzheimer's disease, *Scientific Reports*, 7(1), pp. 1–11. Available at: <https://doi.org/10.1038/s41598-017-06876-8>.

Nelson, P. T., Abner, E. L., Scheff, S. W., Schmitt, F. A., Kryscio, R. J., Jicha, G. A., Smith, C. D., Patel, E., & Markesbery, W. R. (2009). Alzheimer's-type neuropathology in the precuneus is not increased relative to other areas of neocortex across a range of cognitive impairment. *Neuroscience letters*, 450(3), 336–339. <https://doi.org/10.1016/j.neulet.2008.11.006>

Ng, A.S.L., Wang, J., Ng, K.K., Chong, J.S.X., Qian, X., Lim, J.K.W., Tan, Y.J., Yong, A.C.W., Chander, R.J., Hameed, S., Ting, S.K.S., Kandiah, N. and Zhou, J.H. (2021). Distinct network topology in Alzheimer's disease and behavioral variant frontotemporal dementia, *Alzheimer's Research and Therapy*, 13(1). <https://doi.org/10.1186/s13195-020-00752-w>.

Oldham, S. and Fornito, A. (2019). The development of brain network hubs, *Developmental Cognitive Neuroscience*, 36(October 2018), p. 100607. <https://doi.org/10.1016/j.dcn.2018.12.005>.

Patel, K.R., Tobyn, S., Porter, D., Bireley, J.D., Smith, V. and Klawiter, E. (2018). Structural disconnection is responsible for increased functional connectivity in multiple sclerosis, *Brain Structure and Function*, 223(5), pp. 2519–2526. <https://doi.org/10.1007/s00429-018-1619-z>.

Persson, K., Bohbot, V.D., Bogdanovic, N., Selbæk, G., Brækhus, A. and Engedal, K. (2018). Finding of increased caudate nucleus in patients with Alzheimer's disease, *Acta Neurologica Scandinavica*, 137(2), pp. 224–232. <https://doi.org/10.1111/ane.12800>.

Rolls, E.T., Cheng, W. and Feng, J. (2021). Brain dynamics: Synchronous peaks, functional connectivity, and its temporal variability, *Human Brain Mapping*, 42(9), pp. 2790–2801. <https://doi.org/10.1002/hbm.25404>.

Rubinov, M. and Sporns, O. (2010). Complex network measures of brain connectivity: Uses and interpretations, *NeuroImage*, 52(3), pp. 1059–1069. <https://doi.org/10.1016/j.neuroimage.2009.10.003>.

Scarapicchia, V., Mazerolle, E.L., Fisk, J.D., Ritchie, L.J. and Gawryluk, J.R. (2018). Resting state BOLD variability in Alzheimer's disease: A marker of cognitive decline or cerebrovascular status?, *Frontiers in Aging Neuroscience*, 10(FEB), pp. 1–13. <https://doi.org/10.3389/fnagi.2018.00039>.

Seo, E.H., Lee, D.Y., Lee, J.M., Park, J.S., Sohn, B.K., Lee, D.S., Choe, Y.M. and Woo, J.I. (2013). Whole-brain Functional Networks in Cognitively Normal, Mild Cognitive Impairment, and Alzheimer's Disease, *PLoS ONE*, 8(1). <https://doi.org/10.1371/journal.pone.0053922>.

Increased Functional Connectivity in Alzheimer's

Snowden, S.G., Ebshiana, A.A., Hye, A., Pletnikova, O., O'Brien, R., Yang, A., Troncoso, J., Legido-Quigley, C. and Thambisetty, M. (2019). Neurotransmitter Imbalance in the Brain and Alzheimer's Disease Pathology, *Journal of Alzheimer's Disease*, 72(1), pp. 35–43.
<https://doi.org/10.3233/JAD-190577>.

Sporns, O. (2013). The human connectome: Origins and challenges, *NeuroImage*, 80, pp. 53–61.
<https://doi.org/10.1016/j.neuroimage.2013.03.023>.

Sporns, O., Chialvo, D.R., Kaiser, M. and Hilgetag, C.C. (2004). Organization, development and function of complex brain networks, *Trends in Cognitive Sciences*, 8(9), pp. 418–425.
<https://doi.org/10.1016/j.tics.2004.07.008>.

Supekar, K., Menon, V., Rubin, D., Musen, M. and Greicius, M.D. (2008). Network analysis of intrinsic functional brain connectivity in Alzheimer's disease, *PLoS Computational Biology*, 4(6).
<https://doi.org/10.1371/journal.pcbi.1000100>.

Tagliazucchi, E., Balenzuela, P., Fraiman, D. and Chialvo, D.R. (2012). Criticality in large-scale brain fmri dynamics unveiled by a novel point process analysis, *Frontiers in Physiology*, 3 FEB.
<https://doi.org/10.3389/fphys.2012.00015>.

Tam, A., Dansereau, C., Badhwar, A.P., Orban, P., Belleville, S., Chertkow, H., Dagher, A., Hanganu, A., Monchi, O., Rosa-Neto, P., Shmuel, A., Wang, S., Breitner, J. and Bellec, P. (2015). Common effects of amnesic mild cognitive impairment on resting-state connectivity across four independent studies, *Frontiers in Aging Neuroscience*, 7. <https://doi.org/10.3389/fnagi.2015.00242>.

Thomas, J.B., Brier, M.R., Bateman, R.J., Snyder, A.Z., Benzinger, T.L., Xiong, C., Raichle, M., Holtzman, D.M., Sperling, R.A., Mayeux, R., Ghetti, B., Ringman, J.M., Salloway, S., McDade, E., Rossor, M.N., Ourselin, S., Schofield, P.R., Masters, C.L., Martins, R.N., Weiner, M.W., Thompson, P.M., Fox, N.C., Koeppe, R.A., Jack, C.R., Mathis, C.A., Oliver, A., Blazey, T.M., Moulder, K., Buckles, V., Hornbeck, R., Chhatwal, J., Schultz, A.P., Goate, A.M., Fagan, A.M., Cairns, N.J., Marcus, D.S., Morris, J.C. and Ances, B.M. (2014). Functional connectivity in autosomal dominant and late-onset Alzheimer disease, *JAMA Neurology*, 71(9), pp. 1111–1122.
<https://doi.org/10.1001/jamaneurol.2014.1654>.

Toussaint, P.J., Maiz, S., Coynel, D., Doyon, J., Messé, A., de Souza, L.C., Sarazin, M., Perlberg, V., Habert, M.O. and Benali, H. (2014). Characteristics of the default mode functional connectivity in normal ageing and Alzheimer's disease using resting state fMRI with a combined approach of entropy-based and graph theoretical measurements, *NeuroImage*, 101, pp. 778–786.
<https://doi.org/10.1016/j.neuroimage.2014.08.003>.

Tzourio-Mazoyer, N., Landeau, B., Papathanassiou, D., Crivello, F., Etard, O., Delcroix, N., Mazoyer, B. and Joliot, M. (2002). Automated Anatomical Labeling of Activations in SPM Using a Macroscopic Anatomical Parcellation of the MNI MRI Single-Subject Brain, *NeuroImage*, 15(1), pp. 273–289. <https://doi.org/https://doi.org/10.1006/nimg.2001.0978>.

Wang, J., Liu, J., Wang, Z., Sun, P., Li, K. and Liang, P. (2019). Dysfunctional interactions between the default mode network and the dorsal attention network in subtypes of amnesic mild cognitive impairment, *Aging*, 11(20), pp. 9147–9166. Available at: <https://doi.org/10.18632/aging.102380>.

Increased Functional Connectivity in Alzheimer's

Wang, J., Zuo, X., Dai, Z., Xia, M., Zhao, Z., Zhao, X., Jia, J., Han, Y. and He, Y. (2013). Disrupted functional brain connectome in individuals at risk for Alzheimer's disease, *Biological Psychiatry*, 73(5), pp. 472–481. <https://doi.org/10.1016/j.biopsych.2012.03.026>.

Wang, L., Li, H., Liang, Y., Zhang, J., Li, X., Shu, N., Wang, Y.Y. and Zhang, Z. (2013). Amnestic mild cognitive impairment: Topological reorganization of the default-mode network, *Radiology*, 268(2), pp. 501–514. <https://doi.org/10.1148/radiol.13121573>.

Xu, X., Li, W., Mei, J., Tao, M., Wang, X., Zhao, Q., Liang, X., Wu, W., Ding, D. and Wang, P. (2020). Feature Selection and Combination of Information in the Functional Brain Connectome for Discrimination of Mild Cognitive Impairment and Analyses of Altered Brain Patterns, *Frontiers in Aging Neuroscience*, 12. <https://doi.org/10.3389/fnagi.2020.00028>.

Xue, C., Yuan, B., Yue, Y., Xu, J., Wang, S., Wu, M., Ji, N., Zhou, X., Zhao, Y., Rao, J., Yang, W., Xiao, C. and Chen, J. (2019). Distinct Disruptive Patterns of Default Mode Subnetwork Connectivity Across the Spectrum of Preclinical Alzheimer's Disease, *Frontiers in Aging Neuroscience*, 11. <https://doi.org/10.3389/fnagi.2019.00307>.

Yamasaki, T., Muranaka, H., Kaseda, Y., Mimori, Y. and Tobimatsu, S. (2012). Understanding the pathophysiology of Alzheimer's disease and mild cognitive impairment: A mini review on fMRI and ERP studies, *Neurology Research International*. <https://doi.org/10.1155/2012/719056>.

Yan, C. and Zang, Y. (2010). DPARSF: a MATLAB toolbox for “pipeline” data analysis of resting-state fMRI, *Frontiers in Systems Neuroscience*, 4, p. 13. Available at: <https://doi.org/10.3389/fnsys.2010.00013>.

Ye, M., Yang, T., Qing, P., Lei, X., Qiu, J. and Liu, G. (2015). Changes of functional brain networks in major depressive disorder: A graph theoretical analysis of resting-state fMRI, *PLoS ONE*, 10(9). <https://doi.org/10.1371/journal.pone.0133775>.

Yokoi, T., Watanabe, H., Yamaguchi, H., Bagarinao, E., Masuda, M., Imai, K., Ogura, A., Ohdake, R., Kawabata, K., Hara, K., Riku, Y., Ishigaki, S., Katsuno, M., Miyao, S., Kato, K., Naganawa, S., Harada, R., Okamura, N., Yanai, K., Yoshida, M. and Sobue, G. (2018). Involvement of the precuneus/posterior cingulate cortex is significant for the development of Alzheimer's disease: A PET (THK5351, PiB) and resting fMRI study, *Frontiers in Aging Neuroscience*, 10(OCT), pp. 1–15. <https://doi.org/10.3389/fnagi.2018.00304>.

Zamani, J., Sadr, A. and Javadi, A. (2021). Evolutionary optimization in classification of early-MCI patients from healthy controls using graph measures of resting-state fMRI, *bioRxiv*. <https://doi.org/10.1101/2021.03.04.433989>.

Zhang, L., Zuo, X.N., Ng, K.K., Chong, J.S.X., Shim, H.Y., Ong, M.Q.W., Loke, Y.M., Choo, B.L., Chong, E.J.Y., Wong, Z.X., Hilal, S., Venketasubramanian, N., Tan, B.Y., Chen, C.L.H. and Zhou, J.H. (2020). Distinct BOLD variability changes in the default mode and salience networks in Alzheimer's disease spectrum and associations with cognitive decline, *Scientific Reports*, 10(1), pp. 1–12. <https://doi.org/10.1038/s41598-020-63540-4>.

Zheng, W., Liu, X., Song, H., Li, K. and Wang, Z. (2017). Altered functional connectivity of cognitive-related cerebellar subregions in alzheimer's disease, *Frontiers in Aging Neuroscience*, 9(MAY). <https://doi.org/10.3389/fnagi.2017.00143>.

Increased Functional Connectivity in Alzheimer's

TABLES

Table 1.

<i>Information of the participants included in this study</i>						
	Group				Between-group differences	
	HC	EMCI	LMCI	AD	<i>f</i>	<i>p</i>
Number	35	29	30	34	-	-
Sex (M/F)	(15 / 21)	(13 / 16)	(18 / 12)	(16 / 18)	-	Chi ² =2.21 <i>p</i> = 0.52
Age \bar{x} (<i>SD</i>)	73.60 (5.75)	71.36 (5.46)	70.63 (8.23)	72.44 (7.09)	1.08	<i>p</i> = 0.36
Years of ed. \bar{x} (<i>SD</i>)	16.37 (2.36)	15.96 (2.41)	16.85 (2.60)	15.5 (2.75)	1.72	<i>p</i> = 0.167
MMSE \bar{x} (<i>SD</i>)	28.53 (1.92)	27.76 (1.94)	27.60 (1.47)	22.69 (2.53)	54.5	<i>p</i> < 0.0001 ^{a b c}
LDELT \bar{x} (<i>SD</i>)	13.50 (3.48)	8.65 (1.80)	4.46 (2.92)	1.31 (1.97)	122.28	<i>p</i> < 0.0001 ^{a b c d e f}
MOCA \bar{x} (<i>SD</i>)	25.49 (1.91)	24.11 (2.50)	21.61 (3.69)	16.5 (5.24)	38.45	<i>p</i> < 0.0001 ^{a b c d f}

Note. ^a AD < EMCI; ^b AD < LMCI; ^c AD < HC; ^d EMCI < LMCI; ^e EMCI < HC; ^f LMCI < HC; The table displays means, standard deviations and differences in age, years of education (Years of ed.), scores in the Mini Mental State Examination (MMSE), in the Scale Logical Memory II (delayed paragraph A recall) (LDELT) and in the Montreal cognitive assessment (MOCA). Statistical analysis of variance (ANOVA) was used to assess differences. Differences in gender were assessed using a Chi Squared test. HC, healthy controls; EMCI, early mild cognitive impairment; LMCI, late mild cognitive impairment; AD, Alzheimer's disease.

Table 2.

Pairs of brain regions showing significant differences in FC between groups when performing a one-way ANOVA

Network	ROI	Network	ROI	P value	Post hoc FC \bar{x} (<i>SD</i>)
Cerebellum	Cerebellum: Crus II (left)	DMN	Parietal lobe	0.0007	AD>EMCI 0.38 (0.2) > 0.13(0.32)
	Cerebellum 2 nd Non-motor: VIIB (right)	Sensory motor	Central region: Postcentral gyrus (left)	0.0021	AD>EMCI 0.47 (0.24) > 0.25 (0.23)
	Vermis 9	Visual II	Occipital superior (Left)	0.0022	AD>NC 0.34 (0.20) > 0.13 (0.25)

Increased Functional Connectivity in Alzheimer's

Visual I	Occipital lobe: medial surface, calcarine fissure (left)	Visual II	Occipital lobe (lateral): Superior occipital gyrus (right)	0.0007	AD > EMCI 0.67 (0.17) > 0.50 (0.20)
	Occipital lobe: inferior surface, Lingual gyrus (right)	Visual II	Occipital inferior gyrus (right)	0.0015	LMCI > EMCI; NC > EMCI 0.62 (0.12) > 0.49 (0.21); 0.62 (0.16)
Auditory	Temporal lobe: middle temporal gyrus (right)	Visual II	Occipital lobe (lateral): Superior occipital gyrus (left)	0.0025	AD < NC 0.11 (0.29) < 0.34 (0.20)
Basal ganglia	Caudate (right)	Dorsal left	Frontal lobe: Inferior frontal gyrus	0.0022	AD > NC 0.45 (0.19) > 0.25 (0.25)
	Subcortical grey nuclei: Caudate nucleus (left)	Dorsal left	Temporal lobe: middle temporal gyrus (left)	0.0022	AD > NC 0.39 (0.21) > 0.22 (0.23)
Thalamus	Sub cortical gray nuclei (right)	Ventrolateral prefrontal cortex	Frontal lobe: Inferior frontal gyrus triangular part (Left)	0.0008	AD > NC 0.50 (0.14) > 0.30 (0.20)

Note. The table displays the ROI to ROI Functional connectivity (FC) results and the differences between groups. HC, healthy controls; EMCI, early mild cognitive impairment; LMCI, late mild cognitive impairment AD, Alzheimer's disease; DMN, default mode network.

Table 3.

<i>Graph theory measures</i>						
Mesure	HC	EMCI	LMCI	AD	<i>p</i>	Group differences
	\bar{x} (<i>SD</i>)	\bar{x} (<i>SD</i>)	\bar{x} (<i>SD</i>)	\bar{x} (<i>SD</i>)		
Path length	1.568 (0.61)	1.606 (0.61)	1.501 (0.577)	1.516 (0.585)	.05	EMCI > LMCI; EMCI > AD

Increased Functional Connectivity in Alzheimer's

Cluster coeff.	0.783 (0.11)	0.776 (0.11)	0.793 (0.04)	0.796 (0.11)	.52	-----
Degree	67.5 (23.98)	51.689 (23.71)	60.534 (24.11)	59.431(24.14)	.02	EMCI<LMCI; EMCI<AD

Note. Table 3 displays results in graph measures: the mean, standard deviation, and the significant differences between groups in path length, cluster coeff. (Clustering coefficient) and degree. The EMCI, early mild cognitive impairment group, presented a higher path length and a lower degree in comparison with the other groups.

Table 4.

Between group differences in mean ROI to ROI dispersion across windows using a one-way ANOVA

Network	ROI	Network	ROI	P value	Post hoc \bar{x} (SD)
Cerebellum	Cerebellum 7b (right)	Sensory motor	Postcentral gyrus (left)	0,0007	AD < EMCI 0.15 (0.07) < 0.21 (0.07)
	Cerebellum 8 (right)	Cerebellum	Cerebellum 7b (right)	0.0008	AD < EMCI; AD < LMCI 0.07 (0.07) < 0.12 (0.06); 0.07 (0.07) < 0.12 (0.07)
Basal ganglia	Caudate (right)	Dorsal right	Middle frontal gyrus orbital (right)	0,0016	HC < EMCI 0.17 (0.063) < 0.22 (0.045)
DMN	Superior frontal gyrus, medial orbital (left)	DMN	Angular gyrus (left)	0,0016	AD < EMCI 0.15 (0.05) < 0.17 (0.052)
	Superior frontal gyrus, medial orbital (left)	Dorsal left	Middle frontal gyrus, orbital (left)	0,0011	AD < EMCI 0.15 (0.06) < 0.17 (0.05)
Auditory	Temporal pole: superior temporal gyrus (left)	Dorsal right	Frontal lobe: Middle frontal gyrus (right)	0,0004	AD < EMCI 0.14 (0.052) < 0.19 (0.062)

Increased Functional Connectivity in Alzheimer's

	Rolandic operculum (left)	Sensory motor	Supplementary motor area (left)	0,0011	LMCI < EMCI; AD < EMCI 0.15 (0.04) < 0.21 (0.07); 0.16 (0.04) < 0.21 (0.07)
Executive function	Superior frontal gyrus orbital (left)	Dorsal left	Supramarginal gyrus (left)	0,0018	HC < EMCI 0.16 (0.05) < 0.22 (0.07)

Note. Overlapping SWA, Sliding Window Analysis, results with a window size of 30 time points (TR = 3 seconds) and an increment of 1 time point for each slide. One-way ANOVA Significant differences between groups at a $p < 0.05$. HC, healthy controls; EMCI, early mild cognitive impairment; LMCI, late mild cognitive impairment AD, Alzheimer's disease.

Table 5:

<i>Differences in FC using the Point Process Analysis</i>					
Network	ROI	Network	ROI	P value	Post hoc
Cerebellum	Cerebellum 10 (right)	Basal ganglia	Amygdala (right)	0,0001	EMCI < LMCI; AD < LMCI 3.03 (2.14) < 6.3 (3.23); 3.61 (2.82) < 6.3 (3.23)
	Cerebellum Crus I (left)	DMN	Angular gyrus (left)	0,0003	LMCI < AD 4.3 (2.71) < 7.05 (0.62)
	Cerebellum crus I (left)	Dorsal left	Middle temporal gyrus (left)	0,0015	EMCI < AD 7.68 (3.21) < 9.97 (3.52)
Visual III	Middle occipital gyrus (right)	DMN	Precuneus (right)	0,0012	LMCI < HC 7.8 (3.74) < 11.22 (3.53)
Basal ganglia	Caudate (right)	Dorsal left	Frontal lobe: Inferior frontal gyrus triangular part (left)	0,0006	EMCI < AD 5.34 (2.37) < 7.9 (2.93)

Increased Functional Connectivity in Alzheimer's

	Parahippocampal (right)	Auditory	Insula (left)	0,0014	HC < AD 3.71 (2.12) < 5.85 (2.74)
	Caudate nucleus (left)	Dorsal left	Inferior frontal gyrus, triangular part (left)	0,0018	HC < AD; EMCI < AD 5.51 (2.48) < 7.76 (3.40); 5.41 (2.47) < 7.76 (3.40)
Thalamus	Sub cortical gray nuclei: Thalamus (right)	Dorsal left	Inferior frontal gyrus triangular part (left)	0,0020	AD > HC 8.97 (3.08) > 6.31 (2.44)
DMN	Superior frontal gyrus, medial orbital (right)	Dorsal right	Parietal superior gyrus (right)	0,0012	HC < LMCI 7.14 (3.82) < 7.36 (3.69)
	Superior frontal gyrus medial orbital (right)	Dorsal right	Angular gyrus (right)	0,0016	EMCI < LMCI; HC < LMCI 6.51 (3.36) < 8.1 (3.35); 7.25 (3.70) < 8.1 (3.35)
Auditory	Insula (left)	Dorsal left	Inferior frontal gyrus triangular part (left)	0,0009	HC < AD 6.8 (2.72) < 9.58 (3.66)
	Insula (left)	Dorsal (right)	Inferior frontal gyrus triangular part (right)	0,0015	HC < AD 5.4 (2.88) < 7.14 (3.87)
Executive function	Superior frontal gyrus medial (left)	Dorsal (right)	Inferior frontal gyrus triangular part (right)	0,0014	EMCI < LMCI 6.96 (3.25) < 8.33 (3.21)

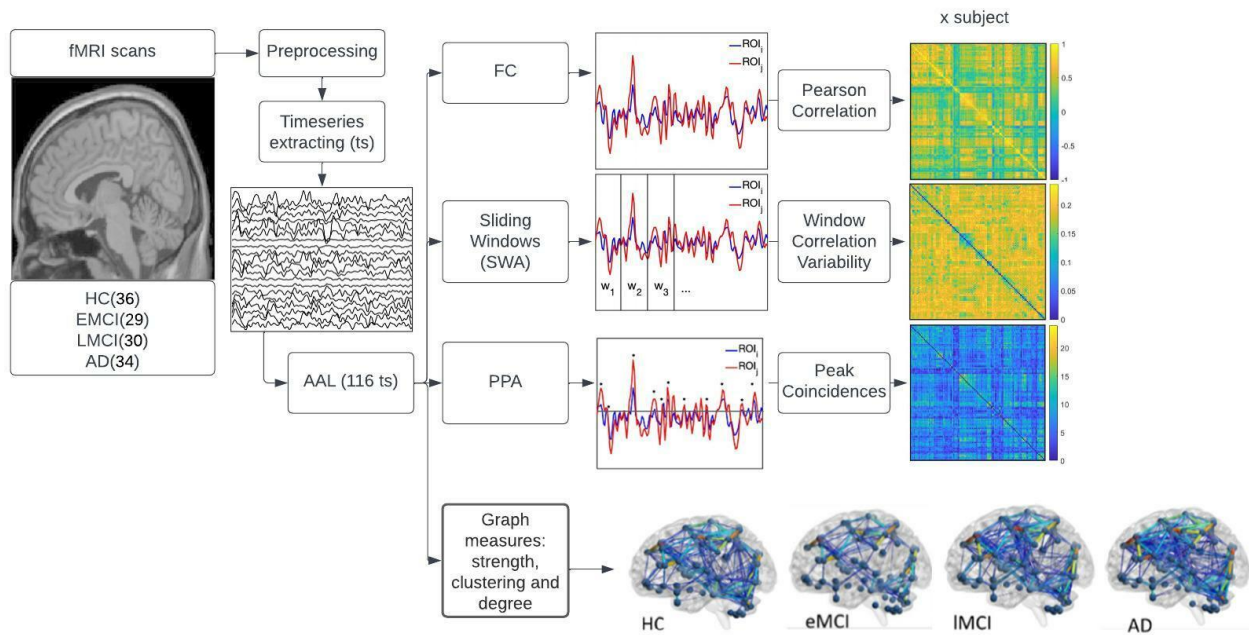
Note. Table 5 displays the differences between groups in dynamic functional connectivity (dFC) between pairs of regions (ROIs) measured by points that surpass a threshold of BOLD signal activation of 1 standard deviation (sd). HC, healthy

Increased Functional Connectivity in Alzheimer's

controls; EMCI, early mild cognitive impairment; LMCI, late mild cognitive impairment AD, Alzheimer's disease; DMN, default mode network.

FIGURES

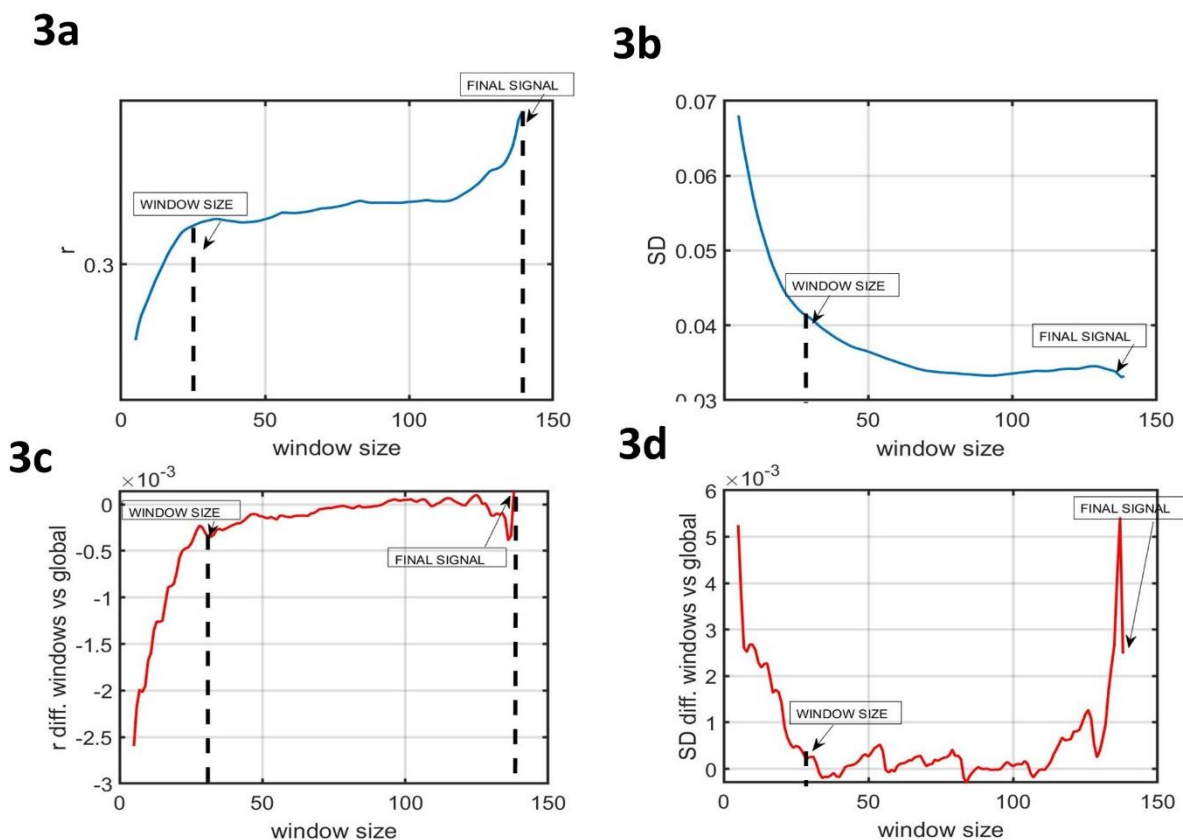
Figure 1



Note. Figure 1 displays the methods used in the study. First the fMRI and T1 image acquisitions were downloaded from the Alzheimer's disease neuroimaging initiative (ADNI) database. Then the images were preprocessed using the DPARSF pipelines. Timeseries from 116 regions of interest (ROIs) were extracted using the automated anatomical labelling (AAL) atlas. These 116 timeseries were used to perform three main analyses displayed on the right side of the figure namely, Functional Connectivity (FC), Sliding Window Analysis (SWA) and Point Process Analysis (PPA). The top right side of the figure shows the FC where the Pearson's Correlation Coefficient of each pair of regions was computed using the mean whole signal of each timeseries; the middle right side of the figure shows the SWA, that consisted on dividing the timeseries into non-overlapping windows, computing the FC for each window and determining the variability in FC across windows; the third plot on the right side of the image shows the PPA, this is a single frame analysis where points that surpass the threshold of $1SD$ of each timeseries were selected, coincident points between pair of regions where summed and displayed in a matrix of addition. The fourth plot on the right side of the image displays the graph measures conducted in the study. To test statistical significance of each analysis a one-way-ANOVA with multiple comparison tests were conducted corrected with Bonferroni at $p < .05$.

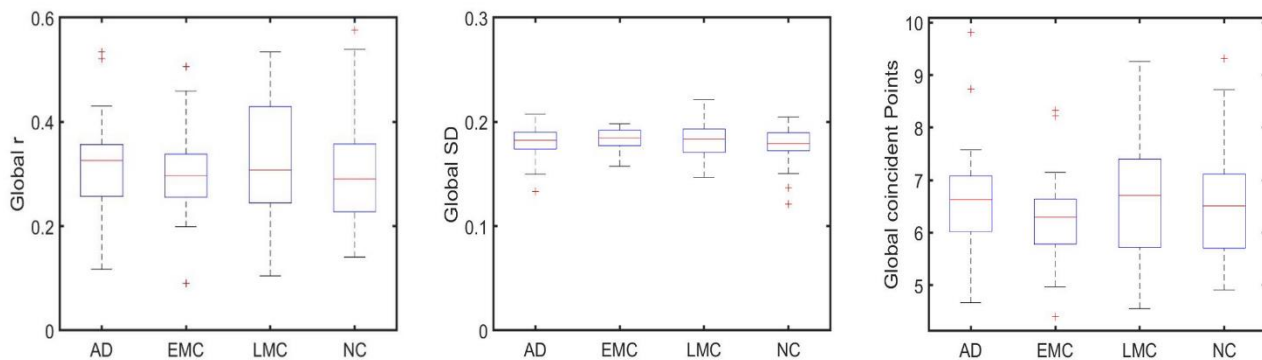
Figure 2

Increased Functional Connectivity in Alzheimer's



Note. The Figure represents the window size analysis before conducting the sliding window correlation analysis. **2a.** Global FC as a function of window size. The Y axis represents the mean FC or correlation of all the ROI to ROI correlations windows of a participant with AD. The X axis shows the 140 time points of the whole time series. Each time point represents 3s (TR= 3s). The mean correlation varies as a function of window size. Shorter windows present a lower mean correlation while windows from 30 or above present a higher correlation. **2b.** The Y axis represents the mean standard deviation (SD) of the SD of all the ROI to ROI correlations across windows of a participant with AD. The X axis shows that this mean SD varies as a function of window size. Shorter windows present a higher variability while windows of 30 time points or above present a lower SD. **2c.** The plot shows the difference between the mean correlation of all ROI to ROIs using a certain window size and the global static **2d.** The difference in the variability amongst windows using window sizes higher than 30 fluctuates around 0, meaning that results in SWA are almost the same, no matter the window length chosen.

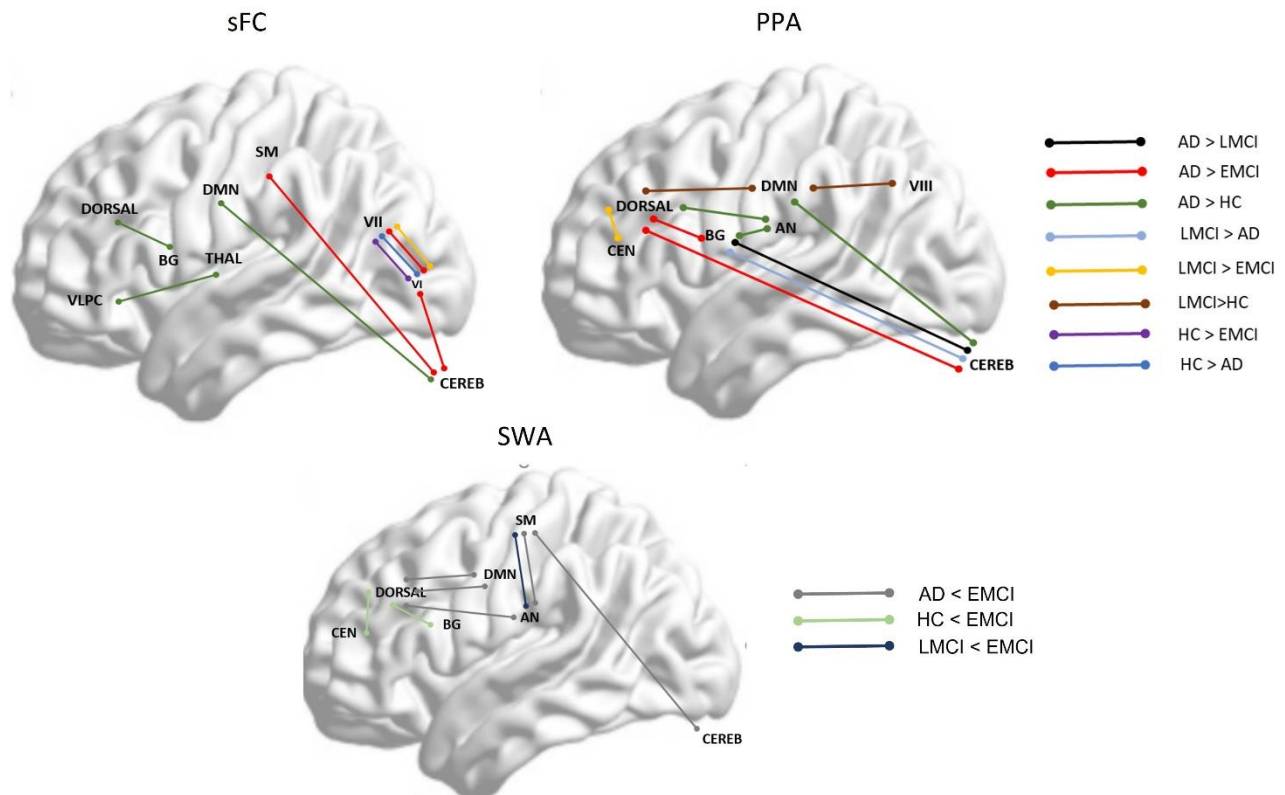
Figure 3



Increased Functional Connectivity in Alzheimer's

Note. Figure 3 shows no significant differences between groups were found globally in FC (subplot on the left), SWA (subplot in the middle) and PPA (subplot on the right).

Figure 4



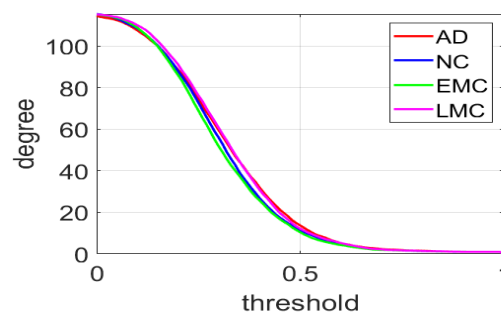
Note. Figure 4 shows between group significant differences between specific brain networks in: static functional connectivity (sFC), point process analysis (PPA) and variability in functional correlation across windows applying sliding window correlation analysis (SWA). Dorsal = dorsal network; DMN = Default Mode Network; SM = Somatosensory network; VLPC = Ventrolateral prefrontal cortex; BG = Basal Ganglia; Thala = thalamus; VI = Visual network I; VII = Visual network II; Cereb = Cerebellum; CEN = Central Executive Network; AN = Auditory Network.

Increased Functional Connectivity in Alzheimer's

Supplementary Material

Supplementary 1. Optimization of thresholding based on mean degree and small-world estimation

After computing the FC, the correlation (FC) matrices were transformed into binary matrices to compute graph measures (raw correlation values were used). Until the moment it does not exist an accurate way to choose a threshold to study brain networks, however, several researchers using rsfMRI datasets used a threshold between 0.2 to 0.5 as it provided scale freeness and enabled differentiation of groups. For this reason, an analysis of our data to ensure these two characteristics was conducted. In this analysis, we assessed the global degree using different correlation thresholds, i.e., from 0.1 to 0.5 at intervals of 0.01. A threshold of 0.3 was finally chosen because the mean degree when using this threshold is not too high not too low, satisfying the smallworldness feature of the brain, this way those nodes that are highly connected with several regions and the ones that are only connected to a few regions were captured. Moreover, this threshold allows a good discrimination across groups (see plot below). Those ROI-to-ROI connections that exceeded a threshold of 0.3 (Pearson's correlation coefficient raw value) were set to 1, whilst those below 0.3 were set to 0.



Note. *The figure shows the mean degree (mean number of nodes connected to another node), y axis and the threshold set, x axis. Smallworldness is most preserved at a threshold between 0.3 and 0.5. Showing that the mean degree is not too high, not too low, revealing a few highly connected networks and many with a low degree. It also shows that differentiation between groups is more evident when binarizing the matrix using one of this range of thresholds.*

Researchers in the following studies used a similar threshold to binarize FC matrices before performing graph theory:

- Ahmadi, H., Fatemizadeh, E., & Motie-Nasrabadi, A. (2020). Multiclass classification of patients during different stages of Alzheimer's disease using fMRI time-series. *Biomedical Physics and Engineering Express*, <https://doi.org/10.1088/2057->

- Aurich, N. K., Filho, J. O. A., da Silva, A. M. M., & Franco, A. R. (2015). Evaluating the reliability of different preprocessing steps to estimate graph theoretical measures in resting state fMRI data. *Frontiers in Neuroscience*, (FEB), <https://doi.org/10.3389/fnins.2015.00048>
- Ng, A. S. L., Wang, J., Ng, K. K., Chong, J. S. X., Qian, X., Lim, J. K. W., Tan, Y. J., Yong, A. C. W., Chander, R. J., Hameed, S., Ting, S. K. S., Kandiah, N., & Zhou, J. H. (2021). Distinct network topology in Alzheimer's disease and behavioral variant frontotemporal dementia. *Alzheimer's Research and Therapy*, 13(1). <https://doi.org/10.1186/s13195-020-00752-w>
- Ye, M., Yang, T., Qing, P., Lei, X., Qiu, J., & Liu, G. (2015). Changes of functional brain networks in major depressive disorder: A graph theoretical analysis of resting-state fMRI. *PLoS ONE*, 10(9). <https://doi.org/10.1371/journal.pone.0133775>

Supplementary 2. Steps Point Process Analysis

Below, an explanation of the three steps conducted in the PPA are explained:

1. **Signals thresholding** ($1sd$). First, signals were thresholded, as shown in the figure below.

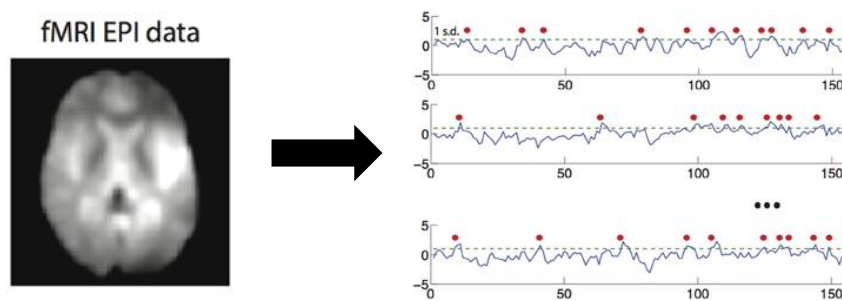


Figure extracted from Cifre et al., 2017 (reference below).

2. **Co-activation matrices:** then, all those points of the timeseries that surpassed $1 SD$ of the BOLD signal were given a 1 (relevant) and the rest were given a 0 (non-relevant), then co-activation matrices for each timepoint were generated, e.g., in timepoint 1 of ROI 1 and ROI 2 the signal is relevant as both surpass $1 SD$, in timepoint 1 ROI 1 and timepoint 1 ROI 3 in time the signal is not relevant as it does not surpass the threshold ($< 1 SD...$). This is conducted for all the 140 timepoints for each 116 pairs or regions. The figure below displays whether each pair of ROIs are coincident in each timepoint.

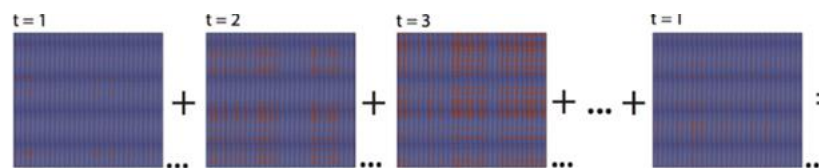


Figure extracted from Tagliazucchi et al., 2016 (reference below).

3. **Matrix of addition:** Then, a matrix of addition was extracted for each pair of ROIs, i.e., connectivity between ROI 1 and ROI 2 in PPA is acquired by adding all the timepoints that were relevant in all the time series. Similar to a correlation matrix, but here instead of correlation between pairs of regions we are computing a summation of the number of relevant points through the timeseries.

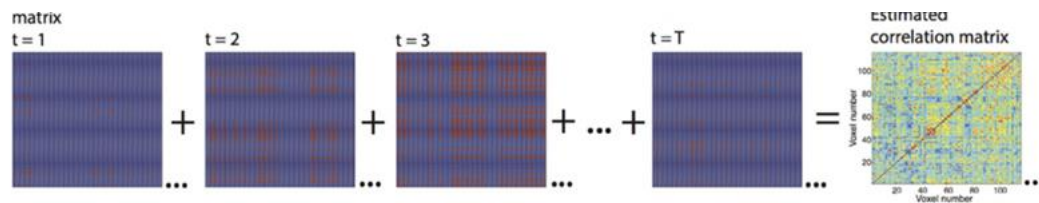


Figure extracted from Tagliazucchi et al., 2016 (reference below).

See these references below for a comprehensive explanation of the method:

Cifre, I., Zarepour, M., Horowitz, G., Cannas, S. and Chialvo, D. (2017). On why a few points suffice to describe spatiotemporal large-scale brain dynamics, arXiv.

<https://doi.org/10.48550/arxiv.1707.00759>.

Cifre, I., Zarepour, M., Horowitz, S.G., Cannas, S.A. and Chialvo, D.R. (2020). Further results on why a point process is effective for estimating correlation between brain regions, *Papers in Physics*, 12(June), pp. 1–8. <https://doi.org/10.4279/pip.120003>.

Tagliazucchi, E., Balenzuela, P., Fraiman, D. and Chialvo, D.R. (2012). Criticality in large-scale brain fmri dynamics unveiled by a novel point process analysis, *Frontiers in Physiology*, 3 FEB.

<https://doi.org/10.3389/fphys.2012.00015>.

Tagliazucchi, E., Siniatchkin, M., Laufs, H., & Chialvo, D. R. (2016). The voxel-wise functional connectome can be efficiently derived from co-activations in a sparse spatio-temporal point-process. *Frontiers in Neuroscience*, 10(AUG). <https://doi.org/10.3389/fnins.2016.00381>.

4. **Study 3. The distance-dependent brain functional connectivity is normal in ipsilateral but disturbed between homologous-contralateral regions in Alzheimer disease (*Ready to submit*)**

The distance-dependent brain functional connectivity is normal in ipsilateral but disturbed between homologous-contralateral regions in Alzheimer disease

Ignacio Cifre^{1,2,*}, Lucia Penalba-Sánchez¹, Jeremi K. Ochab³ Nicolás Rubido^{4,5} and Dante R. Chialvo^{2,6}

¹*Facultat de Psicologia, Ciències de l'educació i de l'Esport, Blanquerna, Universitat Ramon Llull, Barcelona, Spain*

²*Center for Complex Systems & Brain Sciences (CEMSC³), Instituto de Ciencias Físicas (ICIFI), Escuela de Ciencia y Tecnología, Universidad Nacional de San Martín, Buenos Aires, Argentina*

³*Institute of Theoretical Physics and Mark Kac Center for Complex Systems Research, Jagiellonian University, Kraków, Poland*

⁴*University of Aberdeen, Aberdeen Biomedical Imaging Centre, AB25 2ZG Aberdeen, United Kingdom*

⁵*Universidad de la República, Instituto de Física de Facultad de Ciencias, 11400 Montevideo, Uruguay*

⁶*Consejo Nacional de Investigaciones Científicas y Tecnológicas (CONICET), Buenos Aires, Argentina*

Correspondence*:

Ignacio Cifre. FPCEE, Cister 34, 08022, Barcelona, Spain
ignaciocl@blanquerna.url.edu

2 ABSTRACT

3 Neuro-degenerative diseases induce a spectrum of brain alterations, including gray and white
4 matter disturbances. The focus of the present work is to determine the manner in which the
5 functional connectivity (FC) between pairs of brain regions decays as a function of their mutual
6 distance. We find that in Alzheimer's disease (AD) patients, the FC between homologous
7 contralateral regions decays faster (with distance) than in healthy subjects (HS). In contrast,
8 we observe no differences in the decay for intra-hemispheric regions, suggesting a probable
9 involvement of the Corpus Callosum. Our analysis uncovers a FC deficit between contralaterally
10 distant homologous areas, which in turn is significantly correlated with the patient's executive
11 function and cognitive impairment scores but not with their age and degree of brain atrophy.
12 Overall, our results highlight a new aspect of the structural/functional changes in AD patients and
13 its possible consequences over brain function.

14

15 **Keywords:** Alzheimer's disease; Aging; Functional Neuroimaging; Corpus Callosum.

INTRODUCTION

16 Alzheimer’s disease (AD) is a progressive and degenerative disease that affects the central nervous system
 17 in many different ways; it produces inflammation (1; 2) leading to atrophy and cellular death (3; 4; 5).
 18 These effects cause various behavioral alterations, such as memory loss, reduction in daily activities (6),
 19 anosognosia (7), and other psychological symptoms which are present even years before a diagnosis
 20 is reached (8). Despite the intensive research activity on AD - there are over 12 thousand PubMed
 21 “Alzheimer’s disease” entries just in 2020 and 257 of those are systematic reviews - we still lack a complete
 22 understanding of what are its causes, how it develops, or how to treat it.

23 The loss of white matter across the brain due to AD has been particularly studied in the Corpus Callosum
 24 area, leading to the suggestion that AD may be seen as an inter-hemispheric *disconnection syndrome* (9).
 25 This idea, for example, motivated studies using behavioral experiments (10; 11; 12), where patients were
 26 seen to perform better on ipsi-hemispheric tasks. The same motivation was behind electro-encephalography
 27 studies (13), which revealed lower coherence between hemispheres. Results in the same line were reported
 28 using magneto-encephalography (14; 15), and diffusion tensor imaging (16), where the Corpus Callosum’s
 29 fractional anisotropy alterations were found to be related to frontal inter-hemispheric differences with
 30 respect to healthy subjects (HSs). However, white-matter losses in the Corpus Callosum are not AD-specific,
 31 or location specific (other regions also experience white-matter losses), but rather a common aspect of
 32 neuro-degenerative diseases. In particular, Fronto-Temporal Dementia (bvFTD) (17; 18; 19) has been
 33 found to be more affected frontally than at the Corpus Callosum (20; 21).

34 During the last two decades, resting-state functional imaging (rsfMRI) became central in neuroimaging,
 35 in particular to develop biomarkers of neuro-degenerative diseases (22; 23). For example, studies have
 36 revealed alterations of the Resting-State Networks (RSN) in AD patients, particularly of the Default-Mode
 37 Network (DMN), as reported by (24; 25; 26) (for a detailed review, see Table 1 of (23)) and bvFTD patients,
 38 reported in, for instance, (27; 28; 29). Other reports demonstrated alterations to the network’s topological
 39 characteristics of AD patients (30; 31; 32), showing decrease in clustering coefficients, path length, and
 40 other network characteristics, such as hub connectivity (33; 30; 34). In spite of this vast literature, it is still
 41 unclear how potential alterations in the Corpus Callosum due to AD may alter the functional connectivity,
 42 probably with the exception of the results in (35).

43 In this work, we study an AD dataset demonstrating a striking alteration of the functional connectivity
 44 between brain regions which depend on their mutual distance and hemispheric location (ipsi/contralateral).
 45 The results show that the correlations between the BOLD time-series recorded from homologous
 46 contralateral regions decay more rapidly (with distance) in patients with AD than in healthy subjects,
 47 suggesting a key role of the Corpus Callosum in the functional alterations of the disease.

	HS (n=22)	AD(n=17)	Difference
Sex			
Male	8	7	
Female	14	10	n.s.
Age	75.23	74.00	n.s.
MMSE	28.82(1.13)	21.154(3.41)	p<.001
MoCA	25.17(2.24)	16.6(4.27)	p<.001

Table 1. Sample Demographics

DATASETS AND METHODS

48 The datasets analyzed here were obtained from the Alzheimer's Disease Neuroimaging Initiative (ADNI)
49 database (<https://adni.loni.usc.edu>, (36; 37; 38; 39)). The data corresponding to subject scores were
50 obtained from the same database at <https://adni.loni.usc.edu/data-samples/access-data/>, for MMSE and
51 MoCA in the Section "Study Data", subsection Assessments Neuropsychological and for the Atrophy
52 in the Section "Study Data", subsection Imaging. The data-set is composed of 22 Healthy Subjects (HS;
53 14 women; age $\bar{X} = 76.5[7.57]$) and 17 participants with Alzheimer's Disease (AD; 7 women; age
54 $\bar{X} = 76.64[8.02]$) (Further details are shown in Table 1).

55 Data acquisition and preprocessing

56 Functional volumes were acquired using a Philips Intera 3T, consisting of 48 slices (3.3mm
57 thickness)(number of volumes=140; TR = 3000ms; TE = 30ms; Flip angle = 90; matrix 64x64). Functional
58 data were preprocessed using statistical parametric mapping software (SPM12; [http:// fil.ion.ucl.ac.uk/spm](http://fil.ion.ucl.ac.uk/spm))
59 and DPARFS toolbox (<http://rfmri.org/DPARSF>). After deleting the first five volumes, the images were
60 slice-time corrected, aligned to the mean volume of the session scanning, normalized (EPI template)
61 and smoothed (using an 8-mm full-width half-maximum Gaussian kernel). The final spatial resolution of
62 the images was 3x3x3mm. A total of 116 time-series of the mean BOLD activity from each ROI were
63 extracted following the parcellation on the AAL atlas (40). These time series were correlated (using Pearson
64 correlation, unless stated otherwise), to obtain a 116x116 correlation matrix for each subject. To describe
65 the correlation between the ROI's activity as a function of distance, the Euclidean distances between each
66 pair of ROI centroids were extracted from the AAL atlas data. We remark that these values do not represent
67 necessarily geodesic distances, (i.e., those that the tracks may traverse to connect with the interacting
68 ROI's).

RESULTS

69 Functional connectivity is usually described as a scalar measure, i.e., a single number that represent the
70 correlation between two regions. In this work, instead, we attempt to explore FC as a function that estimate
71 how the correlation decays as a function of the distance. Therefore, this section is organized as follows:
72 First, the similarities and differences of scalar FC (see Fig. 1) are presented. Then, how FC decays as a
73 function of distance is explored (in Fig. 2). Such work unveils the fact that BOLD correlation decays faster
74 between homologous contralateral ROIs. Then, control for possible artifacts are described (Figs. 4 and 5)
75 including the analysis of the correlation decay in the brain three main axis but within the same hemisphere.
76 In these computations, the FC value may involve tracks of comparable lengths, but excludes any structure
77 traversing the Corpus Callosum. Then it is tested whether the decay could be related to subjects' motion,
78 such as head rotation or translation (Fig. 3), as it has been shown that movement can alter functional
79 connectivity. Subsequently, it is explored whether the differences may be related with other participant's
80 variables, such as brain atrophy, executive functioning and cognitive impairment scores (Fig. 5).

81 Figure 1 illustrates the basic statistics computed in the two groups of subjects studied. Panels A and B
82 shows the histogram of the Pearson correlation ($\langle r \rangle$) values computed for the BOLD signal recorded
83 from all pairs of ROIs. As expected, the distributions are centered at null values, for both AD and HS
84 groups, however notice that there are significant differences, specially for relatively small $\langle r \rangle$ values.
85 The group average correlation matrices for the 116×116 ROIs are depicted in Panels C and D. In these
86 matrices (as well as those in E and F) the ROIs entries are grouped according to which left (L) and right
87 (R) hemispheres and which resting state network they belong (denoted with labels and color codes). Panel
88 E depicts the distance matrix for the AAL atlas used in this study because, as it was mentioned already, we

89 are interested not only on the potential alterations of the FC values, but also on its decay with the ROIs
 90 mutual distance.

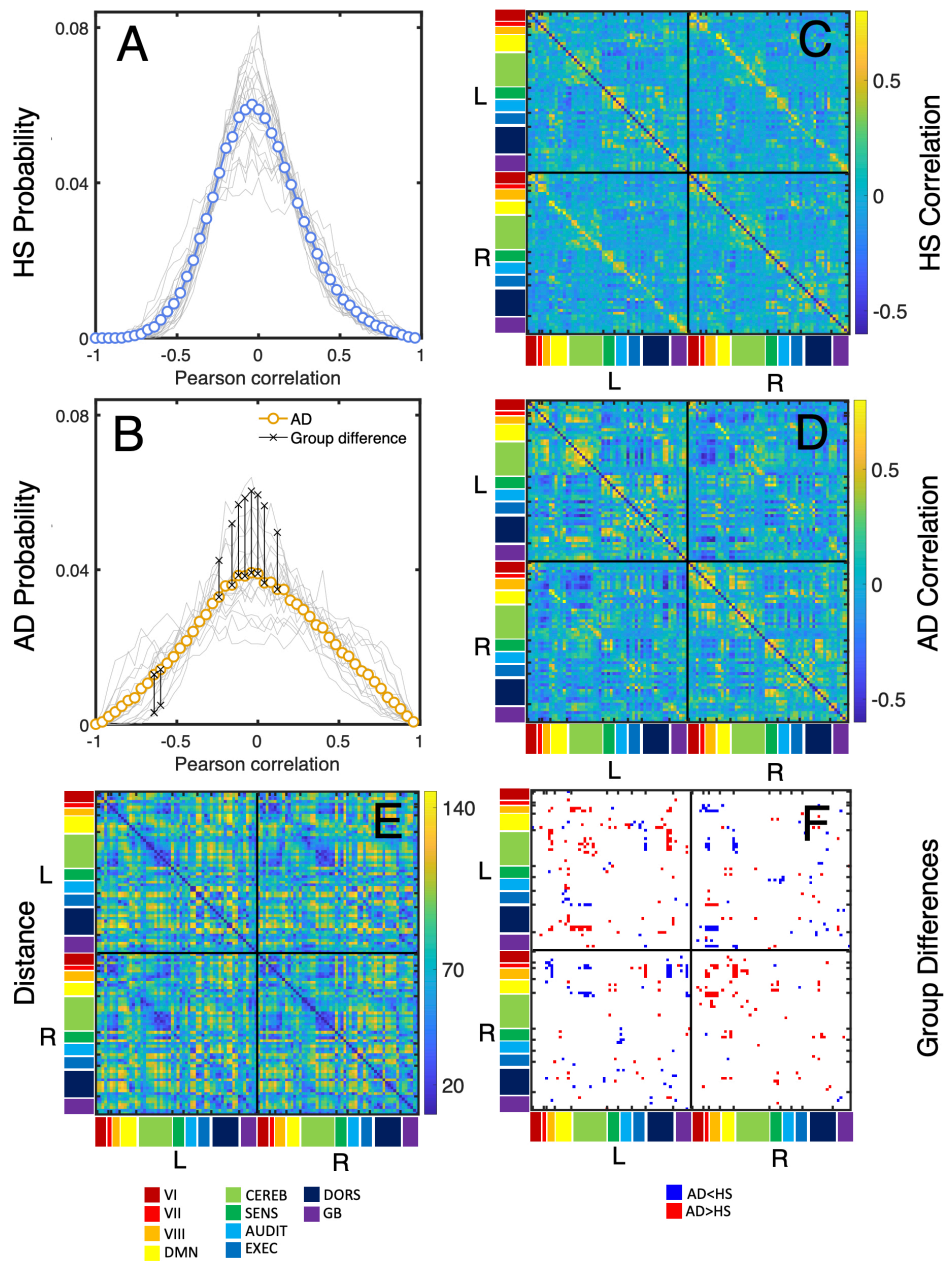


Figure 1. Summary of the basic correlation statistics computed from the BOLD time series in the Healthy Subjects (HS) and Alzheimer Disease (AD) groups. Panels A and B show the distribution of correlations between all pairs of ROIs in HS and AD subject, using solid lines with circles for the group average and thinner gray lines for the single subject distributions. The AD and HS correlation values exhibiting significant differences are denoted with asterisks in Panel B (t-Student test, with Bonferroni corrections at $p < .001$). Panels C and D correspond to the group average correlation matrix between pairs of ROIs BOLD time series for the HS and AD subjects, respectively. As a reference, Panel E illustrates the mutual distances between ROIs, (from the AAL atlas (40)). The results in Panel F identify the ROIs pairs that exhibit significant group FC differences (t-Student test, with Bonferroni corrections $p < .001$).

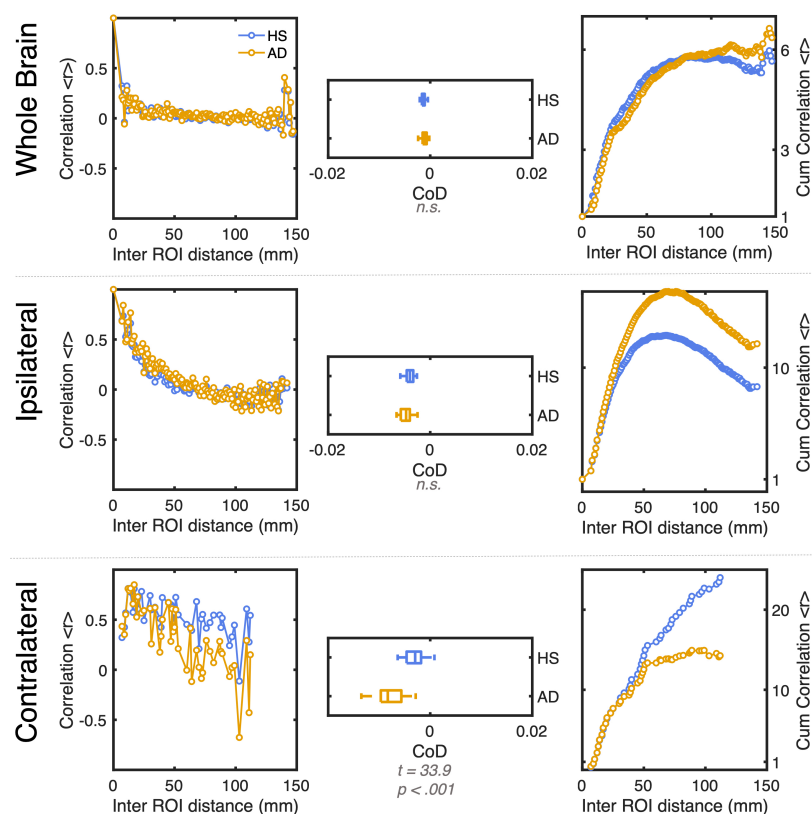


Figure 2. Distance-dependent correlations between ROIs as a function of their centroids distance. On the left panels the values correspond to the standard Pearson correlation and those on the right panels to their cumulative values, both as a function of distance. Top panels shows for the Whole brain ($n = 116 \times 116$), middle ones for ipsilateral ROIs ($n = 58 \times 58$) and the bottom panel the homologous contralateral ROIs ($n = 58$). The center panels show, as bar plots, the fitted average slopes of decay, CoD for all cases. Note that the AD group exhibits a significantly ($p < .001$) faster decay of the correlation for the homologous contralateral ROIs.

91 Distance-dependent functional connectivity

92 It is accepted that, in general, the FC of two brain regions nearby is relatively high and that it progressively
 93 decays with distance (41; 42). The interest here is limited to determine if a *large-scale* pattern of FC decay
 94 can be a useful healthy metric. Of course, considering the intricacies of the brain morphology and structure
 95 a precise fitting is out of the question, rather the objective is to find a simple non-parametric index that
 96 suffice to identify such potential pattern of decay. We compare the correlations decays as a function of
 97 the distance between the ROIs. Three cases are considered here, as presented in Fig. 2: In panel A the
 98 whole-brain correlations (i.e., for all pairs of ROIs) are considered. In the results of panel B only the
 99 computations of the ipsilateral correlations are considered (i.e., between ROIs from the same hemisphere).
 100 Finally, the results on panel C show the correlations from the activity of homologous contralateral regions
 101 (for instance: auditory left with auditory right, somatosensory left with somatosensory right, and so on).
 102 For better visualization (but not for statistical purposes) on the right panels the same data is plotted
 103 as cumulative correlations. This format helps to emphasize the monotonic increasing behaviour of the
 104 correlations vs. distance function exhibited by the homologous contralateral pairs, which contrast with the
 105 non-monotonicity of the other cases.

106 As a simple metric of the pattern of decay, we computed the linear slopes of the correlation decays,
 107 dubbed here CoD . This index estimates the decay rate (i.e., the negative slope) for the Pearson correlation

108 value between pairs of ROIs as a function of the distance between the ROIs' centroids). The resultant slopes
 109 helped us to quantify the possible differences between the two groups of subjects. Simple inspection of the
 110 bottom plots of Fig. 2 reveals that the homologous contralateral correlations of the AD patients decay faster
 111 in comparison with the HS group. The statistical analysis, as shown in the box-plots of Fig. 2 confirm that,
 112 there are significant differences between the CoD obtained from homologous contralateral ROIs ($t = 33.9$;
 113 $p < .001$). These results are robust, despite the small sample and the simplicity of the CoD definition, we
 114 found that similar differences are obtained under changes in the definition of the CoD (see Appendix).
 115

116 Changes in the CoD are unrelated to head motion

117 Since it is well-known that resting-state functional connectivity can be severely contaminated by the
 118 subject's head motion during recording (43) this issue need to be analyzed. This was done by computing
 119 the linear regression between the value of CoD and the mean rotation, as well as between CoD and the
 120 mean translation. Results are shown in Fig. 3, where it can be seen that none of the regression models
 121 resulted in significant correlations for either data-set or group studied.

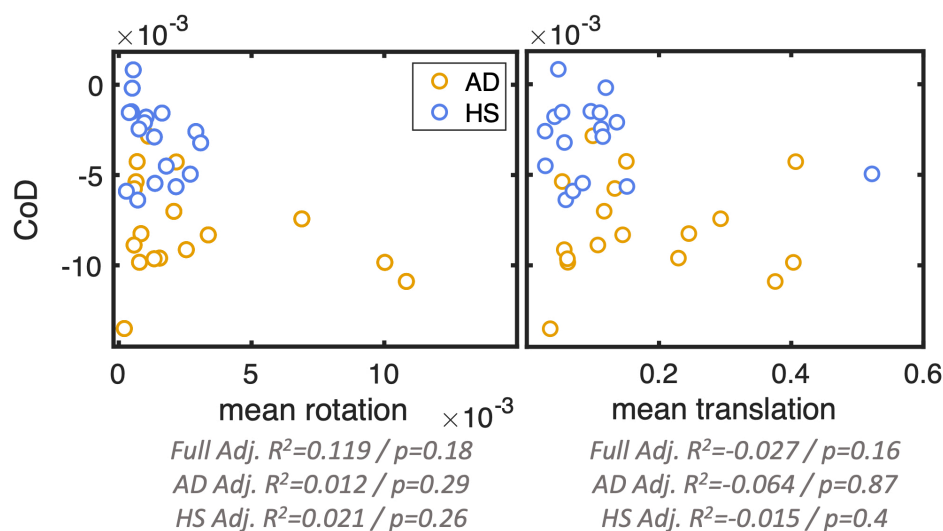


Figure 3. Linear regression between movement and correlation decay with distance, CoD . The linear regression between subjects' averaged-rotation (left panel) and translation (right panel) with CoD for the full sample and for each group (all $p > .05$) are denoted inside each subplot by the R^2 for each regression and its p-value.

122 Changes in the CoD are absent in intra-hemispheric data

123 A second test, conducted to clarify the origin of the differences found, is to compare the correlations
 124 between ipsi-lateral pairs of ROIs with comparable distance to those of the homologous contra-lateral ROI
 125 pairs. In that way, if an unknown hidden process affects the correlation globally must also appear in these
 126 test datasets. To do that, the correlation results were split into 3 main axes: antero-posterior, left-right, and
 127 superior-inferior, where the correlation and distance are computed for each pair of ROIs as long as one
 128 of these planes is crossed. For example, when computing antero-posterior ROI pairs, the correlation is
 129 computed only if there is a change in the Y coordinate's sign between the ROIs while X and Z coordinates
 130 remain unchanged. The results of these calculations show no existence of significant differences except
 131 for an isolated pairs of ROIs belonging to the X plane (see arrow in Fig. 4B, (all $p < .01$, Bonferroni
 132 corrected).

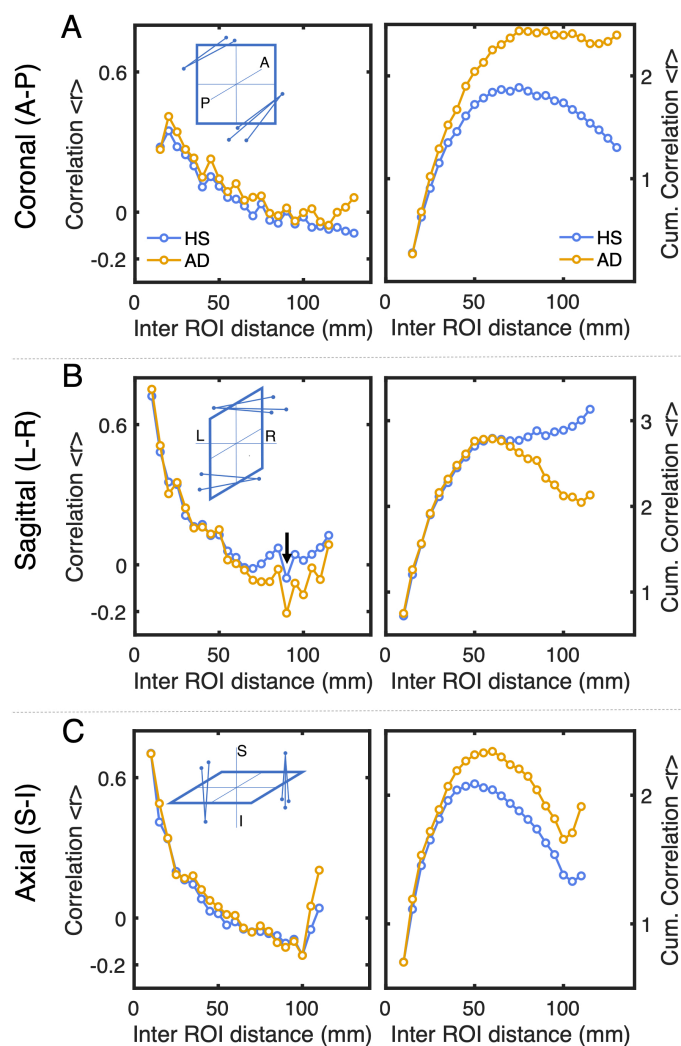


Figure 4. Intra-hemispheric distance-dependent correlations computed between areas crossing the anterior-posterior coronal plane (panel A, pairs of ROIs computed $n = 730$), the sagittal mid-plane (panel B, pairs of ROIs computed $n = 946$) or the superior-inferior axial plane (panel C, pairs of ROIs computed $n = 950$). Correlations represent (similar to Fig. 2) averages for each group. No significant differences were found between the CoD values from the HS vs AD groups. The black arrow in panel B denotes the only significantly different result (all $p < .01$, Bonferroni corrected), which corresponds to one ROI pair with $d \sim 80$ mm. Insets box diagrams show schematically how the planes are defined. Note that here, in contrast with Fig. 2, all ROIs are selected within the same hemisphere.

133 Changes in CoD relates to Cognitive Impairment and Executive Function scores but not 134 with Age and Atrophy score

135 In order to study whether other measures are related to contra-lateral correlation decays, CoD_m , we
136 apply a linear regression model where CoD is set as dependent variable and Age, Atrophy, Cognitive
137 impairment (measured using Mini Mental State Examination test, MMSE (44)) and Executive Functioning
138 (measured using Montreal Cognitive Assessment, MOCA (45)) values are set as predictors. This model has
139 an adjusted $R^2 = 0.362$ (F-statistic vs. constant model: 4.55, p-value $p = .008$), where MMSE and MOCA
140 result as significant predictors ($R^2 = .311$ and $R^2 = .29$ respectively, both $p < .01$), while Atrophy and
141 Age result non-significant (Fig. 5).

142

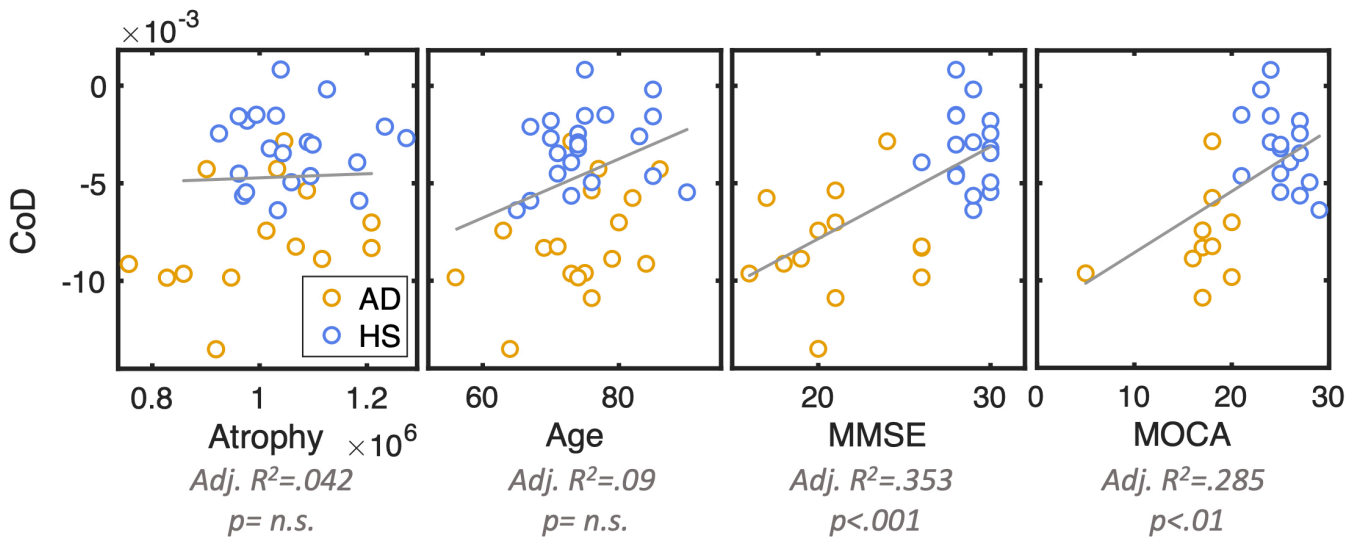


Figure 5. Linear regressions between subjects' variables and their correlation decay slopes, CoD (Fig. 2). Left panel shows age, middle left panel shows atrophy (computed mean from atrophy z-scores on ADNI database), middle right panel shows Cognitive impairment (MMSE score (44)) and right panel shows Executive function (MOCA score (45)). Adjusted R^2 and p-values correspond to each individual regression.

DISCUSSION

143 In this study, we have explored the idea that Alzheimer's Disease may be evaluated as a disconnection
 144 syndrome due to the white matter alteration of long tracks, including the corpus callosum (9). This idea has
 145 been supported by a diversity of results from studies on structural connectivity, electroencephalography
 146 and behavioral studies, like (10; 11; 12) among others. In this work, we evaluate how that degeneration can
 147 be reflected on a differential decay of the functional connectivity over distance in patients in respect to that
 148 of healthy aging subjects. Such index, which we have named as CoD was measured on HS and AD data
 149 from the public available ADNI database.

150 Overall, the results show that healthy subjects exhibit significantly higher correlations on distant
 151 homologous contralateral areas compared to patients with AD (Fig. 2). Interestingly, these differences
 152 are absent when the analysis is done over similar but homotopic distances (as antero-posterior pairs of
 153 ROIs, which are even more distant than contralateral areas (Fig. 4). This finding suggests that mainly tracks
 154 traversing the Corpus Callosum may be responsible for the observed differences. Despite several other
 155 observations reporting structural differences ((17; 18; 19)), to our knowledge, the present results are the
 156 first demonstration at the level of fMRI.

157 Furthermore, regressing CoD with phenotypic measures (Fig. 5), shows that there is a significant
 158 relationship between CoD and executive functions as well as cognitive impairment (47; 48), while it seems
 159 that no relation can be uncovered in this sample for age and brain atrophy.

160 Limitations

161 Several caveats are known to affect the fMRI studies of neuro-degenerative patients. Perhaps the most
 162 important is the well-known fact that head motion produces important artifacts affecting the estimation
 163 of functional connectivity (43). This concern was addressed here by applying regression of both head
 164 rotation and translation to test whether the observed CoD differences were caused by motion. We found no
 165 evidence for a significant association between CoD and measures of head motion. Hence, we consider that
 166 head motion is unlikely to explain the present results. Each group's size was moderate, which of course it

167 can be an important drawback, but also it highlights the magnitude of the disturbance we uncovered which
168 is able to reach significance despite the small sample size. Future work is warranted.

CONCLUSIONS

169 In conclusion, the present results describe the stereotypical way that the correlation of the BOLD signal
170 between brain regions decays as a function of its (Euclidean) distance. The main findings show that the
171 correlation between homologous contralateral ROIs decays more rapidly in AD patients than in healthy
172 subjects. In contrast, we observe no differences when similar computations were conducted within the
173 same hemisphere. These results may be relevant to interpret the functional changes observed in neuro-
174 degenerative diseases, highlighting the need for a combined evaluation of structural/functional changes
175 of the process. The results of this unprecedented study, highlight the merits of a distance-dependent FC
176 metric. Further research is needed to confirm the reliability of these results in other brain conditions, as
177 well as to explore its eventual value as a biomarker signature for neuro-degenerative diseases.

FUNDING

178 Work supported by the MICINN (Spain) grant PID2021-125534OB-I00 by CONICET and Escuela de
179 Ciencia y Tecnología, UNSAM (Argentina) and by the Foundation for Polish Science (FNP) project
180 TEAMNET “Bio-inspired Artificial Neural Networks” (POIR.04.04.00-00-14DE/18-00). The open-access
181 publication of this article is supported in part by the program “Excellence Initiative - Research University”
182 at the Jagiellonian University in Kraków (Poland). Work conducted under the auspice of the Jagiellonian
183 University-UNSAM Cooperation Agreement.

REFERENCES

- 184 [1]Halliday G, Robinson SR, Shepherd C, Kril J. Alzheimer’s disease and inflammation: A review
185 of cellular and therapeutic mechanisms. *Clinical and Experimental Pharmacology and Physiology*.
186 2000;27(1-2):1-8.
- 187 [2]Kinney JW, Bemiller SM, Murtishaw AS, Leisgang AM, Salazar AM, Lamb BT. Inflammation as a
188 central mechanism in Alzheimer’s disease. *Alzheimer’s and Dementia: Translational Research and
189 Clinical Interventions*. 2018;4:575-90. Available from: [https://doi.org/10.1016/j.trci.
190 2018.06.014](https://doi.org/10.1016/j.trci.2018.06.014).
- 191 [3]Teipel SJ, Bayer W, Alexander GE, Zebuhr Y, Teichberg D, Kulic L, et al. Progression of corpus
192 callosum atrophy in Alzheimer disease. *Archives of Neurology*. 2002 feb;59(2):243-8. Available from:
193 <doi=10.1001/archneur.59.2.243>.
- 194 [4]Whitwell JL, Dickson DW, Murray ME, Weigand SD, Tosakulwong N, Senjem ML, et al.
195 Neuroimaging correlates of pathologically defined subtypes of Alzheimer’s disease: A case-control
196 study. *The Lancet Neurology*. 2012;11(10):868-77.
- 197 [5]Pini L, Pievani M, Bocchetta M, Altomare D, Bosco P, Cavedo E, et al. Brain atrophy in Alzheimer’s
198 Disease and aging. *Ageing Research Reviews*. 2016;30:25-48. Available from: [http://dx.doi.
199 org/10.1016/j.arr.2016.01.002](http://dx.doi.org/10.1016/j.arr.2016.01.002).
- 200 [6]Grossberg GT. The ABC of Alzheimer’s disease: Behavioral symptoms and their treatment.
201 *International Psychogeriatrics*. 2002;14(SUPPL. 1):27-49.
- 202 [7]Mak E, Chin R, Ng LT, Yeo D, Hameed S. Clinical associations of anosognosia in mild cognitive
203 impairment and Alzheimer’s disease. *International Journal of Geriatric Psychiatry*. 2015;30(12):1207-
204 14.

- 205 [8]Bäckman L, Jones S, Berger AK, Laukka EJ, Small BJ. Cognitive impairment in preclinical Alzheimer's
206 disease: A meta-analysis. *Neuropsychology*. 2005;19(4):520-31.
- 207 [9]Delbeuck X, Linden MVD, Collette F. Alzheimer's Disease as a Disconnection Syndrome?
208 *Neuropsychology Review*. 2003;13(2):79-92.
- 209 [10]Lakmache Y, Lassonde M, Gauthier S, Frigon JY, Lepore F. Interhemispheric disconnection syndrome
210 in Alzheimer's disease. *Proceedings of the National Academy of Sciences of the United States of*
211 *America*. 1998;95(15):9042-6.
- 212 [11]Jacobson MW, Delis DC, Bondi MW, Salmon DP. Do neuropsychological tests detect preclinical
213 Alzheimer's disease: Individual-test versus cognitive-discrepancy score analyses. *Neuropsychology*.
214 2002;16(2):132-9.
- 215 [12]Reuter-Lorenz PA, Mikels JA. A split-brain model of Alzheimer's disease? Behavioral evidence for
216 comparable intra and interhemispheric decline. *Neuropsychologia*. 2005;43(9):1307-17.
- 217 [13]Pogarell O, Teipel SJ, Juckel G, Gootjes L, Möller T, Bürger K, et al. EEG coherence reflects regional
218 corpus callosum area in Alzheimer's disease. *Journal of Neurology, Neurosurgery and Psychiatry*.
219 2005;76(1):109-11.
- 220 [14]Stam CJ, De Haan W, Daffertshofer A, Jones BF, Manshanden I, Van Walsum AMVC, et al. Graph
221 theoretical analysis of magnetoencephalographic functional connectivity in Alzheimer's disease. *Brain*.
222 2009 oct;132(1):213-24. Available from: [doi/10.1093/brain/awn262](https://doi.org/10.1093/brain/awn262).
- 223 [15]Stam CJ, van Straaten ECW. The organization of physiological brain networks. *Clinical*
224 *Neurophysiology*. 2012;123(6):1067-87. Available from: [http://dx.doi.org/10.1016/j.](http://dx.doi.org/10.1016/j.clinph.2012.01.011)
225 [clinph.2012.01.011](http://dx.doi.org/10.1016/j.clinph.2012.01.011).
- 226 [16]Wang Z, Wang J, Zhang H, Mchugh R, Sun X, Li K, et al. Interhemispheric functional and structural
227 disconnection in Alzheimer's disease: A combined resting-state fMRI and DTI study. *PLoS ONE*.
228 2015;10(5):1-16.
- 229 [17]Yamauchi H, Fukuyama H, Nagahama Y, Katsumi Y, Hayashi T, Oyanagi C, et al. Comparison of the
230 pattern of atrophy of the corpus callosum in frontotemporal dementia, progressive supranuclear palsy,
231 and Alzheimer's disease. *Journal of Neurology Neurosurgery and Psychiatry*. 2000;69(5):623-9.
- 232 [18]Matsuo K, Mizuno T, Yamada K, Akazawa K, Kasai T, Kondo M, et al. Cerebral white matter
233 damage in frontotemporal dementia assessed by diffusion tensor tractography. *Neuroradiology*.
234 2008;50(7):605-11.
- 235 [19]Jiskoot LC, Panman JL, Meeter LH, Doppert EGP, Donker Kaat L, Franzen S, et al. Longitudinal
236 multimodal MRI as prognostic and diagnostic biomarker in presymptomatic familial frontotemporal
237 dementia. *Brain*. 2019;142(1):193-208.
- 238 [20]Zhang Y, Schuff N, Du AT, Rosen HJ, Kramer JH, Gorno-Tempini ML, et al. White matter damage in
239 frontotemporal dementia and Alzheimers disease measured by diffusion MRI. *Brain*. 2009;132(9):2579-
240 92.
- 241 [21]Lu PH, Lee GJ, Shapira J, Jimenez E, Mather MJ, Thompson PM, et al. Regional differences in white
242 matter breakdown between frontotemporal dementia and early-onset Alzheimer's disease. *Journal of*
243 *Alzheimer's Disease*. 2014;39(2):261-9.
- 244 [22]Vemuri P, Jones DT, Jack CR. Resting state functional MRI in Alzheimer's disease; 2012.
- 245 [23]Badhwar AP, Tam A, Dansereau C, Orban P, Hoffstaedter F, Bellec P. Resting-state network dysfunction
246 in Alzheimer's disease: A systematic review and meta-analysis. *Alzheimer's and Dementia: Diagnosis,*
247 *Assessment and Disease Monitoring*. 2017;8:73-85. Available from: [https://doi.org/10.](https://doi.org/10.1016/j.dadm.2017.03.007)
248 [1016/j.dadm.2017.03.007](https://doi.org/10.1016/j.dadm.2017.03.007).

- 249 [24]Lehmann M, Madison CM, Ghosh PM, Seeley WW, Mormino E, Greicius MD, et al.
250 Intrinsic connectivity networks in healthy subjects explain clinical variability in Alzheimer's
251 disease. *Proceedings of the National Academy of Sciences of the United States of America*.
252 2013;110(28):11606-11.
- 253 [25]Zhong Y, Huang L, Cai S, Zhang Y, von Deneen KM, Ren A, et al. Altered effective connectivity
254 patterns of the default mode network in Alzheimer's Disease: An fMRI study. *Neuroscience Letters*.
255 2014;578:171-5.
- 256 [26]Brueggen K, Fiala C, Berger C, Ochmann S, Babiloni C, Teipel SJ. Early Changes in Alpha Band Power
257 and DMN BOLD Activity in Alzheimer's Disease: A Simultaneous Resting State EEG-fMRI Study.
258 *Frontiers in Aging Neuroscience*. 2017;9:319. Available from: <https://www.frontiersin.org/article/10.3389/fnagi.2017.00319>.
- 260 [27]Jalilianhasanpour R, Beheshtian E, Sherbaf G, Sahraian S, Sair HI. Functional Connectivity in
261 Neurodegenerative Disorders. *Topics in Magnetic Resonance Imaging*. 2019 dec;28(6):317-24.
262 Available from: <https://journals.lww.com/10.1097/RMR.0000000000000223>.
- 263 [28]Filippi M, Agosta F, Scola E, Canu E, Magnani G, Marcone A, et al. Functional network connectivity
264 in the behavioral variant of frontotemporal dementia. *Cortex*. 2013 oct;49(9):2389-401. Available
265 from: <http://dx.doi.org/10.1016/j.cortex.2012.09.017>.
- 266 [29]Hafkemeijer A, Möller C, Dopper EGP, Jiskoot LC, van den Berg-Huysmans AA, van Swieten JC, et al.
267 A Longitudinal Study on Resting State Functional Connectivity in Behavioral Variant Frontotemporal
268 Dementia and Alzheimer's Disease. *Journal of Alzheimer's Disease*. 2016 nov;55(2):521-37. Available
269 from: <doi=10.3233/JAD-150695>.
- 270 [30]Supekar K, Menon V, Rubin D, Musen M, Greicius MD. Network analysis of intrinsic functional brain
271 connectivity in Alzheimer's disease. *PLoS Computational Biology*. 2008 jun;4(6):e1000100. Available
272 from: <doi/10.1371/journal.pcbi.1000100>.
- 273 [31]Buckner RL, Sepulcre J, Talukdar T, Krienen FM, Liu H, Hedden T, et al. Cortical Hubs
274 Revealed by Intrinsic Functional Connectivity: Mapping, Assessment of Stability, and Relation
275 to Alzheimer's Disease. *Journal of Neuroscience*. 2009 feb;29(6):1860-73. Available from:
276 <http://www.jneurosci.org/cgi/doi/10.1523/JNEUROSCI.5062-08.2009>.
- 277 [32]Sedeño L, Couto B, García-Cordero I, Melloni M, Baez S, Sepúlveda JPM, et al. Brain
278 network organization and social executive performance in frontotemporal dementia. *Journal of*
279 *the International Neuropsychological Society*. 2016 feb;22(2):250-62. Available from: </doi/10.1017/S1355617715000703>.
- 281 [33]Liu Y, Wang K, YU C, He Y, Zhou Y, Liang M, et al. Regional homogeneity, functional connectivity
282 and imaging markers of Alzheimer's disease: A review of resting-state fMRI studies. *Neuropsychologia*.
283 2008;46(6):1648-56.
- 284 [34]Dai Z, Yan C, Li K, Wang Z, Wang J, Cao M, et al. Identifying and mapping connectivity patterns of
285 brain network hubs in Alzheimer's disease. *Cerebral Cortex*. 2015;25(10):3723-42.
- 286 [35]Liu Y, Yu C, Zhang X, Liu J, Duan Y, Alexander-Bloch AF, et al. Impaired long distance
287 functional connectivity and weighted network architecture in alzheimer's disease. *Cerebral Cortex*.
288 2014;24(6):1422-35.
- 289 [36]Weiner MW, Veitch DP, Aisen PS, Beckett LA, Cairns NJ, Cedarbaum J, et al. 2014 Update of
290 the Alzheimer's Disease Neuroimaging Initiative: A review of papers published since its inception.
291 *Alzheimer's and Dementia*. 2015;11(6):e1-e120.
- 292 [37]Niu Y, Wang B, Zhou M, Xue J, Shapour H, Cao R, et al. Dynamic complexity of spontaneous
293 bold activity in Alzheimer's disease and mild cognitive impairment using multiscale entropy analysis.

- 294 Frontiers in Neuroscience. 2018;12(OCT):1-13.
- 295 [38]Jie B, Liu M, Shen D. Integration of temporal and spatial properties of dynamic connectivity networks
296 for automatic diagnosis of brain disease. Medical Image Analysis. 2018 jul;47:81-94.
- 297 [39]Huang CC, Huang WM, Chen CH, Zhou ZY, Lin CP. The combination of functional and structural MRI
298 is a potential screening tool in Alzheimer's disease. Frontiers in Aging Neuroscience. 2018;10(SEP):1-
299 9.
- 300 [40]Tzourio-Mazoyer N, Landeau B, Papathanassiou D, Crivello F, Etard O, Delcroix N, et al. Automated
301 anatomical labeling of activations in SPM using a macroscopic anatomical parcellation of the MNI
302 MRI single-subject brain. NeuroImage. 2002 jan;15(1):273-89. Available from: [/doi/10.1006/
303 nimg.2001.0978](https://doi.org/10.1006/nimg.2001.0978).
- 304 [41]Salvador R, Suckling J, Coleman MR, Pickard JD, Menon D, Bullmore E. Neurophysiological
305 architecture of functional magnetic resonance images of human brain. Cereb. Cortex. 2005; 15,
306 1332–1342. Available from: <http://dx.doi.org/10.1093/cercor/bhi016>.
- 307 [42]Expert P, Lambiotte R, Chialvo DR, Christensen K, Jensen HJ, Sharp DJ, Turkheimer F. Self-similar
308 correlation function in brain resting-state functional magnetic resonance imaging. Journal of The Royal
309 Society Interface. 2011; 8 (57), 472-479
- 310 [43]Power JD, Schlaggar BL, Petersen SE. Recent progress and outstanding issues in motion correction in
311 resting state fMRI. NeuroImage. 2015;105:536-51. Available from: [http://dx.doi.org/10.
312 1016/j.neuroimage.2014.10.044](http://dx.doi.org/10.1016/j.neuroimage.2014.10.044).
- 313 [44]Folstein MF, Folstein SE, McHugh PR. "Mini-Mental State": A Practical Method for Grading the
314 Cognitive State of Patients for the Clinician. Journal of Psychiatric Research. 1975;12(3):189-98.
- 315 [45]Nasreddine ZS, Phillips NA, Bédirian V, Charbonneau S, Whitehead V, Collin I, et al. The Montreal
316 Cognitive Assessment, MoCA: A Brief Screening Tool For Mild Cognitive Impairment. Journal of the
317 American Geriatrics Society. 2005;53.
- 318 [46]Smith SM, Fox PT, Miller KL, Glahn DC, Fox PM, Mackay CE, et al. Correspondence of the brain's
319 functional architecture during activation and rest. Proceedings of the National Academy of Sciences of
320 the United States of America. 2009;106(31):13040-5.
- 321 [47]Meguro K, Constans JM, Shimada M, Yamaguchi S, Ishizaki J, Ishii H, et al. Corpus callosum atrophy,
322 white matter lesions, and frontal executive dysfunction in normal aging and Alzheimer's disease. A
323 community-based study: The Tajiri Project. International Psychogeriatrics. 2003;15(1):9-25.
- 324 [48]Oosterman JM, Oosterveld S, Rikkert MGO, Claassen JA, Kessels RPC. Medial temporal lobe
325 atrophy relates to executive dysfunction in Alzheimer's disease. International Psychogeriatrics.
326 2012;24(9):1474-82.

APPENDIX

327 **Similar findings are obtained with an alternative definition of CoD**

328 As mentioned in the main text the present findings are robust to alternative calculations of the rate of
329 correlation decay. Fig. 6 shows the result of considering the correlation versus distance as piece-wise linear.
330 We find similar conclusions for the two CoD computed, each one for distances shorter or longer than
331 ~ 70 mm.

333 **Significant differences in pair correlations are found throughout most of the RSNs**

334 As seen in the results presented in Fig. 1F there are multiple pairs of ROIs which in our sample exhibit
335 significant differences, some of them in which the functional connectivity of AD is larger than the ones of
336 HS and viceversa. Despite that, no single pattern emerges indicating that certain RSN are more altered than

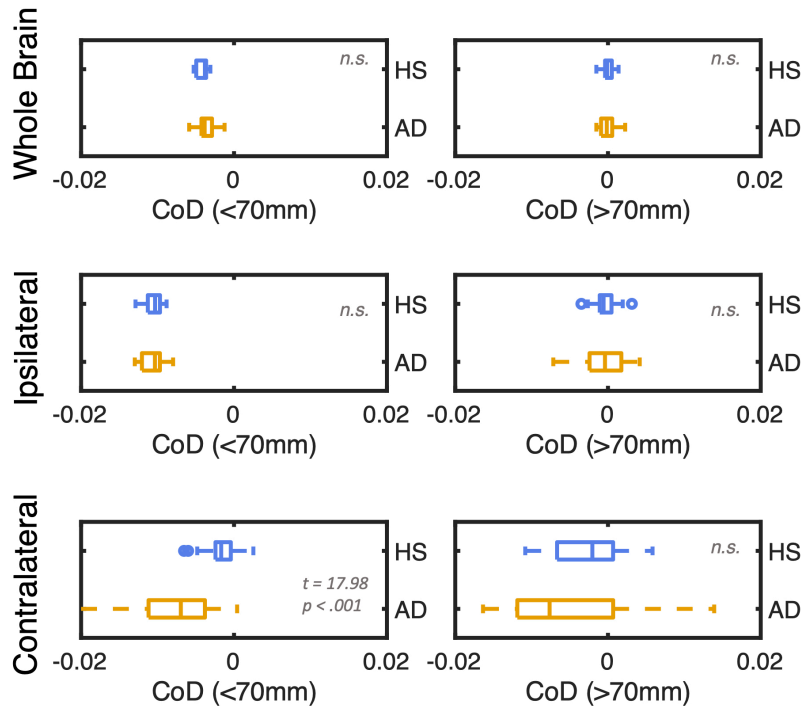


Figure 6. Correlation decay slopes, *CoD* compared across groups as in Fig. 2, fitting the decay for distances shorter or longer than ~ 70 mm. Note, similar to the results presented in Fig. 2, that significant differences are only found for homologous contralateral pairs of ROIs.

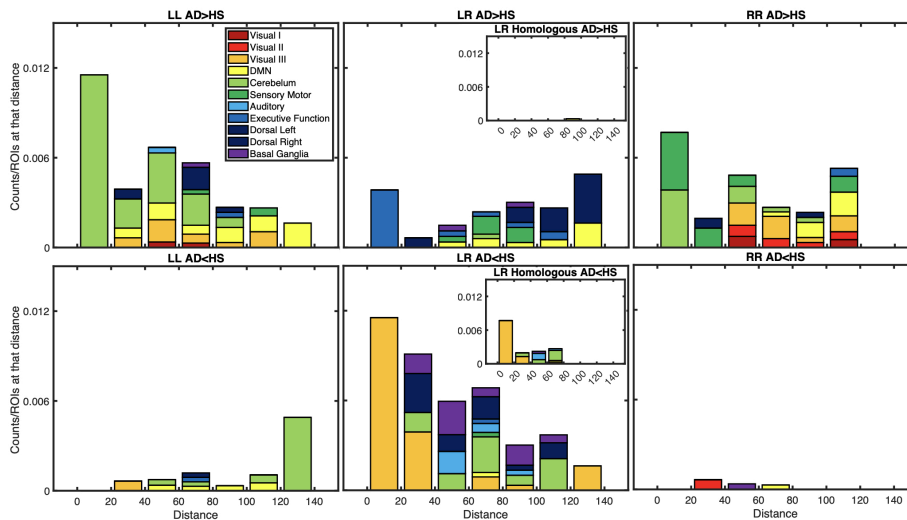


Figure 7. The significant differences shown in Fig. 1 spread over most RSN without a preference. The figure shows the number of cases (normalized by the number of ROIs at that distance) in which a given ROI-pair exhibits significant differences in the correlation, grouped by RSN. Insets in the middle plots show the results only for the homologous contralateral pairs of ROIs.

337 others. To explore that, in Fig 7 we plot as stacked bars the results of counting the number of significant
 338 ROIs (i.e., the dots in Fig. 1F) within each and across hemispheres, being coloured according to the RSN
 339 they belong to. The labels LL and RR correspond to the intra-hemispheric correlations Left and Right
 340 respectively. The label LR refers to the inter-hemispheric Right-Left ones (which are exactly symmetric

341 with the Left-Right). We could no find a prevalent pattern, suggesting that our analysis is unable to establish
342 if the disturbances prevails on a given RSN.

- 5. Study 4. Classification of sleep quality and aging as a function of brain complexity:
A multiband non-linear EEG analysis (*Submitted*).**

Title:

Classification of sleep quality and aging as a function of brain complexity: a multiband non-linear EEG analysis

Authors:

Lucía Penalba-Sánchez^{1,2,3}, Gabriel Silva⁴, Mark Crook-Rumsey^{5, 6}, Alexander Sumich³, Pedro Miguel Rodrigues⁴, Patrícia Oliveira-Silva², Ignacio Cife¹

¹ Facultat de Psicologia, Ciències de l'educació i de l'Esport, Blanquerna, Universitat Ramon Llull, Barcelona, Spain

² HNL - Human Neurobehavioral Laboratory, Research Centre for Human Development (CEDH), Faculdade de Educação e Psicologia, Universidade Católica Portuguesa, Porto, Portugal;

³ NTU Psychology, School of Social Sciences, Nottingham Trent University

⁴ CBQF - Centro de Biotecnologia e Química Fina – Laboratório Associado, Escola Superior de Biotecnologia, Universidade Católica Portuguesa

⁵ UK DRI Centre for Care Research and Technology, Imperial College London, UK

⁶ UK DRI, Department of Basic and Clinical Neuroscience, Maurice Wohl Clinical Neuroscience Institute, London, UK

Corresponding author:

Lucía Penalba-Sánchez

Address: Passeig de Sant Gervasi, 47, 08022 Barcelona

Email address: lucia.penalba.sanchez@gmail.com

Abstract

Study objectives: Understanding and classifying brain states as a function of sleep quality with age has important implications for developing targets for lifestyle-based interventions involving sleep hygiene. The current study uses an algorithm that captures non-linear features of brain complexity to differentiate awake electroencephalography (EEG) states, as a function of age and sleep quality.

Methods: Fifty-eight participants (aged 20 – 80) were assessed using the Pittsburgh Sleep Quality Inventory (PSQI) and awake resting state EEG. Groups were formed based on age and sleep quality (younger adults $n = 24$, mean age = 24.7 years, $SD = 3.43$, males $n = 14$, good sleepers $n = 11$; older adults $n = 34$, mean age = 72.87; $SD = 4.18$, males $n = 13$, good sleepers $n = 9$). Ten non-linear features were extracted from multiband EEG analysis to feed several classifiers followed by a leave one out cross-validation.

Results: Brain state complexity accurately predicted i) age in good sleepers, with 75% mean accuracy (across all channels) for lower frequencies (alpha, theta and delta) and 95% accuracy at specific channels (temporal, parietal); and ii) sleep quality in older groups with a moderate accuracy (70 and 72%) across subbands with some regions showing greater differences. It also differentiated younger good sleepers from older poor sleepers with 85% mean accuracy across all subbands, and 92% at specific channels. Lower accuracy levels (<50%) were achieved in predicting sleep quality in younger adults.

Conclusions: The algorithm discriminated excellently older vs younger groups and could be used to explore intragroup differences in older adults to predict sleep intervention efficiency depending on their brain complexity.

Keywords: *sleep quality, PSQI, EEG, non-linear multiband analysis, classification, machine learning, healthy aging*

Statement of Significance:

Classifying older and younger adults considering their brain configuration is a first step to develop sleep age-based interventions. This is the first study to i) extract 10 non-linear measures of brain complexity from EEG data from healthy young and older individuals with subjective good and bad sleep quality; ii) classify participants by their age and sleep quality feeding machine learning (ML) methods with an algorithm based on the mix of non-linear measures, and iii) understand which EEG subbands and brain regions are more altered when comparing young vs older adults with good and bad sleep quality as well as between groups of age.

Abbreviations: YG = Young adults with good sleep quality; YB = Young adults with bad sleep quality; OG = Older adults with good sleep quality; OB = Older adults with bad sleep quality; Y = Younger adult groups; O = Older adult groups.

Introduction

Good sleep quality is essential for maintaining one's cognitive and mental health over the lifespan¹⁻³, with critical repercussions at a personal, societal, and economic level. Understanding, poor sleep quality in the older adults is particularly important, as it is associated with risk of several noncommunicable diseases (e.g., diabetes, cardiovascular diseases and obesity) and may contribute to cognitive decline and memory impairments⁴⁻⁷, through mechanisms such as increases in blood pressure, evening cortisol levels, proinflammatory cytokines, and sympathetic tone.⁶⁻⁸

Changes in sleep patterns are part of a healthy aging process⁹ but these changes do not imply a decrease in sleep quality. Research shows that there are many older individuals that report to have an optimal sleep quality or even better than in middle age and that they remain free of sleep disorders such as obstructive sleep apnea or insomnia.^{3,10} Individual differences, associated with age such as a decrease in the amplitude of brain electrical activity and synchronization¹¹, a small decline in white matter volume and mild atrophy in cortical regions might be factors contributing to a decline in sleep quality.^{12,13}

In order to increase sleep quality, interventions have been conducted showing a stronger effect in younger in comparison to older adults, especially in cognitive outcomes. This diminished success in the older samples could be attributed first, to applying the interventions without adjusting them to their age and second, to the inclusion of participants with mild cognitive impairment or higher rates of atrophy in the hippocampus and frontal regions, areas involved in the acquisition and consolidation of new memories. These participants, despite presenting an improvement in physiological sleep, such as an increase in deep sleep waves, and sleep spindles, could not strengthen memories due to reduced thalamic-cortical network support.³

A good sleep might not contribute to good memory consolidation when certain circuits are impaired but might be highly useful to slow down other physiological processes such as insulin

levels or psychological ones such as mood swings and stress, preventing diabetes or psychological disorders.^{1,3} Exploring whether individuals with good and bad sleep quality can be classified as a function of their brain configuration is essential to developing interventions that efficiently tackle sleep disturbances. Neuroimaging, self-reported sleep questionnaires, non-linear signal processing techniques and ML might enable researchers and clinicians to discriminate groups considering time/space dependent mechanisms of the awake resting state brain, namely complexity, activity and connectivity.¹

In the present study, we aimed to answer the question “Can we differentiate the sleep quality of younger and older adults as a function of brain complexity using wake resting state EEG data?”. Until now, this has been difficult to address when using linear statistical approaches because the brain is a dynamic, complex, and chaotic system.

EEG is a promising widely used tool in sleep medicine that tracks the changes in the electrical activity of cortical regions over time caused by post-synaptic potentials from thousands of neurons.¹⁴ It has an excellent temporal resolution, and it is inexpensive and easy to transport.¹⁵ Most studies exploring sleep quality and /or aging with waking EEG data have used linear methods of analysis, treating the whole time series as deterministic. However, EEG data from human brains reveals that the brain behaves under deterministic chaos, i.e., its behaviour is neither stochastic nor completely predictable.¹⁶ Considering this, several neuroscientists have started to frame their research using the theory of non-linear dynamics and chaos, as it fits better the biophysiological data.¹⁷⁻¹⁹ Under this paradigm, researchers have extracted non-linear features, i.e., measures, from the EEG time series to study different aspects of the human brain such as the relationship between brain complexity, age and sleep.^{20,21}

Brain’s complexity can be defined as the ability of the neuronal circuits to interact at different spatial and temporal scales enabling the individual to flexibly adapt to the environment. Complexity has been associated with increased health and greater probabilities of survival and

has been reported to be decreased in patients with cognitive impairment and neurodegenerative diseases.^{22,23} Healthy aging has been associated with a shift in local / global complexity balance, with more information being encoded at a local level and less at a global one. A lack of this shift in older individuals predicts worse cognitive outcomes. One of the functions of sleep is regulating the complex organization of the dynamic brain, by balancing the cortical excitatory-inhibitory activity.²⁴ Recently some descriptors of complexity have been extracted from EEG signals to understand aging processes and sleep quality. The most used are the Correlation Dimension (D_2), Long Range Temporal Correlations (LRTC), energy, and entropy. Some investigators extracted the correlation dimension (D_2), a measure of connectedness of the system, before and after sleep deprivation. Using classic statistics, they concluded that participants with sleep deprivation showed reduced D_2 values reflecting a decrease in topological complexity.²⁵

Another way to measure complexity is by assessing the memory of the system using Long-Range Temporal Correlations (LRTC) measures. Colombo et al., (2016)²⁴ extracted one of the LRTC features from the signals, namely the Hurst Exponent (H), to measure statistical self-dependence of the brain activity over multiple scales of time and space, i.e., the self-similarity of the time series. The authors explored the impact that subjective insomnia has on complexity for each frequency subband. Using non-parametric statistics, they found that participants with worse sleep quality presented a higher LRTC suggesting a decrease in brain balanced excitability.

Energy has been seen to change as a function of sleep and age.²⁶ Investigators explored the influence of the amount of sleep hours of young adults on energy change, by feeding a support vector machine (SVM), k-nearest neighbour (KNN) and discriminative graph regularized extreme learning machine (GELM), with EEG power spectral density (PSD) for each subband. The results indicated that GELM was the best classifier to discriminate between conditions in the gamma

frequency (62.16 % accuracy) and 83.57% when including the channels that achieved higher accuracies.²⁶

Entropy is a measure of complexity that indicates the level of disorder in a dynamic system. High levels of entropy signify less order and increased irregularity which translates into a dysfunctional brain organization that needs to be compensated by other networks. Studies have reported an increase in entropy in healthy aging in comparison to younger and middle-aged adults.²⁷ Additional findings on entropy revealed that the aging brain is characterized by being less complex, implying a reduced repertoire of behaviours or a reduced flexibility to adjust to different situations, more irregular and less connected across hemispheres and modules.²⁸

A recent study showed that by mixing all these measures of complexity into a single algorithm and feeding several classifiers with this information healthy older adults and older adults with Mild Cognitive Impairment (MCI) can be classified excellently.²⁹

Evidence showed the potentiality of non-linear measures of complexity to better understand aging and / or sleep. Nonetheless, until now, previous studies exploring healthy samples as a function of age and sleep used i) one non-linear feature and classical statistics to explore differences in sleep between groups of young adults²⁴⁻²⁶; ii) one or more non-linear features (i.e., when using more than one these were explored separately,) and classical statistics to explore differences in brain configuration between young and older adults¹⁸; iii) one or more non - linear features and ML techniques to classify sleep (Wang, Li et al., 2016); and iiiii) one non-linear feature and ML to classify younger adults vs older adults.²⁸

The aim of the present study was to determine whether older and younger adults with good and bad sleep quality can be classified as a function of brain complexity. The PSQI³⁰, wake rsEEG data, an algorithm that integrates combination of EEG non-linear features of complexity extracted from the EEG data and ML techniques were used.

Method

Participants

The cohort used in this study overlaps with that in a previous publication³¹. The study was approved by the Health Research Authority, UK (REC reference: 17/EM/1010), and participants provided informed consent.

Fifty-eight right-handed volunteers were included in the current study. Participants were divided into four groups (see below) depending on their age (i.e., younger adults aged 20-34, older adults aged ≥ 65) and their sleep quality (good vs bad), as assessed using the PSQI³⁰. For a PSQI description see section “data-description”.

- Group 1: $n = 11$ young adults with good sleep quality (YG) (scores < 5 in PSQI); $n = 5$ females and $n = 6$ males (mean age = 23.36; $sd = 2.70$)
- Group 2: $n = 13$ young adults with bad sleep quality (YB) (scores > 5); $n = 5$ females and $n = 8$ males; (mean age = 25.53; $sd = 3.54$)
- Group 3: $n = 9$ older adults with good sleep quality (OG) (scores < 5 in PSQI³⁰); $n = 4$ females and $n = 5$ males; (mean age = 73.77; $sd = 5.45$)
- Group 4: $n = 25$ older adults with bad sleep quality (OB) (scores > 5 in the PSQI); $n = 17$ females and $n = 8$ males; (mean age = 72.56; $sd = 3.40$)

Young participants were recruited from the Nottinghamshire area. Older participants were recruited through the Trent aging panel, an internal Nottingham Trent University database of older adult study volunteers.

Participants presented normal or corrected to normal vision, no history of psychiatric, cognitive, or neurological disorder, and no medication that could interfere with the EEG recordings. Participants were asked not to consume alcohol 24 hours before the recordings and caffeine and nicotine 3 hours prior. To guarantee that none of the participants presented MCI they were assessed with the Hopkins Verbal Learning Test-Revised (HVLT-R).³² The HVLT-R in comparison

to other scales such as the Mini-Mental State Examination (MMSE) ³³ has very high sensitivity and specificity enabling to capture of subtle differences in cognitive decline.

Data description

Sleep quality assessment (PSQI):

Sleep quality was assessed using the standardized self-rated questionnaire PSQI.^{13,30} It is composed of 19 items that measure 7 domains, i.e., sleep quality, sleep latency, sleep duration, sleep efficiency, sleep disturbances, use of sleep medication, and daytime dysfunction, all of them are summarized in a global score. Given poor sleep quality in normal aging has been associated with all the elements measured by the PSQI ³⁰, the global PSQI score was used to differentiate bad vs good sleep in the current study. This tool has been reported to be optimal to assess sleep quality. It has a diagnostic sensitivity of 89.6 and a specificity of 86.5 (kappa .75 $p < .001$). Scores range from 0 to 21. Scores > 5 are indicative of poor sleep or significant sleep disturbance.³⁰

EEG Data collection:

Eyes closed resting state EEG data was recorded using a 128-channel Active Two Acquisition system (BioSemi, Amsterdam, Netherlands) at a sampling rate of 2048 Hz and processed at 24-bits. Seven additional channels were applied around the face to help with artifact detection. To reduce the computational load of data 32 channels, were used for the data analysis: 'A1', 'A7', 'A15', 'A17', 'A19', 'A23', 'A28', 'A30', 'B2', 'B4', 'B11', 'B16', 'B22', 'B26', 'B29', 'C4', 'C7', 'C11', 'C15', 'C16', 'C21', 'C24', 'C28', 'C29', 'C30', 'D4', 'D10', 'D16', 'D19', 'D23', 'D26', 'D31' (localizations are displayed in Figure 1). The location of channels captures the electrical activity through all the regions of the scalp. The use of these scalp widespread 32 channels has been reported to be optimal by several researchers.¹⁴ The location correspondence of the biosemi electrodes in 10/5 international system is displayed in Supplementary material.

EEG Data preprocessing:

MATLAB ver. R2018a and EEGLAB³⁴ were used to preprocess the EEG data. Raw EEG data was converted into 32 real value data vectors representing data extracted from each of the EEG channels. Data was imported referenced to linked mastoids, high and low pass filtered between 0.1 Hz and 45 Hz, downsampled to 256 Hz and the DC component has been removed. Bad channels were visually inspected, manually removed, and interpolated. An independent component analysis (ICA – runica) was used to discard those components that showed ocular and muscular artifacts, i.e., runica – visual inspection of scalp topographies and activity spectra – rejection of noisy data “eye blinking / muscle”. To reduce computational demands, from the five minutes of EEG recorded data, only one minute was used for the data analysis, i.e., a total of 15361-time points and 32 channels. The first minute of the signal was selected to capture the most attentive moment and avoid sleepiness in older adults with bad sleep quality. Revising other studies one minute of data is sufficient to conduct this type of analysis.³⁵

EEG signal processing and feature extraction:

The subsections below describe the steps followed by the data pre-processing. These include multi-band decomposition, feature extraction, data normalization, and classification (see Figure 2 for an overview of the methods).

Multiband decomposition

For each participant and channel, the EEG time series were split into 5s windows, i.e., a total of 12 windows. Then, a global windowing average was calculated, obtaining a 5s mean signal per each channel and each participant. After, an EEG signal decomposition into frequency subbands was performed for each participant, per channel. EEG subbands *delta* (δ , 0.1-4 Hz), *theta* (θ , 4-8 Hz), *alpha* (α , 8-16 Hz), *beta* (β , 16-32 Hz), and *gamma* (γ , 32-45) were extracted from the broadband signal using discrete wavelet transform (DWT). DWT is one of the most used tools to perform time-frequency analysis for non-stationary data (Vetterli & Kovačević, 1995). In contrast

to the classic Fourier Transform, where the frequency is extracted, but time frequency is lost, using DWT, wavelets are localized both in frequency and time, ensuring optimal time and frequency resolutions.

In the present study, DWT was used, with a biorthogonal 3.5 wavelet. This type of wavelet is often preferred as it adjusts to the EEG original signals with very little deformation³⁶. DWT was performed through an octave band critically decimated filter bank.^{37,38} The signal was transformed into approximation and details, using a scalar function and a wavelet function. The values obtained for each participant, each channel, and each subband were used as input values for the feature extraction.

Feature extraction

The non-linear nature of the EEG data was assessed with the tool provided by³⁹ Then, two main steps were conducted [1] reconstruction of the attractor from the state space from observations, [2] extraction of features of complexity [2.1] features from attractor: correlation dimension, Lyapunov exponent and approximate entropy (descriptors of the attractor) from state space, [2.2] features from time series: long-term memory measures, fractal measures, energy, and entropy.

[1] Attractor reconstruction from the state space with time delay embedding

Detecting an order or structure behind the EEG time series is a challenging task as the data is complex and chaotic.⁴⁰ In consequence, the extraction of certain descriptors or features directly from the time series is not an easy procedure. However, when reconstructing this type of data from “time-series or time-trace” to “state space” a hidden order can be observed. The state space represents every single *state* of the dynamic system, the brain, in an m-dimensional plot forming a geometric structure called an *attractor*. Note that a state of a dynamic system can be defined as the configuration of the system at a specific time. In the present study, each state is represented by EEG channel values at a specific time point of the time series. The most

implemented approach to reconstructing the phase space of EEG signals is the “time delay embedding”. The minimal dimension of the state space, i.e., acquired by “embedding” enables the extractions of non-linear features to explore the whole dynamic system and the interactions within it in a non-ambiguous way. Some of these non-linear features are the topology (connectedness), general structure, prediction of states, the correlation dimension, and the causality between variables.^{29,41}

In the present study, a reconstruction of the state space using time delay embedding is given by:

$$x_i = [x(i), x(i + \tau), \dots, x(i + (m - 1)\tau)],$$

Where τ is the incorporation delay and m is the dimensionality. The values τ and m were obtained following the methods in Faust and Bairy (2012)⁴². The vector sequence x_i , $i = 1, 2, \dots, M$, where, $M = N - (m - 1)\tau$, form the reconstructed attractor.^{42,43}

[2] Feature extraction

The ten features presented below were extracted per channel (32 channels), each participant and each subband.

[2.1] Features extracted from the reconstructed attractor

Once the phase space was determined, the correlation dimension and Lyapunov exponent and the approximate entropy were extracted. These measures enable us to determine the complexity and balance of the brain:

Correlation dimension (D_2): it is a measure that describes the complexity of the system based on the topology or connectedness of the attractor; in other words, it estimates the space and distribution occupied by different points of the fractal attractor. For instance, two points in the attractor might be very close in time but far in space. It is estimated based on the correlation integral, a function of variable distances:

$$C(r, M) = \frac{2}{M(M-1)} \sum_{i=1}^M \sum_{j=1; j \neq i}^M \theta(r - \|x_i - x_j\|)$$

Where M is the number of data points or length of the attractor and Θ is the Heaviside function, i.e., this function attributes a value of 0 for negative inputs and of 1 for positive ones. $C(r)$ determines the probability that two pairs of points of the attractor $\{x_i, x_j\}$ present a distance between them equal to or less than r .^{29,41,42} From this, the correlation dimension can be estimated as:

$$D_2 = \lim_{r \rightarrow 0} \frac{\log C(r, M)}{\log(r)}$$

Lyapunov exponent (LLE), measures the stability of the attractor and quantifies chaos. Chaotic or strange attractors perform two processes: [1] a process of expansion that consists of trajectories starting from the same or similar point diverging and then [2] a process of folding as time evolves, in other words, trajectories go back to the initial state converging (close to each other). LLE determines the rate of expansion and folding. The largest the rate (LLE), the more chaotic is the attractor. LLE rate of an attractor should be a positive value to be chaotic. For each state of the state, the largest exponent LLE can be extracted by finding the state x_j that satisfies $\min_j \|x_i - x_j\|$, such that $|i - j| > T_m$, where T_m is the mean period. The estimates are given by^{29,44}

$$\lambda(i) = \frac{1}{M+2} \sum_{K=1}^M \frac{1}{kT_s} \ln \frac{\|x_{i+k} - x_{j+k}\|}{\|x_i - x_j\|}$$

where T_s is the sampling period. The LLE is defined by the slope of the best linear approximation of $\lambda(i)$.⁴⁴

Approximate entropy (APet): computes the rate at which information of the dynamic system is lost over time.⁴³ It is defined as:

$$\text{ApET}(m,r,N) = \frac{1}{N-m+1} \sum_{i=1}^{N-m+1} \log [C_i^m (r)] - \frac{1}{N-m} \sum_{i=1}^{N-m} \log [C_i^{m+1} (r)],$$

Where

$$C_i^m (r) = \frac{1}{N-m+1} \sum_{j=1}^{N-m+1} \theta(r - ||x_i - x_j||),$$

is the probability of the point x_i on the attractor to be segregated from the other points by a distance inferior or equal to r .

[2.2] Features extracted directly from the time series

In this subsection, the features extracted directly from the time series are described. These are long-term memory measures (Hurst Exponent, Detrended Fluctuation Analysis), fractal dimension measures (Higuchi algorithm, Katz Algorithm), energy, and entropy.

Long Term Memory Measures

The **Hurst Exponent (H)** is used to assess long-range statistical self-dependence of a time series, i.e., self-correlation, smoothness, and self-similarity of a single time series.^{42,43} It can be estimated as:

$$H = \frac{\log (R/S)}{\log (N)},$$

R/S is a rescaled range. H is estimated by the slope of the best linear approximation of $\log[R(n)/S(n)]$ as a function of $\log(N)$, see²¹ for computation details of $R(n)/S(n)$. The more irregular the EEG signal is, the closer to 0 will be H.⁴¹

Detrended Fluctuation Analysis ($\Delta\Delta$): Similarly, to Hurst Exponent, detrended fluctuation, measures the statistical dependency on non-linear signals. However, this latter one, explores exclusively self-similarity, in other words, long-range correlations of a time series.^{43,45,46} From $x(n)$, the cumulative deviation series is calculated as follows:

$$y(k) = \sum_{i=1}^k [x(i) - \bar{X}].$$

A linear approximation denoted by $y_m(k)$ is estimated for each m -long segment of $y(k)$. The following formula defines the average fluctuation of the signal as a function of m :

$$F(m) = \sqrt{\frac{1}{N} \sum_{k=1}^N [y(k) - y_m(k)]^2}.$$

The scale exponent Δ signifies the correlation properties of the signal $x(n)$, represented by the slope of the best linear approximation of $\log F(m)$ as a function of $\log m$.⁴⁶

Fractal Dimension Measures:

Fractal Dimension with Higuchi algorithm (FDh): a fractal is a geometric figure that is divided by smaller identical subfigures, it presents self-similarity at different scales. This type of figure is used to model and assess real-world problems as its shape is more natural than conventional geometric figures. The brain presents attractors with the structure of a fractal. In EEG processing, the fractal dimension measures the complexity of the brain by detecting transient events in the waveforms.⁴² This feature can be calculated directly from the signals, reconstruction of the attractor is not needed. There are several algorithms to compute the FD,

in the present study the Higuchi Algorithm was used due to its excellent capacity for accuracy achieved in seminal research.⁴²

For $m = 1, \dots, n$ and $k = 1, \dots, k_{max}$, where k_{max} is obtained experimentally despite $k_{max} = 8$ was initially proposed, a distance measure is computed as.⁴¹⁻⁴³

$$L_m(K) = \frac{N-1}{[a]k} \sum_{i=1}^{[a]} |x(m+ik) - x(m+(i-1)k)|,$$

where $a = (N - m)/k$ and $[a]$ represents the largest integer equal to or less than a . The averaged distance is computed as $L(k) = \sum_m^k = L_{m(k)/k}$ for $k = 1, \dots, k_{max}$. The FD estimate, denoted by FDH, is then given by the slope of the best linear approximation of $\ln[L(k)]$ as a function of $\ln(1/k)$.

Fractal dimension with Katz Algorithm (FDk): Additionally, the Katz⁴⁷ algorithm (FDk) was used to determine FD:

$$FD_K = \frac{\log(L/a)}{\log(d/a)},$$

where L is the sum of the distances between the successive points of $x(n)$, a is the average distance between the successive points, and d is the greatest distance between $x(1)$ and the remaining points of $x(n)$.

Energy and entropy:

Energy (EN): energy is one of the most used measures to explore aging processes. It detects the slowing down of brain frequencies or shifts from high frequencies to low frequencies in aging has been widely reported.⁴³

$$EN = \sum_{n=1}^N |x(n)|^2.$$

Entropy (ETs and ETL): Similarly to LLE, entropy measures the loss of information of its dynamics. A positive entropy denotes chaos, it means that it takes more time to expand than to fold back, i.e., produces more information than it destructs. Entropy detects the amount of randomness or uncertainty in the EEG signal, in other words, it assesses how ordered or disordered the peaks of the signal are. A low entropy reflects predictability or repetition in the EEG signal patterns. The Shannon (ETs) and Logarithmic (ETL) entropies ^{29,48,49} can be estimated as:

$$ET_S = - \sum_{n=1}^N |x(n)|^2 \log[|x(n)|^2]$$

And

$$ET_L = - \sum_{n=1}^N \log[|x(n)|^2]$$

|After extracting the non-linear features DE, LLE, H, Δ , FDh, FDk, EN, ETs, ETL, and APet, data was organized per pairs of groups. Features were normalized using z-scores per each pair of groups, i.e., YG and OB, YB and OB, YG and OG, OB and OG, YG and YB. The normalized values obtained per each feature were used as input for the ML techniques SVM, KNN, LR and DT.

To ensure the results are generalizable, a leave one-out cross-validation procedure was used. Due to the limited amount of data, all were used in the cross-validation.

Results

Best classifier

The topographic maps in Figure 3 display the results of the best classifier for each pair of groups. Mean accuracies were assessed to select the best classifier. See supplementary material where the accuracies reached in each classifier are displayed.

Discriminatory capacity

Generally, as displayed in Figure 4, the results showed an *excellent* mean accuracy capacity of the algorithms to discriminate the following groups [1] YG vs OB (different age, only bad sleep in older) [2] YB vs OB (different age, bad sleep in both), [3] YG vs OG (different age, same good sleep), and [4] YB vs OG (different age, bad sleep in young) (see points 1 to 4 in Figure 4 showing accuracy levels); a *good* accuracy [5] OG vs OB (same age, different sleep quality) and a *low* accuracy [6] YG vs YB (same age, different sleep quality) (see Figure 4). Considering these results, when comparing groups of different ages, i.e., YG-OB, YB-OB, YG-OG, YB-OG, “bad sleep” in combination with “older age” constitute the variables that allow better to differentiate the groups, followed by “aging” (independently of sleep) and last, “bad sleep” in young. Additionally, when comparing groups of the same age, i.e., OG vs OB, YG vs YB, the older groups are easier to discriminate than the younger ones. This could be explained by the fact that the brain complexity and energy are not that affected in young participants that do not sleep well or because the algorithms used are better to capture differences between young vs old.

Regarding mean accuracies in the different subbands, results showed an excellent classification accuracy in the alpha, theta, and delta subbands when comparing young vs older adults, especially when comparing the YG vs OB, with an accuracy of 80 % in alpha, 82 % in theta and 85% in delta (see Table 1). The older groups', i.e., OG vs OB mean discriminatory capacity in all subbands was lower than when comparing Y vs O but preserved (over 70%). Lower *mean accuracy levels* were found when comparing the YG vs YB (see Table 1). Nonetheless, the classification accuracies of specific EEG channels, show an optimal discrimination between the young groups in all the sub-bands except in gamma (see Table 1 YG vs YB, highlighted in blue).

Differences in specific regions across groups

In this subsection, the most relevant results of accuracy levels in specific channels will be presented.

Young versus old

As displayed in the topography maps in Figure 3 and the biosemi plots in Figure 5 the YG vs OB are the study groups that present a higher discriminatory capacity. Generally, the areas that show higher differences between age groups are the frontotemporal regions (affected in gamma, alpha, and theta). Additionally, some occipital and parietal regions are markedly affected especially in the theta and delta subbands.

Regarding specific channels, the regions that enable a higher discriminatory capacity between the Y vs O in the slow rhythms, i.e., delta and theta, are within the temporal-parietal and occipital (especially the channel *B16*). This might indicate age-related changes, independently of sleep quality, as it is present when comparing all pairs of groups Y vs O, but it is not present when comparing OG vs OB nor YG vs YB. Conversely, the occipital (EEG channel *A 30*) seems to be related to bad sleep quality in O (see Table 2), this area cannot discriminate between young with good sleep vs old with good sleep). Additionally, channel *A23* in the Occipital seems to be related to bad sleep both in young and older adults.

Regarding the alpha subband, the frontotemporal region *C11* is the most different when comparing the YG vs OB, and it is associated with a bad sleep quality only in older adults, as this result is also present when comparing the YB vs OB and the OG vs OB.

Results in the gamma and beta subbands in Y vs O suggest that some occipital regions especially the *A23* are associated with a bad sleep quality in older participants (this is evident as in all pairs of groups where OB is present, this region shows a great accuracy performance). Conversely, the left frontotemporal region (*D23*) is associated with older adults with good sleep, as we can

see only this region is different between YG-OG, and YB-OG (see Figure 5 and supplementary material).

Old good versus old bad

When comparing the OG vs OB, an overall $\geq 71\%$ accuracy in all subbands was achieved. As mentioned in the last section, results show that regions C11 (frontotemporal in alpha) and A23 (occipital in gamma and beta) are associated with bad sleep in the older group.

Young good versus young bad

The highest mean accuracy achieved by the YG vs YB was 50 % in the alpha subband. However specific channels in beta, alpha, theta, and delta reached accuracy levels $> 70\%$.

The parietal central line (channel A19) in the alpha subband, seems to be associated with bad sleep in young adults, note that the algorithms can discriminate this region between the groups YG vs YB as well as between YB vs OG, (see Figure 1). Other channels that allow differentiating YG and YB but not other pairs of groups are the channel D19 (parietal) in the beta, B29 (fronto-central) in theta, and D31 (inferior parietal) in the delta subband.

Discussion

The aim of this study was to classify young and older adults with good and bad sleep quality as a function of brain complexity. Whilst similar algorithms have been used to discriminate healthy older adults from those with neurodegenerative diseases using resting state EEG data ²⁹, the current study is the first to demonstrate the utility in classifying groups based on healthy ageing and sleep quality.

The algorithm achieved excellent mean accuracies when comparing young vs older adults. Moderate to high accuracies when comparing the older adult groups, e.g., older with good sleep

quality with older adult with bad sleep quality, and low accuracies when classifying the younger groups, i.e., younger adults with bad sleep vs younger adults with good sleep quality. Additionally, the algorithm enabled excellent discrimination between all pairs of groups in specific subbands and regions.

Brain configuration in the lower frequencies, i.e., alpha, theta and delta subbands, seems to play an important role in the aging process, especially in temporal and parietal regions. This can be seen when comparing the older vs younger groups, independently of their sleep quality. This is aligned with several studies that indicate changes in older adults in the slower rhythms in several regions, achieving accuracy levels of 75.5%.^{50,51} These changes, have been hypothesized by several authors to be caused by a generalized slowing of the nervous tissue, a decrease of cerebral perfusion and metabolism and inhibition mechanisms.⁵²

Additionally, results showed that, although age, allowed discrimination between groups (e.g., YG vs OG), even a higher accuracy is achieved when both age and sleep quality are taken into account (i.e., young adults with good sleep quality vs older adults with bad sleep quality). This may reflect an interaction between aging and sleep quality on brain function.

Evidence suggests that changes in theta and delta frequencies are associated with sleep deprivation and bad sleep quality.⁵³ According to a systematic review, the hypothesis underlying this finding is that delta is a marker of homeostatic sleep drive, the more we are awake, or sleep deprived the higher is delta.⁵⁴ Changes in the delta subband apart from denoting typical brain aging seem to be associated with sleep deprivation and bad sleep quality independently of age. Münch et al. (2004)⁵³ found that young cohorts show a more pronounced delta activity in frontal while the older present a decrease. This, according to the authors might indicate a “pre-frontal tiredness” due to a bad sleep quality and the aggregated “frontal tiredness” due to ageing. Our results, although cannot show directionality, showed that frontal along with some temporal regions seem to be altered in the delta and theta subbands in older adults with bad sleep quality

in comparison to younger adults with good sleep. Furthermore, our findings suggest that the occipital region is generally affected both in young and older adults with bad sleep quality, however while the former group only seem to present alterations in the delta and theta subbands, the latter presents differences in the occipital in all the subbands, especially markedly in the gamma, beta and alpha subbands. This finding is aligned with a study that found differences in the occipital regions when comparing older vs young.⁵⁵

When comparing the young cohorts, the algorithm achieved good discrimination accuracies only in specific regions and subbands. More precisely, occipital and parietal regions seem to be affected in young adults with bad sleep quality in the alpha, beta and delta frequencies. Additionally, some areas in the fronto temporal left in gamma and beta are associated with younger adults with good sleep. The low mean classification accuracy of the young groups, i.e., YG versus YB, might reflect that sleep does not alter significantly the brain configuration in younger adults and that bad sleep quality in older adults affects the brain configuration in a more widespread manner than in younger adults. Another hypothesis could be that the algorithm is not good enough to discriminate between younger groups.

This study presents some limitations. First, only the first minute of data was used to decrease processing computational time. Although, it has been demonstrated that one minute of EEG data is sufficient for this type of analysis, future studies should include longer time series or assess whether the accuracy levels change over different time windows. Second, a search for the best combination of non-linear features was not performed. A recent study conducted by some of the co-authors indicated that this combination of features is optimal to classify healthy older adults and older adults with neurodegenerative diseases.⁴³ Accuracy levels in the younger groups might be improved by using another combination of features. This takes several days of computational work. We propose future studies to investigate whether another combination of features allows better discrimination of young samples. Third, the effects of age and the ones

on sleep quality are not easy to disentangle and although we can determine the classification accuracies with high confidence and which subbands are more affected in each pair of groups, answering the questions “which of these changes are more associated with a bad sleep quality and which ones with age?” or “is there a decrease or increase in delta or theta subbands”? is not possible, only inferences can be made by comparing all the results of all pairs of groups. Four, this study has a small sample. To reduce the possible overfitting as much as possible a leave-one-out cross-validation was used. However, future work should be conducted to validate this method with bigger samples. Five, cognitive impairment was assessed using the HVLIT, and it is assumed that the older adults were healthy, however they could have some preclinical early pathologic aging that was not controlled such as tauopathy and beta-amyloid accumulation and / or higher atrophy in the hippocampus and frontal regions than the expected for healthy aging. Six, within-group differences were not explored, for instance “is it possible to discriminate the individuals with a very bad sleep quality from those with a moderate bad sleep quality?” or “can brain complexity be used to classify individuals with specific sleep disturbances such as latency or number of awakenings per night?”. These gaps and questions should be investigated as might be the base to create individualized interventions.

In conclusion, this study demonstrates that the algorithm is efficient in classifying the older vs the younger participants with good and bad sleep quality included in the present study. It is the first study that classifies excellently younger and older adults with good and bad sleep as a function brain configuration, using a mix of non-linear features.

Future studies using EEG and non-linear features along with ML techniques might enable to predict which intervention is better depending on age, lifestyle, and brain configuration to improve sleep quality.⁵⁶

Acknowledgements

The authors would like to thank all the participants of the present study.

Additionally, financial support was provided by the MICINN (Spain) grant PID2021-125534OB-I00

Disclosure statement

The authors have no conflicts of interest to report.

References

1. Scullin MK, Bliwise DL. Sleep, Cognition, and Normal Aging: Integrating a Half-Century of Multidisciplinary Research. *Perspect Psychol Sci*. Published online 2015:97-137. doi:10.1177/1745691614556680
2. Hoch CC, Dew MA, Reynolds CF, et al. Aging and Sleep Longitudinal Changes in Diary-and Laboratory-Based Sleep. A Three-Year Follow-Up. Vol 20.; 1997. <https://academic.oup.com/sleep/article/20/3/192/2732095>
3. Scullin MK. Do Older Adults Need Sleep? A Review of Neuroimaging, Sleep, and Aging Studies. *Curr Sleep Med Rep*. 2017;3(3):204-214. doi:10.1007/s40675-017-0086-z
4. Abichou K, la Corte V, Hubert N, et al. Young and Older Adults Benefit From Sleep, but Not From Active Wakefulness for Memory Consolidation of What-Where-When Naturalistic Events. *Front Aging Neurosci*. 2019;11. doi:10.3389/fnagi.2019.00058
5. Stickgold R, Walker MP. Memory consolidation and reconsolidation: What is the role of sleep? *Trends Neurosci*. 2005;28(8):408-415. doi:10.1016/j.tins.2005.06.004
6. McEwen BS, Sapolsky RM. *Stress and Cognitive Function Introduction Catecholamines and Glucocorticoids*. Vol 5.; 1995.
7. Vgontzas AN, Zoumakis E, Bixler EO, et al. Adverse Effects of Modest Sleep Restriction on Sleepiness, Performance, and Inflammatory Cytokines. *Journal of Clinical Endocrinology and Metabolism*. 2004;89(5):2119-2126. doi:10.1210/jc.2003-031562
8. McEwen BS. Sleep deprivation as a neurobiologic and physiologic stressor: allostasis and allostatic load. *Metabolism*. 2006;55(SUPPL. 2). doi:10.1016/j.metabol.2006.07.008
9. Gulia KK, Kumar VM. Sleep disorders in the elderly: a growing challenge. *Psychogeriatrics*. 2018; 18(3):155-165. doi:10.1111/psyg.12319
10. Dregan A, Armstrong D. Age, cohort and period effects in the prevalence of sleep disturbances among older people: The impact of economic downturn. *Soc Sci Med*. 2009;69(10):1432-1438. doi:10.1016/J.SOCSCIMED.2009.08.041
11. Mattis J, Sehgal A. Circadian Rhythms, Sleep, and Disorders of Aging. *Trends in Endocrinology and Metabolism*. 2016;27(4):192-203. doi:10.1016/j.tem.2016.02.003
12. Double KL, Halliday GM, Kril JJ, et al. Topography of brain atrophy during normal aging and Alzheimer's disease. *Neurobiol Aging*. 1996;17(4):513-521. doi:10.1016/0197-4580(96)00005-x

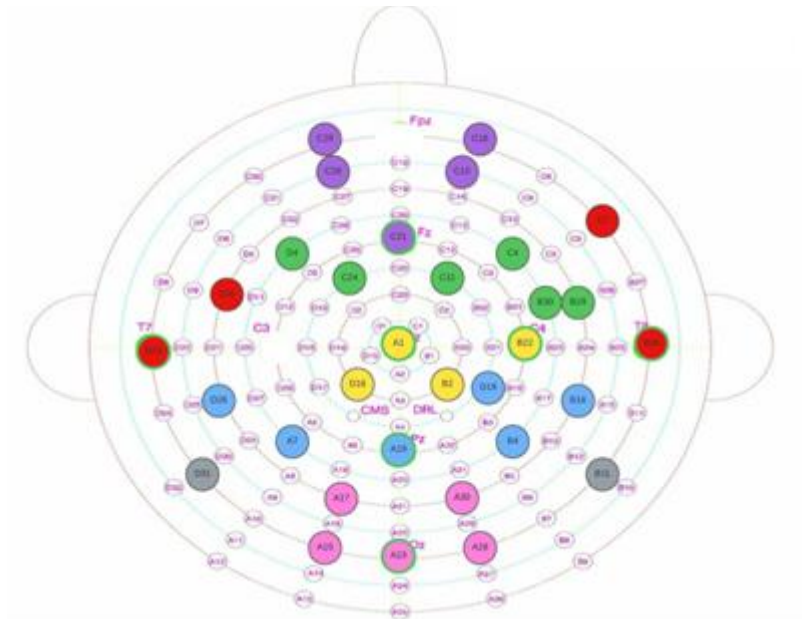
13. Nebes RD, Buysse DJ, Halligan EM, Houck PR, Monk TH. Self-reported sleep quality predicts poor cognitive performance in healthy older adults. *Journals of Gerontology - Series B Psychological Sciences and Social Sciences*. 2009;64(2):180-187. doi:10.1093/geronb/gbn037
14. Cassani R, Estarellas M, San-Martin R, Fraga FJ, Falk TH. Systematic review on resting-state EEG for Alzheimer's disease diagnosis and progression assessment. *Dis Markers*. 2018;2018. doi:10.1155/2018/5174815
15. Sanei S, & CJA. *EEG Signal Processing*; 2007.
16. Babloyantz A, Salazar JM and Nicolis C. Evidence of chaotic dynamics of brain activity during the sleep cycle. *Physics Letter A*. 1985, 111, 152-156.
17. Chialvo D. Life at the Edge: Complexity and Criticality in Biological Function. *Acta Physica Polonica B*. 2018, 49(12), 1955. <https://doi.org/10.5506/aphyspolb.49.1955>
18. Cifre I, Miller Flores MT, Penalba L, Ochab JK, Chialvo DR. Revisiting Nonlinear Functional Brain Co-activations: Directed, Dynamic, and Delayed. *Front Neurosci*. 2021;15. doi:10.3389/fnins.2021.700171
19. Miller P. Dynamical systems, attractors, and neural circuits. *F1000Res*. 2016;5:F1000 Faculty Rev-992. 2016 May 24. doi:10.12688/f1000research.7698.1
20. Faust O, Bairy MG. Nonlinear analysis of physiological signals: A review. *J Mech Med Biol*. 2012;12(4). doi:10.1142/S0219519412400155
21. Qian B & Rasheed K. Hurst exponent and financial market predictability. In P. Locke (Ed.), *Proceedings of IASTED international conference on financial engineering and applications*. 2007 (pp. 203–209). ACTA Press.
22. Hou F, Yu Z, Peng CK, Yang A, Wu C, & Ma, Y. Complexity of Wake Electroencephalography Correlates With Slow Wave Activity After Sleep Onset. *Frontiers in Neuroscience*. 2018 12. <https://doi.org/10.3389/fnins.2018.00809>
23. Yang AC, Jann K, Michel CM, Wang DJJ. Editorial: Advances in Multi-Scale Analysis of Brain Complexity. *Front Neurosci*. 2020;14. doi:10.3389/fnins.2020.00337
24. Colombo MA, Wei Y, Ramautar JR, Linkenkaer-Hansen K, Tagliazucchi E, van Someren EJW. More severe insomnia complaints in people with stronger long-range temporal correlations in wake resting-state EEG. *Front Physiol*. 2016;7(NOV). doi:10.3389/fphys.2016.00576
25. Jeong J, Kim D, Kim S, Chae JH, Go H and Kim KS. Effect of Total Sleep Deprivation on the Dimensional Complexity of the Waking EEG. *Sleep*. 2001;24. 197-202. 10.1093/sleep/24.2.197.
26. IEEE Computational Intelligence Society, International Neural Network Society, Institute of Electrical and Electronics Engineers, IEEE World Congress on Computational Intelligence (2016 : Vancouver BC). *2016 International Joint Conference on Neural Networks (IJCNN) : 24-29 July 2016, Vancouver, Canada*.
27. Wang Z. Brain Entropy Mapping in Healthy Aging and Alzheimer's Disease. *Front Aging Neurosci*. 2020;12. doi:10.3389/fnagi.2020.596122
28. Keshmiri S. Entropy and the Brain: An Overview. *Entropy (Basel, Switzerland)*.2020; 22(9), 917. <https://doi.org/10.3390/e22090917>

29. Silva G, Alves M, Cunha R, Bispo BC, Oliveira-Silva P, Rodrigues PM. Early Detection of Alzheimer's and Parkinson's Diseases Using Multiband Nonlinear EEG Analysis. *Psychol Neurosci*. 2022; doi:10.1037/pne0000287
30. Buysse DJ RC. The Pittsburgh Sleep Quality Index: a new instrument for psychiatric practice and research. *Psychiatry*. *Psychiatry research Elsevier*. 1989;193-213. doi:doi:10.1016/0165-1781(89)90047-4
31. Crook-Rumsey M. *Neurophysiology of Prospective Memory in Typical and Atypical Ageing*. Nottingham Trent University. ProQuest Dissertations Publishing. 2020; 28605687.
32. Benedict RHB, Schretlen D, Groninger L, Brandt J. Hopkins verbal learning test - Revised: Normative data and analysis of inter-form and test-retest reliability. *Clinical Neuropsychologist*. 1998;12(1):43-55. doi:10.1076/clin.12.1.43.1726
33. de Jager CA, Budge MM, Clarke R. Utility of TICS-M for the assessment of cognitive function in older adults. *Int J Geriatr Psychiatry*. 2003;18(4):318-324. doi:10.1002/gps.830
34. Delorme A & Makeig S. EEGLAB: an open-source toolbox for analysis of single-trial EEG dynamics, *Journal of Neuroscience Methods* 134:9-21. 2004;134:9-21.
35. Dobarjeh MG, Wang GY, Kasabov NK, Kydd R, Russell B. A Spiking Neural Network Methodology and System for Learning and Comparative Analysis of EEG Data from Healthy Versus Addiction Treated Versus Addiction Not Treated Subjects. *IEEE Trans Biomed Eng*. 2016;63(9):1830-1841. doi:10.1109/TBME.2015.2503400
36. Rodrigues PM, Bispo BC, Garrett C, Alves D, Teixeira JP, Freitas D. Lacsogram: A New EEG Tool to Diagnose Alzheimer's Disease. *IEEE J Biomed Health Inform*. 2021;25(9):3384-3395. doi:10.1109/JBHI.2021.3069789
37. Malvar HS. Signal processing with lapped transforms. *Artech Hou*. 1992.
38. Vetterli M., & Kovacevic J. Wavelets and subband coding. *Prentice Hall*. 1995.
39. BenSaïda A. A practical test for noisy chaotic dynamics. *SoftwareX*. 2015;3-4:1-5. doi:10.1016/j.softx.2015.08.002
40. Stam CJ. Nonlinear dynamical analysis of EEG and MEG: Review of an emerging field. *Clinical Neurophysiology*. 2005;116(10):2266-2301. doi:10.1016/j.clinph.2005.06.011
41. Rodríguez-Bermúdez G, García-Laencina PJ. Analysis of EEG signals using nonlinear dynamics and chaos: A review. *Applied Mathematics and Information Sciences*. 2015;9(5):2309-2321. doi:10.12785/amis/090512
42. Faust O, Bairy MG. Nonlinear analysis of physiological signals: a review. *J Mech Med Biol*. 2012;12. doi:10.1142/S0219519412400155
43. Silva G, Alves M, Cunha R, Bispo BC, Oliveira-Silva P, Rodrigues PM. Early detection of Alzheimer's and Parkinson's diseases using multiband nonlinear EEG analysis. *Psychol Neurosci*. Published online March 28, 2022. doi:10.1037/pne0000287
44. Rosenstein' MT, Collins JJ, de Luca CJ, Rapp PE. *A Practical Method for Calculating Largest Lyapunov Exponents from Small Data Sets*. 1993; Vol 65.

45. Gifani P, Rabiee HR, Hashemi MH, Taslimi P, Ghanbari M. Optimal fractal-scaling analysis of human EEG dynamic for depth of anesthesia quantification. *J Franklin Inst.* 2007;344(3-4):212-229. doi:10.1016/j.jfranklin.2006.08.004
46. Lee JM, Kim DJ, Kim IY, Park KS, Kim SI. *Detrended Ductuation Analysis of EEG in Sleep Apnea Using MIT=BIH Polysomnography Data.* 2002; Vol 32 www.elsevier.com/locate/complbiomed
47. Katz MJ. Fractals and the analysis of waveforms. *Comput Biol Med.* 1988;18(3):145-156. doi:https://doi.org/10.1016/0010-4825(88)90041-8
48. Das AB, Bhuiyan MIH. Discrimination and classification of focal and non-focal EEG signals using entropy-based features in the EMD-DWT domain. *Biomed Signal Process Control.* 2016;29:11-21. doi:https://doi.org/10.1016/j.bspc.2016.05.004
49. Rodríguez-Sotelo JL, Osorio-Forero A, Jiménez-Rodríguez A, Cuesta-Frau D, Cirugeda-Roldán E, Peluffo D. Automatic sleep stages classification using EEG entropy features and unsupervised pattern analysis techniques. *Entropy.* 2014;16(12):6573-6589. doi:10.3390/e16126573
50. Babiloni C, Triggiani AI, Lizio R, et al. Classification of single normal and Alzheimer's disease individuals from cortical sources of resting state EEG rhythms. *Front Neurosci.* 2016;10(FEB). doi:10.3389/fnins.2016.00047
51. Ishii R, Canuet L, Aoki Y, et al. Healthy and Pathological Brain Aging: From the Perspective of Oscillations, Functional Connectivity, and Signal Complexity. *Neuropsychobiology.* 2018;75(4):151-161. doi:10.1159/000486870
52. Davidson PN, Davidson KA. Electroencephalography in the elderly. *Neurodiagnostic Journal.* 2012;52(1):3-19. doi:10.1080/21646821.2012.11079839
53. Münch M, Knoblauch V, Blatter K, et al. The frontal predominance in human EEG delta activity after sleep loss decreases with age. *European Journal of Neuroscience.* 2004;20(5):1402-1410. doi:10.1111/j.1460-9568.2004.03580.x
54. Long S, Ding R, Wang J, Yu Y, Lu J, Yao D. Sleep Quality and Electroencephalogram Delta Power. *Front Neurosci.* 2021;15. doi:10.3389/fnins.2021.803507
55. Hong JK, Lee HJ, Chung S, Yoon IY. Differences in sleep measures and waking electroencephalography of patients with insomnia according to age and sex. *Journal of Clinical Sleep Medicine.* 2021;17(6):1175-1182. doi:10.5664/jcsm.9156
56. Barracca N. The Brain-Sleep Connection: GCBH Recommendations on Sleep and Brain Health. 2017; doi:10.26419/252Fpia.00014.001.pdf

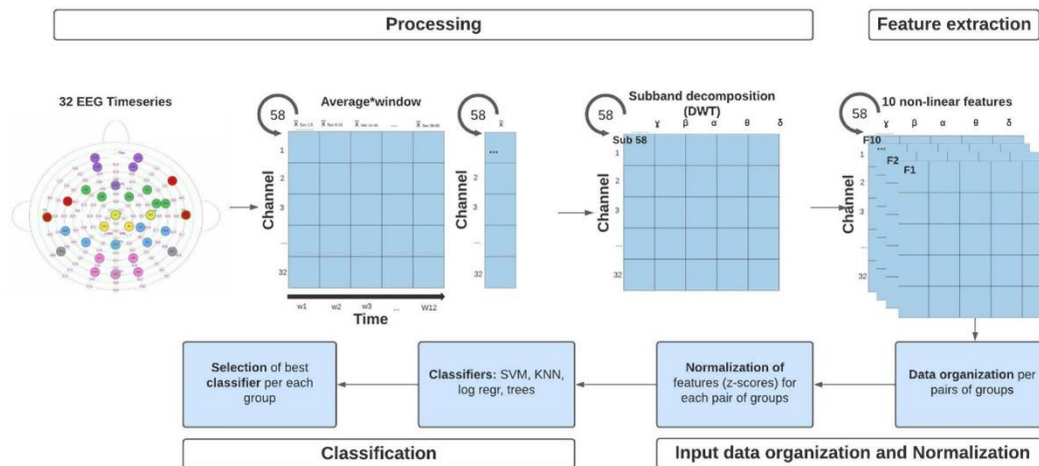
Figure captions

Figure 1. Channels' location



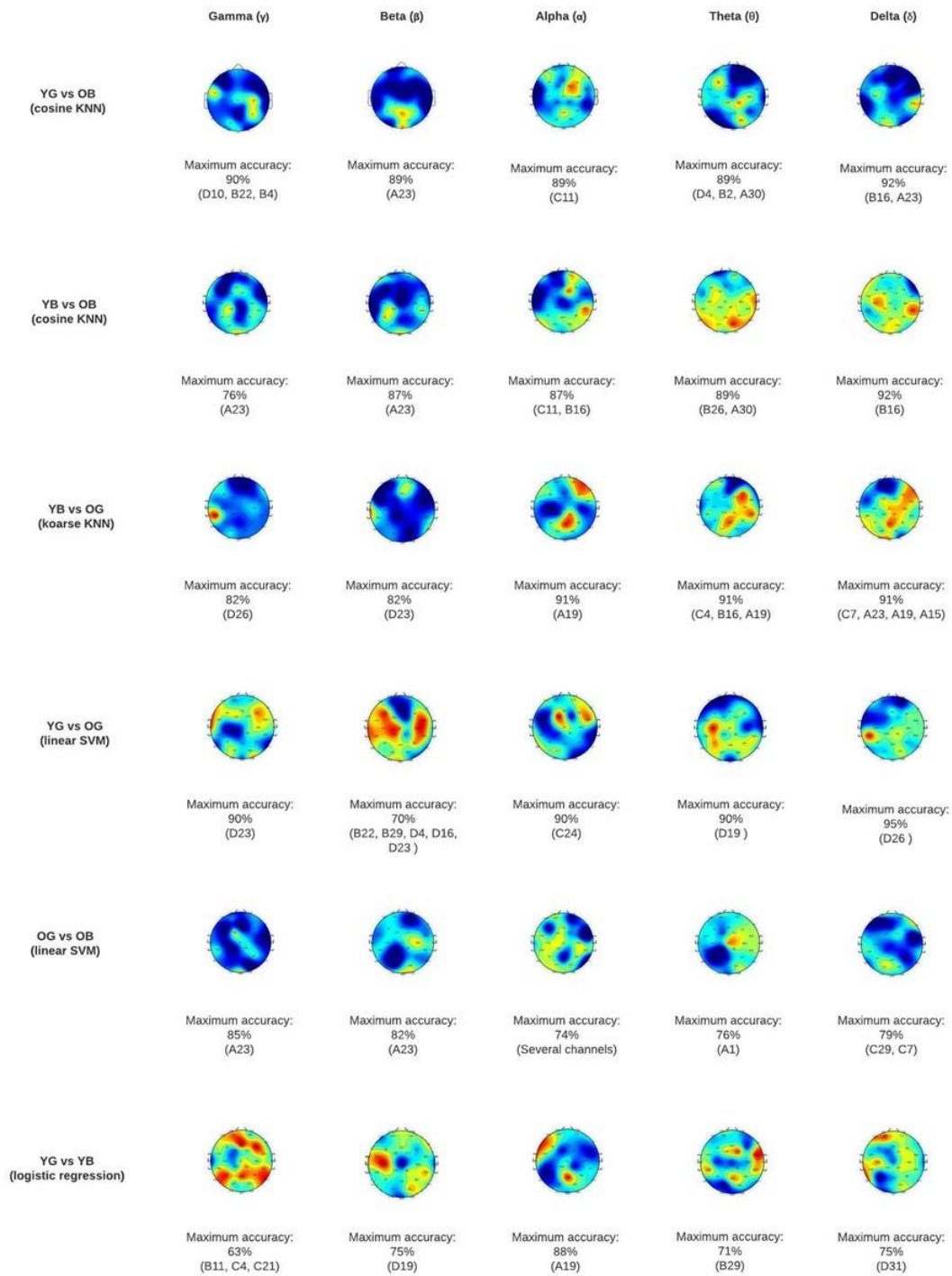
Note. Small circular colours display the signals acquired from the 32 electrodes used for the study. Specific colours signify broader brain regions, in purple frontal areas, in green fronto-central, in yellow central, in red frontotemporal, in blue parietal, in grey inferior parietal, and in pink occipital

Figure 2. Methodology overview



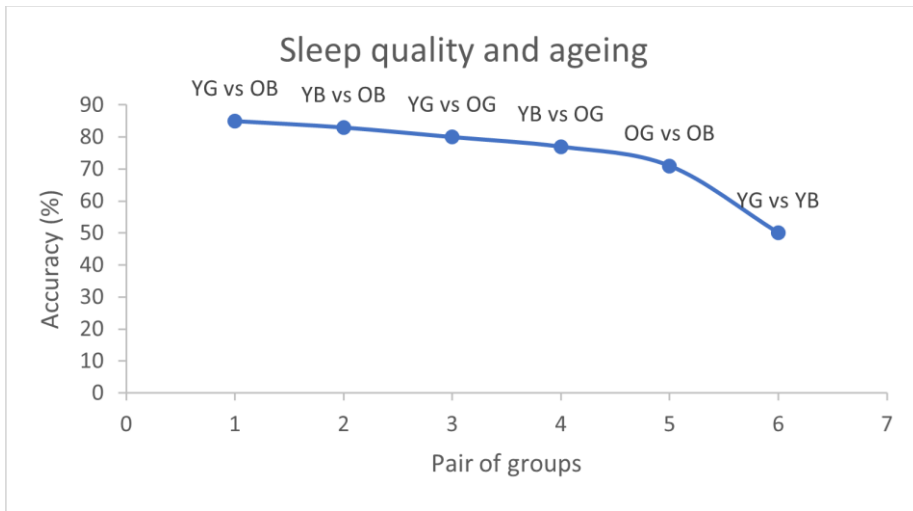
Note. Figure 2 displays an overview of the methodology used in the present study. From left to right, 32 channels were carefully chosen from the 128 acquired, time-series of the 32 channels were selected from them and split into 5-second windows, a global windowing average was performed to comprise each time-series data in just one 5s window, then DWT = Discrete Wavelet Transform has been applied to achieve the conventional sub-bands per subject and electrode. Features were extracted for each sub-band and each subject. Non-linear features were organized per binary groups and z-score normalization was performed per study group pairs. Non-linear features normalized were the input of classifiers. SVM = support vector machine; KNN = K-nearest neighbour; log regr. = logistic regression; trees = decision trees.

Figure 3. Topographic maps



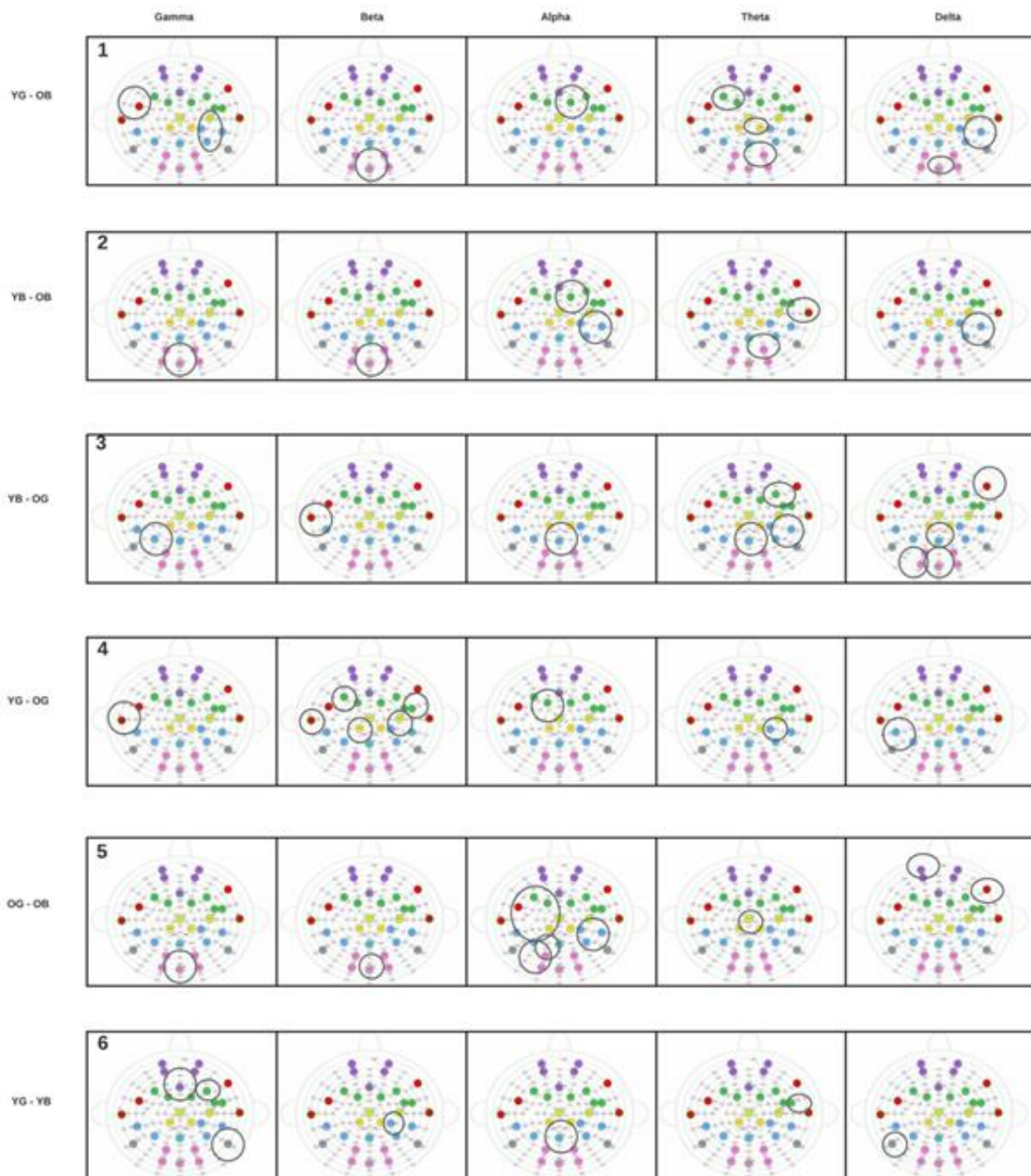
Note. Figure 3 displays the topographic maps classification results at calp Level for Each Pair of Groups. YG =Young adults' good sleep; YB = Young adults' bad sleep; OG = Older adults' good sleep; OB = Older adult bad sleep.

Figure 4. Influence of sleep and age on the discriminatory capacity



Note. 1 = YG (young adults with good sleep quality) vs OB (older adults with bad sleep quality), 2 = YB (young adults with bad sleep quality) vs OB, 3 = YG vs OG (older adults with good sleep quality), 4 = YB vs OG, 5 = OG vs OB, 6 = YG vs YB. Results show the highest mean accuracy level reached in each pair of groups (in the subband with the highest accuracy).

Figure 5. Biosemi plots



Note. Figure 5 displays the Biosemi plots. It shows the regions that allow better discrimination between pairs of groups. Subplots 1 to 4 show differences in brain configuration between pairs of different ages, i.e., young - older; subplots 5 and 6 between pairs of groups of the same age (young – young; older – older). Small circular colours display the signals acquired from the 32 electrodes used for the study. Specific colours signify broader brain regions, in purple frontal areas, in green fronto-central, in yellow central, in red frontotemporal, in blue parietal, in grey inferior parietal, and in pink occipital. Black circles surrounding specific circular colours (EEG channels) signalize regions that allow discriminating with an accuracy of >70% in all subbands between groups, except for the gamma YG-YB, with a 65%.

Tables

Table 1. Classification accuracy of young adults with good sleep vs old adults with bad sleep

Group	Classifier	Mean / max	Gamma	Beta	alpha	Theta	Delta
YG vs OB	Cosine KNN	Mean	70%	73%	80%	82%	85%
		Max	75%	89%	89%	89%	92%
YB vs OB	Cosine KNN	Mean	68%	72%	77%	78%	83%
		Max	76%	87%	87%	89%	92%
YB vs OG	Coarse KNN	Mean	60%	62%	75%	79%	80%
		Max	82%	82%	91%	91%	91%
YG vs OG	Linear SVM	Mean	59%	56%	67%	70%	77%
		Max	90%	70%	90%	90%	95%
OG vs OB	Linear SVM	Mean	72%	72%	72%	71%	71%
		Max	85%	82%	74%	76%	79%
YG vs YB	Logistic regression	Mean	43%	50%	49%	47%	50%
		Max	63%	75%	88%	71%	75%

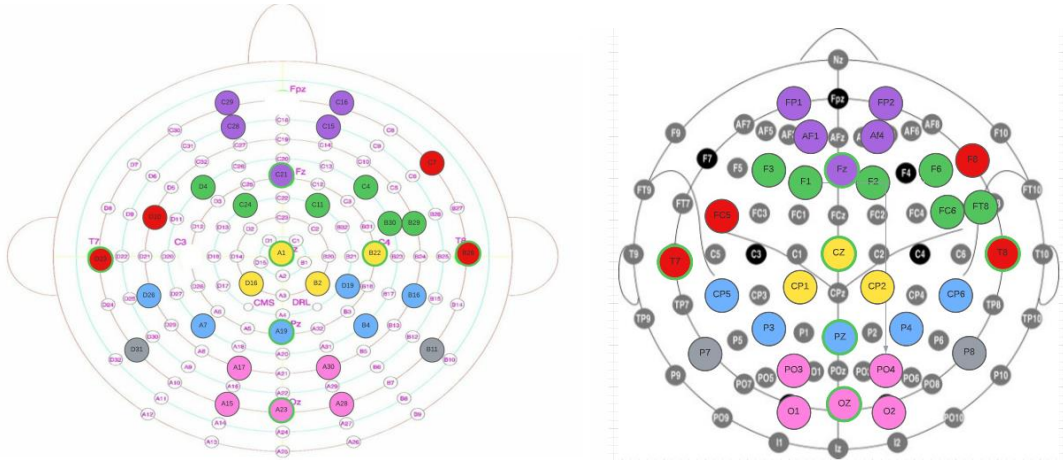
Note. YG = Young adults good sleep; YB = Young adults bad sleep; OG = older adults good sleep; OB = Older adults bad sleep;

Classifier = Machine learning method that classified with a higher accuracy level for each pair of groups; Mean = mean global accuracy level of all channels; Max = maximum accuracy achieved in at least one channel. In light orange mean accuracies => 70; in dark orange mean accuracies =>80; in light blue maximum accuracy in at least one channel =>70; in dark blue maximum accuracy in at least one channel => 80.

Supplementary material

Supplementary 1

Biosemi and 10/5 international system plots



Note. The plot on the left displays the biosemi nomenclature and the one on the right the 10/5 international system nomenclature and the approximate correspondence location. Electrodes in colours are the ones included in the analysis. See below the list where the names of the electrodes in biosemi nomenclature and 10/5 international are specified.

Name of EEG locations – Biosemi (10/5 international)

'A1' Central (CZ)

'A7' Parietal (P3)

'A15' Occipita (O1)

'A17' Occipital (PO3)

'A19' Parietal (PZ)

'A23' Occipital (OZ)

'A28' Occipital (O2)

'A30' Occipital (PO4)

'B2' Central (CP2)

'B4' Parietal (P4)

'B11' Inferior parietal (P8)

'B16' Parietal (CP6)

'B22' Central

'B26' Fronto temporal (T8)

'B29' Fronto central (FT8)

'C4' Fronto central (F6)

'C7' Fronto temporal (F8)

'C11' Fronto central (F2)

'C15' Frontal (AF4)

'C16' Frontal (FP2)

'C21' Frontal (Fz)

'C24' Fronto central (F1)

'C28' Frontal (AF1)

'C29' Frontal (FP1)

'C30' Fronto central (FC6)

'D4' Fronto central (F3)

'D10' Fronto temporal (FC5)

'D16' Centra (CP1)

'D19' Parietal


'D23' Fronto temporal (T7)

'D26' Parietal (CP5)

'D31' Inferior parietal (P7)

Supplementary 2: accuracies reached with different machine learning methods

Young good vs old bad:

FineTree						MediumTree						CoarseTree						LogisticRegression					
Channel	Gamma	Beta	alpha	Theta	Delta	Channel	Gamma	Beta	alpha	Theta	Delta	Channel	Gamma	Beta	alpha	Theta	Delta	Channel	Gamma	Beta	alpha	Theta	Delta
Mean	63%	67%	73%	77%	78%	Mean	63%	67%	73%	77%	78%	Mean	63%	67%	73%	77%	78%	Mean	62%	66%	72%	72%	75%
Max	83%	89%	86%	89%	92%	Max	83%	89%	86%	89%	92%	Max	83%	89%	86%	89%	92%	Max	81%	81%	89%	89%	97%
MediumGuassianSVM						CoarseGuassianSVM						FineKNN						MediumKNN					
Channel	Gamma	Beta	alpha	Theta	Delta	Channel	Gamma	Beta	alpha	Theta	Delta	Channel	Gamma	Beta	alpha	Theta	Delta	Channel	Gamma	Beta	alpha	Theta	Delta
Mean	69%	69%	77%	79%	86%	Mean	69%	69%	69%	69%	69%	Mean	55%	62%	69%	72%	80%	Mean	70%	72%	78%	82%	86%
Max	78%	83%	86%	89%	92%	Max	69%	69%	69%	69%	69%	Max	69%	81%	86%	86%	92%	Max	75%	83%	86%	89%	92%
LinearSVM						QuadraticSVM						CubicSVM						FineGuassianSVM					
Channel	Gamma	Beta	alpha	Theta	Delta	Channel	Gamma	Beta	alpha	Theta	Delta	Channel	Gamma	Beta	alpha	Theta	Delta	Channel	Gamma	Beta	alpha	Theta	Delta
Mean	67%	69%	76%	79%	85%	Mean	59%	66%	75%	79%	84%	Mean	58%	66%	70%	76%	81%	Mean	69%	70%	70%	72%	70%
Max	78%	83%	83%	92%	89%	Max	75%	83%	86%	89%	94%	Max	75%	81%	83%	92%	94%	Max	78%	75%	78%	81%	75%
CoarseKNN						CosineKNN 						CubicKNN						WeightedKNN					
Channel	Gamma	Beta	alpha	Theta	Delta	Channel	Gamma	Beta	alpha	Theta	Delta	Channel	Gamma	Beta	alpha	Theta	Delta	Channel	Gamma	Beta	alpha	Theta	Delta
Mean	69%	69%	69%	69%	69%	Mean	70%	73%	80%	82%	85%	Mean	69%	72%	79%	81%	86%	Mean	64%	68%	77%	81%	85%
Max	69%	69%	69%	69%	69%	Max	75%	89%	89%	89%	92%	Max	78%	86%	86%	89%	92%	Max	75%	83%	83%	92%	92%

Note. Young good vs old bad

Young bad vs old bad:

FineTree						MediumTree						CoarseTree						LogisticRegression					
Channel	Gamma	Beta	alpha	Theta	Delta	Channel	Gamma	Beta	alpha	Theta	Delta	Channel	Gamma	Beta	alpha	Theta	Delta	Channel	Gamma	Beta	alpha	Theta	Delta
Mean	62%	65%	69%	72%	76%	Mean	62%	65%	69%	72%	76%	Mean	62%	65%	68%	73%	77%	Mean	63%	66%	68%	69%	74%
Max	84%	82%	87%	87%	92%	Max	84%	82%	87%	87%	92%	Max	84%	82%	87%	87%	92%	Max	79%	76%	84%	79%	84%
MediumGaussianSVM						CoarseGaussianSVM						FineKNN						MediumKNN					
Channel	Gamma	Beta	alpha	Theta	Delta	Channel	Gamma	Beta	alpha	Theta	Delta	Channel	Gamma	Beta	alpha	Theta	Delta	Channel	Gamma	Beta	alpha	Theta	Delta
Mean	65%	66%	72%	72%	82%	Mean	66%	66%	66%	66%	66%	Mean	53%	57%	67%	70%	78%	Mean	67%	71%	76%	77%	83%
Max	74%	76%	82%	84%	89%	Max	66%	68%	68%	66%	68%	Max	74%	82%	82%	95%	87%	Max	76%	79%	84%	87%	89%
LinearSVM						QuadraticSVM						CubicSVM						FineGaussianSVM					
Channel	Gamma	Beta	alpha	Theta	Delta	Channel	Gamma	Beta	alpha	Theta	Delta	Channel	Gamma	Beta	alpha	Theta	Delta	Channel	Gamma	Beta	alpha	Theta	Delta
Mean	67%	69%	74%	75%	82%	Mean	59%	62%	68%	71%	81%	Mean	56%	58%	69%	73%	79%	Mean	64%	66%	66%	66%	66%
Max	76%	82%	84%	87%	89%	Max	84%	79%	89%	87%	92%	Max	76%	79%	87%	87%	92%	Max	74%	71%	74%	74%	74%
CoarseKNN						CosineKNN						CubicKNN						WeightedKNN					
Channel	Gamma	Beta	alpha	Theta	Delta	Channel	Gamma	Beta	alpha	Theta	Delta	Channel	Gamma	Beta	alpha	Theta	Delta	Channel	Gamma	Beta	alpha	Theta	Delta
Mean	66%	66%	66%	66%	66%	Mean	68%	72%	77%	78%	83%	Mean	67%	71%	76%	76%	82%	Mean	61%	66%	72%	74%	82%
Max	66%	66%	66%	66%	66%	Max	76%	87%	87%	89%	92%	Max	79%	79%	87%	89%	87%	Max	79%	76%	84%	89%	89%

Note. Young bad vs old bad

Young bad vs old good:

FineTree						MediumTree						CoarseTree						LogisticRegression					
Channel	Gamma	Beta	alpha	Theta	Delta	Channel	Gamma	Beta	alpha	Theta	Delta	Channel	Gamma	Beta	alpha	Theta	Delta	Channel	Gamma	Beta	alpha	Theta	Delta
Mean	53%	60%	73%	76%	72%	Mean	53%	60%	73%	76%	72%	Mean	53%	60%	73%	76%	72%	Mean	63%	63%	64%	66%	70%
Max	91%	86%	95%	100%	95%	Max	91%	86%	95%	100%	95%	Max	91%	86%	95%	100%	95%	Max	86%	82%	100%	100%	100%
MediumGaussianSVM						CoarseGaussianSVM						FineKNN						MediumKNN					
Channel	Gamma	Beta	alpha	Theta	Delta	Channel	Gamma	Beta	alpha	Theta	Delta	Channel	Gamma	Beta	alpha	Theta	Delta	Channel	Gamma	Beta	alpha	Theta	Delta
Mean	57%	58%	69%	78%	78%	Mean	59%	59%	59%	59%	59%	Mean	55%	57%	68%	68%	78%	Mean	60%	62%	75%	79%	80%
Max	68%	77%	86%	95%	95%	Max	59%	59%	59%	59%	59%	Max	77%	82%	91%	95%	100%	Max	82%	82%	91%	91%	91%
LinearSVM						QuadraticSVM						CubicSVM						FineGaussianSVM					
Channel	Gamma	Beta	alpha	Theta	Delta	Channel	Gamma	Beta	alpha	Theta	Delta	Channel	Gamma	Beta	alpha	Theta	Delta	Channel	Gamma	Beta	alpha	Theta	Delta
Mean	58%	61%	69%	79%	78%	Mean	58%	60%	66%	75%	79%	Mean	58%	59%	67%	72%	78%	Mean	58%	58%	61%	61%	61%
Max	86%	77%	86%	100%	95%	Max	77%	91%	86%	95%	100%	Max	82%	91%	86%	95%	100%	Max	73%	68%	68%	77%	86%
CoarseKNN						CosineKNN						CubicKNN						WeightedKNN					
Channel	Gamma	Beta	alpha	Theta	Delta	Channel	Gamma	Beta	alpha	Theta	Delta	Channel	Gamma	Beta	alpha	Theta	Delta	Channel	Gamma	Beta	alpha	Theta	Delta
Mean	60%	62%	75%	79%	80%	Mean	59%	59%	77%	83%	78%	Mean	59%	62%	75%	77%	80%	Mean	59%	62%	75%	77%	80%
Max	82%	82%	91%	91%	91%	Max	77%	77%	86%	95%	91%	Max	77%	73%	91%	91%	95%	Max	77%	73%	91%	91%	95%

Note. Young bad vs old good

Young good vs old good:

FineTree						MediumTree						CoarseTree						LogisticRegression					
Channel	Gamma	Beta	alpha	Theta	Delta	Channel	Gamma	Beta	alpha	Theta	Delta	Channel	Gamma	Beta	alpha	Theta	Delta	Channel	Gamma	Beta	alpha	Theta	Delta
Mean	58%	57%	66%	67%	70%	Mean	58%	57%	66%	67%	70%	Mean	58%	57%	66%	67%	70%	Mean	58%	62%	61%	64%	65%
Max	85%	85%	90%	90%	90%	Max	85%	85%	90%	90%	90%	Max	85%	85%	90%	90%	90%	Max	90%	85%	85%	85%	95%
MediumGuassianSVM						CoarseGuassianSVM						FineKNN						MediumKNN					
Mean	58%	53%	68%	71%	76%	Mean	55%	55%	55%	55%	55%	Mean	50%	56%	59%	63%	72%	Mean	57%	57%	72%	77%	80%
Max	80%	75%	80%	90%	95%	Max	55%	55%	55%	55%	55%	Max	75%	85%	80%	95%	90%	Max	75%	70%	85%	85%	90%
LinearSVM ★						QuadraticSVM						CubicSVM						FineGuassianSVM					
Mean	59%	56%	67%	70%	77%	Mean	62%	60%	63%	69%	75%	Mean	59%	60%	63%	70%	72%	Mean	52%	50%	54%	55%	60%
Max	90%	70%	90%	90%	95%	Max	90%	85%	85%	90%	95%	Max	85%	85%	90%	85%	90%	Max	65%	65%	75%	75%	90%
CoarseKNN						CosineKNN						CubicKNN						WeightedKNN					
Mean	55%	55%	55%	55%	55%	Mean	55%	56%	70%	77%	78%	Mean	58%	56%	68%	73%	80%	Mean	56%	52%	64%	73%	77%
Max	55%	55%	55%	55%	55%	Max	75%	75%	80%	85%	90%	Max	75%	80%	80%	90%	90%	Max	75%	75%	85%	85%	85%


Note. Young good vs old good

Old good vs old bad:

FineTree						MediumTree						CoarseTree						LogisticRegression					
Channel	Gamma	Beta	alpha	Theta	Delta	Channel	Gamma	Beta	alpha	Theta	Delta	Channel	Gamma	Beta	alpha	Theta	Delta	Channel	Gamma	Beta	alpha	Theta	Delta
Mean	61%	61%	60%	63%	67%	Mean	61%	61%	60%	63%	67%	Mean	61%	61%	60%	63%	68%	Mean	64%	63%	58%	61%	65%
Max	85%	79%	85%	85%	85%	Max	85%	79%	85%	85%	85%	Max	85%	79%	85%	85%	85%	Max	71%	71%	74%	71%	82%
MediumGuassianSVM						CoarseGuassianSVM						FineKNN						MediumKNN					
Mean	74%	74%	73%	73%	73%	Mean	74%	74%	74%	74%	74%	Mean	64%	63%	59%	59%	62%	Mean	73%	74%	73%	74%	74%
Max	79%	79%	74%	74%	74%	Max	74%	74%	74%	74%	74%	Max	82%	82%	74%	76%	79%	Max	76%	76%	76%	76%	79%
LinearSVM ★						QuadraticSVM						CubicSVM						FineGuassianSVM					
Mean	72%	72%	72%	71%	71%	Mean	68%	67%	63%	65%	67%	Mean	64%	67%	60%	59%	65%	Mean	74%	74%	73%	73%	73%
Max	85%	82%	74%	76%	79%	Max	85%	85%	76%	79%	85%	Max	85%	88%	74%	79%	79%	Max	79%	79%	74%	76%	74%
CoarseKNN						CosineKNN						CubicKNN						WeightedKNN					
Mean	74%	74%	74%	74%	74%	Mean	74%	73%	74%	74%	74%	Mean	74%	74%	73%	73%	74%	Mean	74%	74%	73%	73%	74%
Max	74%	74%	74%	74%	74%	Max	76%	74%	76%	76%	79%	Max	74%	74%	76%	74%	79%	Max	74%	74%	76%	74%	79%

Note. Old good vs old bad

Young good vs young bad

FineTree						MediumTree						CoarseTree						LogisticRegression 					
Channel	Gamma	Beta	alpha	Theta	Delta	Channel	Gamma	Beta	alpha	Theta	Delta	Channel	Gamma	Beta	alpha	Theta	Delta	Channel	Gamma	Beta	alpha	Theta	Delta
Mean	47%	48%	49%	53%	49%	Mean	47%	48%	49%	53%	49%	Mean	47%	48%	49%	53%	49%	Mean	43%	50%	49%	47%	50%
Max	71%	75%	71%	83%	79%	Max	71%	75%	71%	83%	79%	Max	71%	75%	71%	83%	79%	Max	63%	75%	88%	71%	75%
MediumGuassianSVM						CoarseGuassianSVM						FineKNN						MediumKNN					
Channel	Gamma	Beta	alpha	Theta	Delta	Channel	Gamma	Beta	alpha	Theta	Delta	Canais	Gamma	Beta	alpha	Theta	Delta	Channel	Gamma	Beta	alpha	Theta	Delta
Mean	50%	52%	47%	46%	48%	Mean	54%	54%	54%	54%	54%	Média	43%	48%	49%	47%	55%	Mean	57%	61%	56%	56%	59%
Max	63%	79%	63%	67%	58%	Max	54%	54%	54%	54%	54%	Maximo	67%	88%	79%	71%	75%	Max	75%	75%	75%	75%	71%
LinearSVM						QuadraticSVM						CubicSVM						FineGuassianSVM					
Channel	Gamma	Beta	alpha	Theta	Delta	Channel	Gamma	Beta	alpha	Theta	Delta	Canais	Gamma	Beta	alpha	Theta	Delta	Channel	Gamma	Beta	alpha	Theta	Delta
Mean	49%	53%	45%	44%	47%	Mean	43%	48%	49%	52%	56%	Média	46%	51%	49%	53%	55%	Mean	48%	51%	51%	51%	51%
Max	67%	75%	71%	75%	79%	Max	71%	79%	75%	67%	75%	Maximo	67%	79%	71%	71%	71%	Max	71%	71%	75%	71%	67%
CoarseKNN						CosineKNN						CubicKNN						WeightedKNN					
Channel	Gamma	Beta	alpha	Theta	Delta	Channel	Gamma	Beta	alpha	Theta	Delta	Channel	Gamma	Beta	alpha	Theta	Delta	Channel	Gamma	Beta	alpha	Theta	Delta
Mean	54%	54%	54%	54%	54%	Mean	60%	58%	56%	54%	54%	Mean	58%	61%	56%	56%	61%	Mean	47%	47%	46%	47%	51%
Max	54%	54%	54%	54%	54%	Max	83%	79%	71%	71%	79%	Max	75%	75%	75%	71%	75%	Max	67%	75%	63%	71%	67%

Note. Young good vs young bad

Supplementary 3:

EEG brain configuration changes in theta and delta subbands in young vs older adults				
Subband	YG vs OB	YB vs OG	YB vs OB	YG vs OG
Theta	D4	C4	B26	D19
	B2	B16	A30	
	A30	A19		
Delta	B16	C7	B16	D26
	A23	A23		
		A19		
		A15		

Note. Table 2 displays the channels that presented higher differences between the study groups in the theta and delta subbands. YG = Young Adults with Good Sleep Quality; OB = Older Adults with Bad sleep Quality; YB = Young Adults Bad Sleep Quality; OG = Older Adults Good sleep Quality; Highlighted *in blue* the most representative channels indicating bad sleep in ageing; Channels in *in green* indicate age related changes; *In orange* the channel related to bad sleep independently of age. Only the theta and delta subbands are displayed as they are the ones that showed greater accuracy levels. (See below a biosemi plot with the biosemi EEG channels' locations). In *black* changes due to age and / or sleep (difficult to disentangle).

Regions most affected when comparing the older groups	
Subband	OG vs OB
Gamma	A23
Beta	A23
Alpha	Several
Theta	A1
Delta	C29
	C7

Note. Table 3 displays the channels that presented higher differences between the study groups. OG = Older with Good Sleep Quality and the OB = Older with Bad Sleep Quality. In this table, all the subbands are displayed as accuracy levels are homogeneous across them.

General Conclusions

The main aims of this thesis dissertation were i) to describe and demonstrate the methodological advantages of the PPA, ii) to explore the FC, and the dFC in AD and iii) to introduce a non-linear ML technique to classify age and sleep quality as a function of brain complexity.

Here it was demonstrated that the PPA has two main advantages. The first is that only a few data points from the BOLD rsfMRI signal are needed to perform the analysis. The second is that the data points included are based on the relevant neural events, i.e., intrinsic activation events identified by considering the signal's amplitude. This is useful when dealing with big datasets and when comparing the FC of healthy individuals with the FC of patients with a brain disease, which seems to have an increased variability over time. Considering this, our results suggest the PPA is more sensitive capturing changes across the stages of AD.

The AD biological insights extracted from this dissertation can be summarized into two main findings. First, patients with AD seem to present reduced connectivity between contralateral brain regions compared to healthy participants. These differences, however, are not present when exploring the FC of ipsilateral brain regions. These results support the idea that AD is a "disconnection syndrome" caused by the alteration of long white matter tracks, especially of the corpus callosum, associated with increased global atrophy and reduced cognitive functioning (Delbeuck et al., 2003).

The second main finding is that FC and dFC seem to have a non-linear progression change across the stages of the disease. This is characterized by a decrease in several brain regions in EMCI in comparison to healthy subjects, an increased FC in LMCI in comparison to HC and EMCI and an increased FC in mild AD in comparison to all the other groups. This FC pattern of progression had not been reported yet in the literature, probably because most studies using statistical approaches did not split the MCI group into EMCI and LMCI.

These two findings are complementary, and one could be explained by the other. The fact that AD participants in study 3 showed a decreased in FC (as a function of distance) between long distant contralateral brain regions could explain the abnormal increased in FC between several brain regions in study 2. As suggested by other researchers, these increased FC in LMCI and mild AD might indicate compensatory mechanisms that can be adaptive short term but not in the mid-long term. In fact, researchers inferred that an abnormal increased FC between several

regions could be explained by an accumulation of pathologic protein in close regions and that these compensatory mechanisms generate, at the same time, an increase of this pathologic protein, developing a mal(adaptive) loop (Ashraf et al., 2015). Future studies could include patients with moderate and severe AD to explore the progress of FC in these stages. I hypothesize a linear reduction of FC in the last AD stages due to the massive and widespread brain atrophy and its association with decreased connectivity (Badhwar et al., 2017; Wang et al., 2020).

The non-linear dFC method, PPA, represents a gate for several future research ideas. Some of these are i) to conduct further research to validate the method to be used in the context of AD and other neurodegenerative diseases; ii) to apply the PPA to explore other brain diseases; iii) to apply PPA to task fMRI; iv) to apply PPA to other neuroimaging modalities such as to EEG data. The PPA is a "minimalistic"¹ and fast research tool that needs to be validated. Ultimately, this method might be able to be used in a clinical context to make predictive, prognostic and clinical diagnoses of AD and other brain diseases. The PPA might be a promising tool to distinguish healthy patients and patients with brain pathology in a highly efficient way. In addition to the advantages already reported, one of the main aspects to consider when applying PPA is the threshold set to select the relevant points that denote strong activity in the PPA. This is the only free parameter. This topic was deeply explored by Tagliazucchi et al. (2012). In their paper, they demonstrated that any threshold of the BOLD signal between 1 and 2 *SD* is optimal, as results remain unchanged. Using a threshold within this range is fundamental to extract uncontaminated BOLD temporal points.

Some additional ideas for future studies that will potentially enable the identification of FC biomarkers for AD are related to the characterization of the samples. To deeply understand the neural underpinnings of AD, it is relevant to keep in mind that the first stage of the disease, known as preclinical AD, is characterized by tauopathy, betamyloidosis and a lack of presence of cognitive symptoms². The presence of just one biomarker (amyloidosis or tauopathy) is not considered preclinical AD. However, it indicates risk for AD (AR-AD), albeit less so than someone with a preclinical AD (Dubois et al., 2019). Considering these facts, and as suggested by other authors, future studies exploring connectivity could consider a deeper biological characterization of the samples, especially of the healthy and MCI participants. This finer

¹ Minimalistic here means that only a few datapoints are needed, which means less computational demands.

² AD was discovered in the late 20th century, examining patients postmortem who had brain pathology associated with AD, i.e., tauopathy and betamyloidosis, but who had not shown any symptom. This concept has now evolved being possible to explore the presence of AD biomarkers in vivo (Dubois et al., 2019).

description of the samples in studies exploring FC could help determine the likeliness of healthy participants to develop MCI and of MCI to develop a clinical AD (Canevelli et al., 2019).

The algorithm used to classify age and sleep quality achieved excellent accuracy levels, especially when comparing the young vs. the older groups. The main advantage of this non-linear ML approach is the ability to include several features (not only synchronicity between regions) to capture the brain complexity and enable classification. Future studies with a more significant sample should be conducted to validate the method. In addition, this algorithm could be used in future research to classify sleep quality in MCI vs. healthy older adults. Additionally, future investigations could include a feature search selection to determine which of the features of complexity extracted from the signal are best to classify age and sleep quality. This step was not performed in study 4 because high accuracies in the older groups, which were the main target, were already reached. However, the algorithm could probably be adjusted to classify with higher accuracy the younger groups. Another idea for future studies would be to perform ANOVA to determine the directionality of the findings and extract biological meaning, i.e., mixing classical statistics and ML. Eventually, this tool could be employed in clinical practice to classify patients' sleep quality and to select the most appropriate intervention considering brain complexity.

In conclusion, this thesis presented novel methods to study FC, dFC and global brain complexity in the context of aging and AD using rsfMRI and rsEEG DATA with classical statistics and ML. The results obtained revealed that these methods are sensitive to capturing synchronicity and complexity changes across healthy older adults and AD groups. Further studies are needed to validate these methods and findings. If results are as expected, the PPA and the non-linear multiband EEG algorithm could potentially be used as a clinical tool for early diagnosis of AD, sleep disturbances associated with age and other brain diseases. For a graphical display of the general conclusions, see "My Ph.D. studies chart".

References

- Ashraf, A., Fan, Z., Brooks, D.J. and Edison, P. (2015). Cortical hypermetabolism in MCI subjects: a compensatory mechanism?, *European Journal of Nuclear Medicine and Molecular Imaging*, 42(3), pp. 447–458. <https://doi.org/10.1007/s00259-014-2919-z>.
- Badhwar, A. P., Tam, A., Dansereau, C., Orban, P., Hoffstaedter, F., & Bellec, P. (2017). Resting-state network dysfunction in Alzheimer's disease: A systematic review and meta-analysis. *Alzheimer's and Dementia: Diagnosis, Assessment and Disease Monitoring*, 8, 73–85. <https://doi.org/10.1016/j.dadm.2017.03.007>

- Canevelli, M., Bacigalupo, I., Gervasi, G., Lacorte, E., Massari, M., Mayer, F., ... Cesari, M. (2019). Methodological Issues in the Clinical Validation of Biomarkers for Alzheimer's Disease: The Paradigmatic Example of CSF. *Frontiers in Aging Neuroscience*, 11.
- Delbeuck X, Linden MVD, Collette F. (2013). Alzheimer's Disease as a Disconnection Syndrome? *Neuropsychology Review* ;13(2):79-92.
- Dubois, B., Hampel, H., Feldman, H. H., Scheltens, P., Aisen, P., Andrieu, S., ... Cliff, R.J., Proceedings of the Meeting of the International Working Group (IWG) and the American Alzheimer's Association on "The Preclinical State of AD"; July 23, 2015; Washington DC, USA (2016). Preclinical Alzheimer's disease: Definition, natural history, and diagnostic criteria. *Alzheimer's & dementia: the journal of the Alzheimer's Association*, 12(3), 292–323. <https://doi.org/10.1016/j.jalz.2016.02.002>
- Tagliazucchi, E., Balenzuela, P., Fraiman, D., & Chialvo, D. R. (2012). Criticality in large-scale brain fmri dynamics unveiled by a novel point process analysis. *Frontiers in Physiology*, 3 FEB. <https://doi.org/10.3389/fphys.2012.00015>
- Wang, X. H., Zhao, J., Du, Y. H., Ding, X. T., & Men, G. Z. (2020). Alteration of functional connectivity in patients with Alzheimer's disease revealed by resting-state functional magnetic resonance imaging. *Neural Regeneration Research*, 15(2), 285. <https://doi.org/10.4103/1673-5374.265566>

My Ph.D. Studies:

Novel non-linear approaches to understanding the dynamic brain: knowledge from rsfMRI and EEG studies.

